DASA 1369

AN EXPERIMENTAL DRAG FACILITY

by

M. L. Whitfield
E. M. Briggs
R. K. Gregory
R. C. DeHart

Project No. 1029-3

Contract DA 49-146-XZ-062

FINAL REPORT

Prepared for

Defense Atomic Support Agency
Washington 25, D. C.

March 15, 1963

SOUTHWEST RESEARCH INSTITUTE
SAN ANTONIO, TEXAS

DASA 1369

SOUTHWEST RESEARCH INSTITUTE
8500 Culebra Road, San Antonio 6, Texas

Department of Structural Research

AN EXPERIMENTAL DRAG FACILITY

by

M. L. Whitfield
E. M. Briggs
R. K. Gregory
R. C. DeHart

Project No. 1029-3

Contract DA 49-146-XZ-062

FINAL REPORT

Prepared for

Defense Atomic Support Agency
Washington 25, D.C.

March 15, 1963

APPROVED:

Robert C DeHart

R. C. DeHart, Director
Department of Structural
Research

ABSTRACT

Experiments performed during the initial phase of a program sponsored by the Defense Atomic Support Agency (DASA) under contract DA 49-146-XZ-062 have shown that solid propellants can substantially supplement and prolong the positive pressure pulse in a standard shock tube, provided that proper design and operational procedures are observed. The extra energy from the solid propellant allows for expedient simulation of nuclear blast wave conditions within the tube.

Three types of solid propellant rocket motors from standard stock were utilized. Pressure, temperature, and velocity characteristics of gas flow generated by the motor and discharged through a nozzle into the tube were recorded as a function of time at several locations down the tube. In addition, a unique technique for generating a shock wave at a preselected time during the high velocity gas flow was developed.

TABLE OF CONTENTS

TABLE OF CONTENTS (Cont'd)

LIST OF ILLUSTRATIONS

LIST OF ILLUSTRATIONS (Cont'd)

LIST OF ILLUSTRATIONS (Cont'd)

LIST OF ILLUSTRATIONS (Cont'd)

LIST OF ILLUSTRATIONS (Cont'd)

LIST OF TABLES

LIST OF SYMBOLS

A_p	area within wetted perimeter, ft^2
A_l	cross-sectional area facing flow on probe, ft^2
C_{p_a}	specific heat at actual temperature, Btu/lb °R
C_{p_s}	specific heat at standard temperature, Btu/lb °R
h	convective heat transfer coefficient, Btu/hr ft^2 °R
K	effective thermal conductivity, Btu-ft/hr ft^2 °R
L	probe immersion depth, ft
M	Mach number
M_x	Mach number in front of shock
M_y	Mach number behind shock
P_{ox}	stagnation pressure in front of shock, psi
P_{oy}	stagnation pressure behind normal shock, psi
P_s	static pressure, psi
P_t	total or stagnation pressure, psi
P_t'	stagnation pressure behind normal shock, psi
P_x	static pressure in front of normal shock, psi
P_y	static pressure behind normal shock, psi
q	dynamic pressure, psi
r	probe correction factor
T	temperature, °R
T_o	stagnation temperature, °R

LIST OF SYMBOLS (Cont'd)

T_p	measured temperature of probe, °R
T_{p_a}	adiabatic temperature of probe, °R
T_r	temperature of radiant heat shield, °R
T_w	wall temperature, °R
T_∞	stream temperature, °R
$(\Delta T_p)_c$	stem conduction error, °R
$(\Delta T_p)_r$	radiant heat transfer error, °R
V	velocity, ft/sec
ϵ	surface emissivity
γ	ratio of specific heats
ρ	density, lb sec^2/ft^4
σ	Stefan-Boltzmann constant, Btu/hr ft^2 $(°R)^4$

1. INTRODUCTION

1.1 General

During the nuclear moratorium, simulation of nuclear blast waves was of prime importance because of the continuing need to develop information which would improve the nation's defense posture. Since the duration of a nuclear blast wave is longer than the duration of the blast wave generated in so-called standard shock tubes, various means for generating longer duration shocks needed investigation. One of the most plausible concepts was the addition of energy behind the shock wave in a standard shock tube. The feasibility of this suggestion was theoretically demonstrated by work under a prior DASA contract.[1] It was still necessary, however, to investigate the various problems of practical application of the proposed technique. Accordingly, a program for experimentally establishing the feasibility of using solid propellants to prolong the shock wave duration in a shock tube was sponsored at SwRI by DASA under contract DA 49-146-XZ-062. Work concerning the simulation of an atomic blast is reported herein.

The solid propellant driven tunnel has the additional inherent capability of being able to produce an environment similar to that experienced by an object re-entering the atmosphere from space. Consequently, the scope of the original project was broadened to include an "evaluation of the drag facility principle to determine its usefulness for investigating the shock loading of re-entry bodies in flows of over 7000 fps." The research conducted on this extended scope of the contract is contained in a separate report, Reference 2.

1.2 Scope of Work

The primary objective of the research was to investigate experimentally the feasibility of generating in a long tube conditions typical of a nuclear blast wave by controlled burning of solid propellants. Dynamic pressures of 100 psi and 1 second duration were to be generated in an 8-in. diameter tunnel through the use of currently available rocket motors. Sufficient measurements of flow parameters were to be made to confirm the actual environment conditions in the tunnel and to provide a means for comparison with existing theory. Also, a method for providing a strong shock front in the event it did not naturally occur was to be devised.

1.3 Summary of Results

The general test procedure consisted of firing a preselected rocket motor expanding the flow through an expansion nozzle into tunnels having the dimensions shown in Figures 2.1 and 2.3 and measuring the flow parameters. The flow parameters were measured by means of various calibrated instrumentation devices. Quantities measured were dynamic pressure, stagnation pressure, static pressure, temperature, stagnation temperature, and velocity. Continuous recordings of these instruments were taken throughout the duration of the gas flow. These data are shown in Appendix A.

The results of the experiments are summarized in Table 1.1. The dynamic pressure of the flow was directly measured in two tests with two Broadview dynamic pressure gages. In shot 2 a dynamic pressure of 73 psi was measured at station 13 (13 ft from the nozzle exit), and in shot 4 the dynamic pressure was 58 psi at station 82; however, it is believed that temperature effects caused some inaccuracy in the measurements. Independent measurements of stagnation pressure and static pressure gave a more reliable value for dynamic pressure that compared favorably with theoretical predictions, as shown for example in Table 1.1 by the better correlation with theory in shots 6 through 12. Dynamic pressures varied from 18 and 20 psi for the Turbine Spinners (T-S) to 100 psi for the Cajuns and 150 psi for the Redhead/Roadrunner (RH/RR) in the 8-in. tube and were 30 and 50 psi for the RH/RR's in the 17-in. tube as determined from the stagnation pressure and static pressure records.

Sustained duration of the dynamic pressures was demonstrated to be from 0.6 sec for the small Turbine Spinners, to 1.6 and 2 sec for the RH/RR, to 2.4 sec for the Cajun as shown in Table 1.1. Some variation of the durations was measured. This was attributed primarily to variations of the motor burning time which was influenced by fluctuations in ambient temperature and/or varying exposures to atmospheric humidity.

The static pressures associated with these dynamic pressures were about 4 psia for the Turbine Spinners, about 15 psia for the Cajuns, and about 12 psia for the RH/RR in the 8-in. tube and were about 1 and 4.5 psia for the RH/RR's in the 17-in. tunnel, as shown in Table 1.1.

For independent and controlled generation of the shock front, a separate shock wave generator was developed as shown in Figure 2.19. It consisted of a massive ring housing that contained cavities for up to eight high explosive charges. To generate a strong clean shock front, all the charges had to detonate absolutely simultaneously, which required

TABLE 1.1. EXPERIMENTAL RESULTS

		Measured*			Predicted**			
Test	Motor	M	q, psi	P_s at q max, psia	M	q, psi	V, fps	Tunnel Diameter
1	T-S	5.5	20	4.4	5.4	18	7500	8"
2	Cajun	3.3	103	15	3.2	120	6700	8"
3	T-S	4.9	18	4	5.4	18	7500	8"
4	Cajun	3.3	100	15	3.2	120	6700	8"
5	T-S	-	-	7	5.4	18	7500	8"
6	RH/RR	3.5	150	12	3.7	140	6780	8"
7	RH/RR	5.2	35	2.5	5.17	30	7500	17"
8	RH/RR	5.2	30	1	5.17	30	7500	17"
9	RH/RR	5.2	30	1	5.17	30	7500	17"
10	T-S	-	-	14	Subsonic			17"
11	RH/RR	5.2	30	1	5.17	30	7500	17"
12	RH/RR	4.4	54	4.5	5.17	30	7500	17"

*At Station No. 1
**At the Nozzle Exit
Isentropic Conditions

a high voltage, high energy detonation source. Such a source was developed and successfully used to fire up to six 8-gram pentolite explosive charges. This explosive energy blown into the supersonic flow formed a clean shock front as it was swept down the tube to impinge on the model. Peak overpressures at the model varied from 20 psi with 2 charges to 100 psi with 6 charges.

In the 17-in. tunnel which was constructed to facilitate a larger model for the aforementioned re-entry study, the flow was more efficiently expanded to higher flow velocity and much lower density which resulted in a lower dynamic pressure (from 30-50 psi) and a lower static pressure (1-2 psi) than the 8-in. tunnel.

1.4 Conclusions

Exploratory tests concerning the economic and operational feasibility of a solid propellant driven tunnel have indicated that it is possible to create a variety of environments in the tunnel by superposing shock waves on hypervelocity flow and that the primary difficulty in the development of such a test facility is the instrumentation. Initial research has shown that the discharge of the gas generated by the burning of a solid propellant into a shock tube is a reasonable means for increasing the duration of the blast wave generated in a shock tube. Experiments have also shown that the use of solid propellant type motors for generating high velocity flow in existing tunnels is practicable. Programmed detonation of explosives subsequent to motor firing allows for superposing a shock wave on the flow.

The primary difficulty in the development of instrumentation for the facility arose from temperature and acceleration effects on the gages. Water cooling and damped mountings to some extent offset these difficulties, but specially designed equipment and transducers are needed to improve the accuracy with which data can be obtained.

The flow in the tunnel was relatively turbulent and pulsated which made optical measurements difficult. Turbulence control techniques such as those used in wind tunnels are needed if steady flow conditions are to be established in the tube.

The gas being generated by the solid propellant is somewhat lighter than air and has a lower ratio of specific heats. Special propellant formulations are available and could be tailored for specific blast load problems.

This research has indicated that improved results can be achieved. Higher dynamic pressures could be generated with higher flow rates and/or higher molecular weight propellants. Static pressures more closely simulating that of surface nuclear blasts could be generated with higher chamber pressures and/or by deliberately causing a normal shock in the nozzle to convert the flow to subsonic flow. The duration of the gas flow could be varied with specially designed propellant grains. The shock pressures could be controlled by variation of yield and/or number of explosive charges.

2. DESCRIPTION OF THE FACILITY

2.1 Rocket Motors

From aerodynamic theory of isentropic expansion it was determined that a gas flow rate of 40 to 50 lb/sec was required to achieve a 100-psi dynamic pressure in an 8-in. pipe. This determination was based on the use of a typical ammonium nitrate rocket motor which burns at 3000°R and 2000 psia. Three different rocket motors were utilized in the test series. The characteristics of these motors are given in the following paragraphs and summarized in Table 2.1.

Two of Thiokol Chemical Company's "Cajun" motors, in which the propellant was ammonium perchlorate, were used. The combustion temperature of these motors was 4520°R. These motors were readily available and had a long history of reliability.

Rocketdyne Division of North American Aviation supplied six "Redhead/Roadrunner" motors which could deliver approximately the desired flow rate. These ammonium nitrate motors as they are normally produced have nearly a 6-second burning time. By decreasing the wall thickness and throttling the flow to increase the pressure to about 2000 psia it was possible to reduce the burning duration for these motors to about 1.8 sec. These motors were specially modified for this work.

Four small motors (Turbine Spinners) supplied by Rocketdyne were used for functionality tests for various tunnel and instrument configurations. Although the amount of gas generated by the Turbine Spinner was so small that large expansion of the gas flow was needed in order to fill the 8-in. pipe, it was still possible to conduct successful checkout tests.

TABLE 2.1. ROCKET MOTOR CHARACTERISTICS

Manufacturer		Rocketdyne	Rocketdyne	Thiokol
Name		Turbine Spinner	RH/RR	Cajun
Wt, lb		6.5	100	120
Chamber pressure, psia		2000	2000	1200
Burning time, sec		0.7	1.8	2.8
Propellant		RDS 135	RDS 233	TE-82
Flame temperature, TC °F		2544	2697	4160
Burning rate		0.270	0.270	
Ratio of specific heats		1.250	1.244	1.25
Molecular weight of exhaust gas		20.94	21.09	26.5
Exhaust products % molecular				
Water	H_2O	34.78	35.68	35.1
Carbon monoxide	CO	14.47	14.45	8.3
Nitrogen	N_2	21.55	21.71	8.3
Hydrogen	H_2	21.18	3.01	8.9
Hydrogen chloride	HCL			16.6
Sulfur dioxide	SO_2			0.16
Carbon dioxide	CO_2	7.28	7.09	15.3
Hydrogen sulfide	H_2S			5.6
Sulfur	S_2			1.5
Solids		3.85	.75	0.49

2.2 Tunnels

An 8-in. diameter pipe tunnel 100 ft long was fabricated from bolt-flanged pipe sections approximately 20 ft in length as shown in Figures 2.1 and 2.2. Wall thickness was 0.500 in. The interchangeable sections allowed for flexibility in placement and interchange of instrumentation. As shown in Figure 2.1, the tunnel was anchored at the forward end and secured with pipe rollers at four locations.

For the investigation described in Reference 2, a 17-in. diameter 29-ft long tunnel was constructed (see Figs. 2.3 and 2.4) for use with Rocketdyne's Redhead/Roadrunner, Figure 2.5 (Ref. 2). The assembly was designed for Mach 5.2 flow at a rate of 54.3 lb/sec using normal supersonic criteria. Tunnel walls, which were 7/16 in. thick, were lined with polished stainless steel to a thickness of 0.07 in. A 6-in. diameter window was provided for optical measurements. In the middle of the tunnel a bolted coupling allowed ready access to the model and the inside of the windows (Figs. 2.3 and 2.4).

The tunnel facilities were equipped with a reinforced concrete, dirt covered bunker around the forward end of the tunnel as can be seen in Figures 2.1 and 2.2.

2.3 Instrumentation

2.3.1 General

The most difficult problem encountered involved the development of instrumentation installations that would survive the extreme environment. Some instruments designed to operate at even higher temperatures than those encountered in these tests could not withstand the high velocity flow. The requirement for fast response transducers capable of measuring the shock front generated as a part of the study described in Reference 2 increased the difficulties to be overcome severalfold.

Temperature effects on pressure transducers necessitated special precautions, such as water cooling. Even temperature measurement was difficult with such high velocity flow because of radiant and conductive heat losses.

The location of the instrumentation is shown in Figure 2.1 for the early tests in the 8-in. tunnel. This was later modified for tests 5 and 6 as shown on Figure 2.6. Instrumentation locations for the 17-in. tunnel are shown in Figures 2.3 and 2.4.

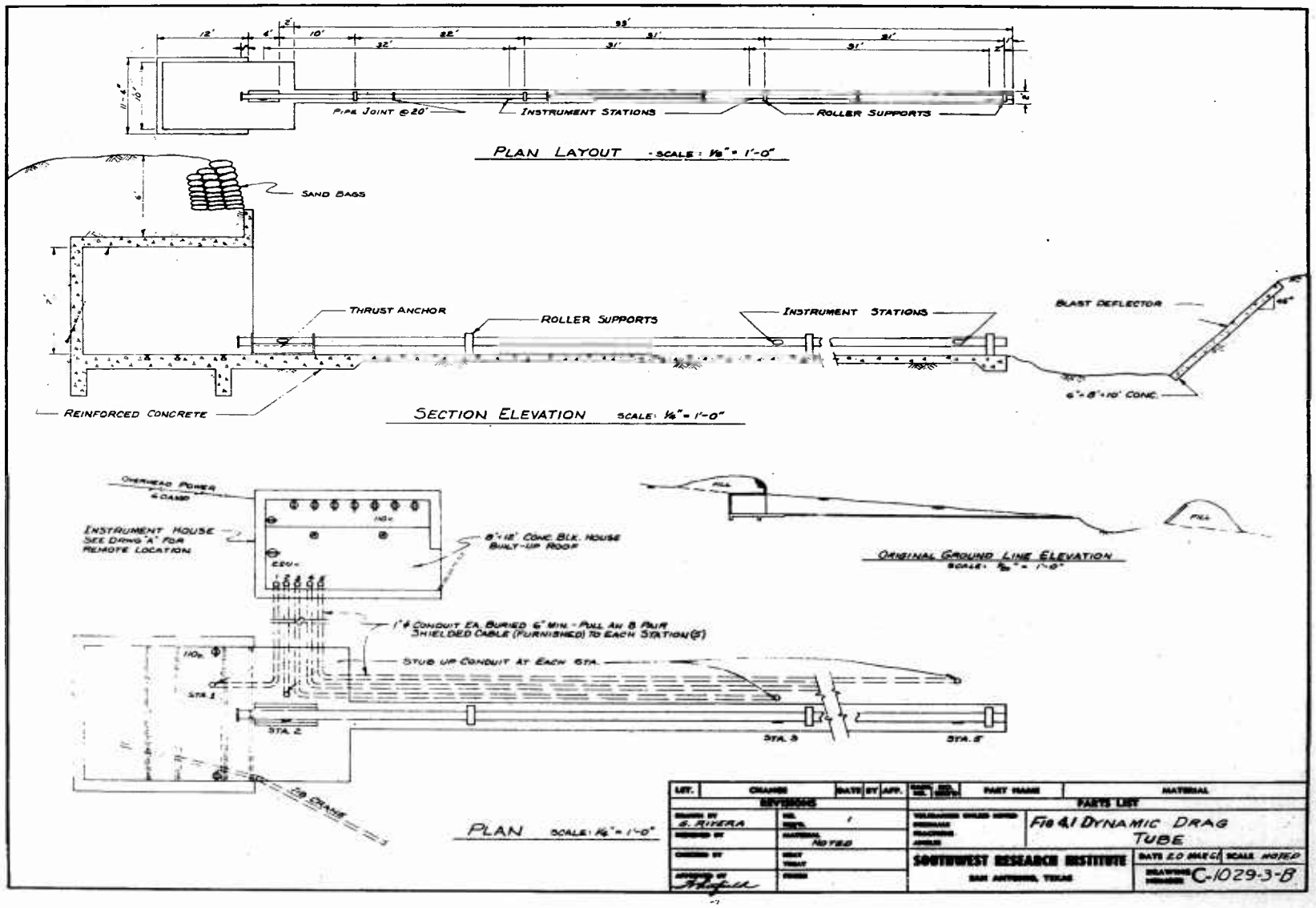

FIGURE 2.1. DYNAMIC DRAG TUBE

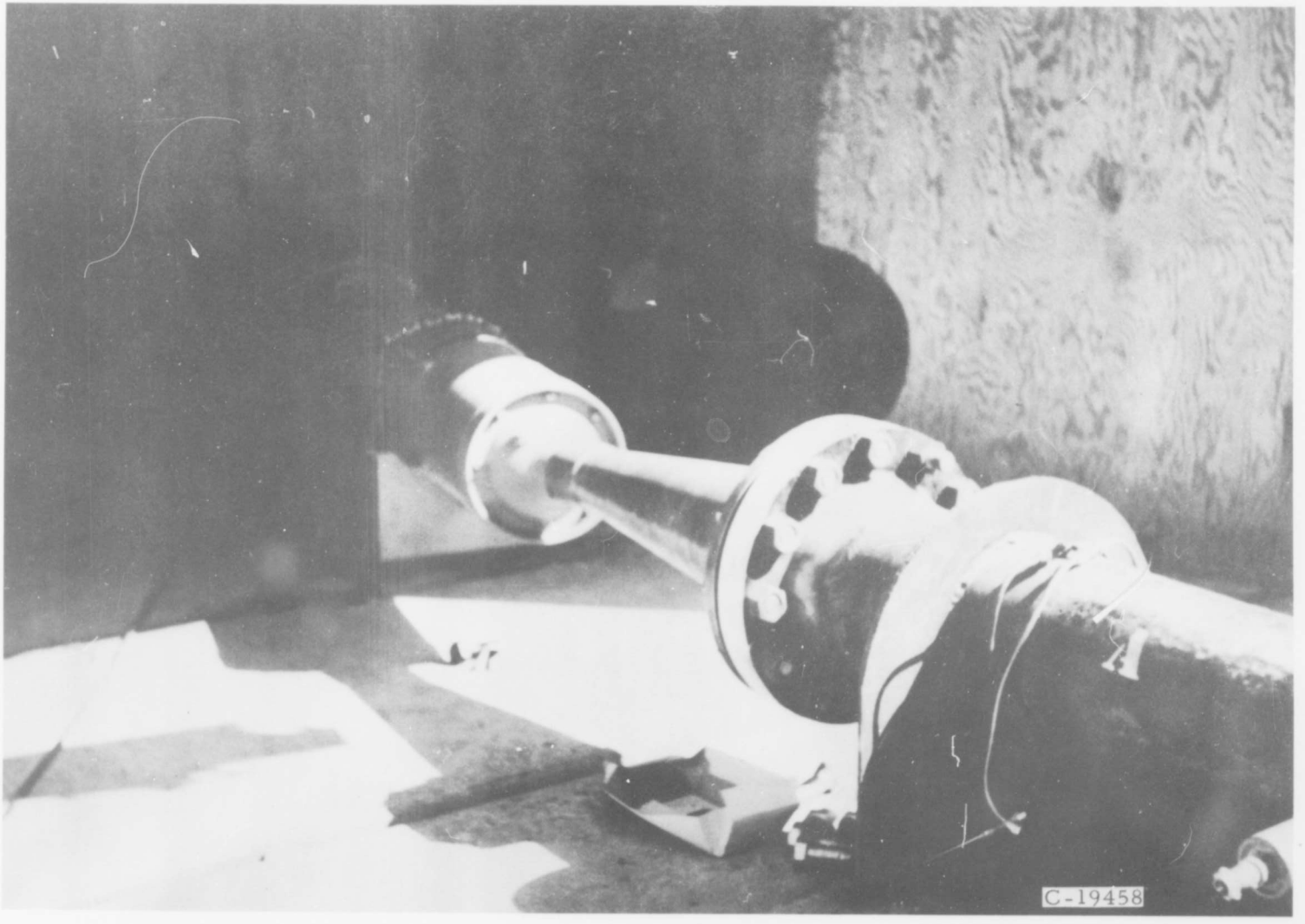

FIGURE 2.2. VIEW LOOKING UPSTREAM AT "READHEAD/ROADRUNNER" ON 8-IN. TUBE

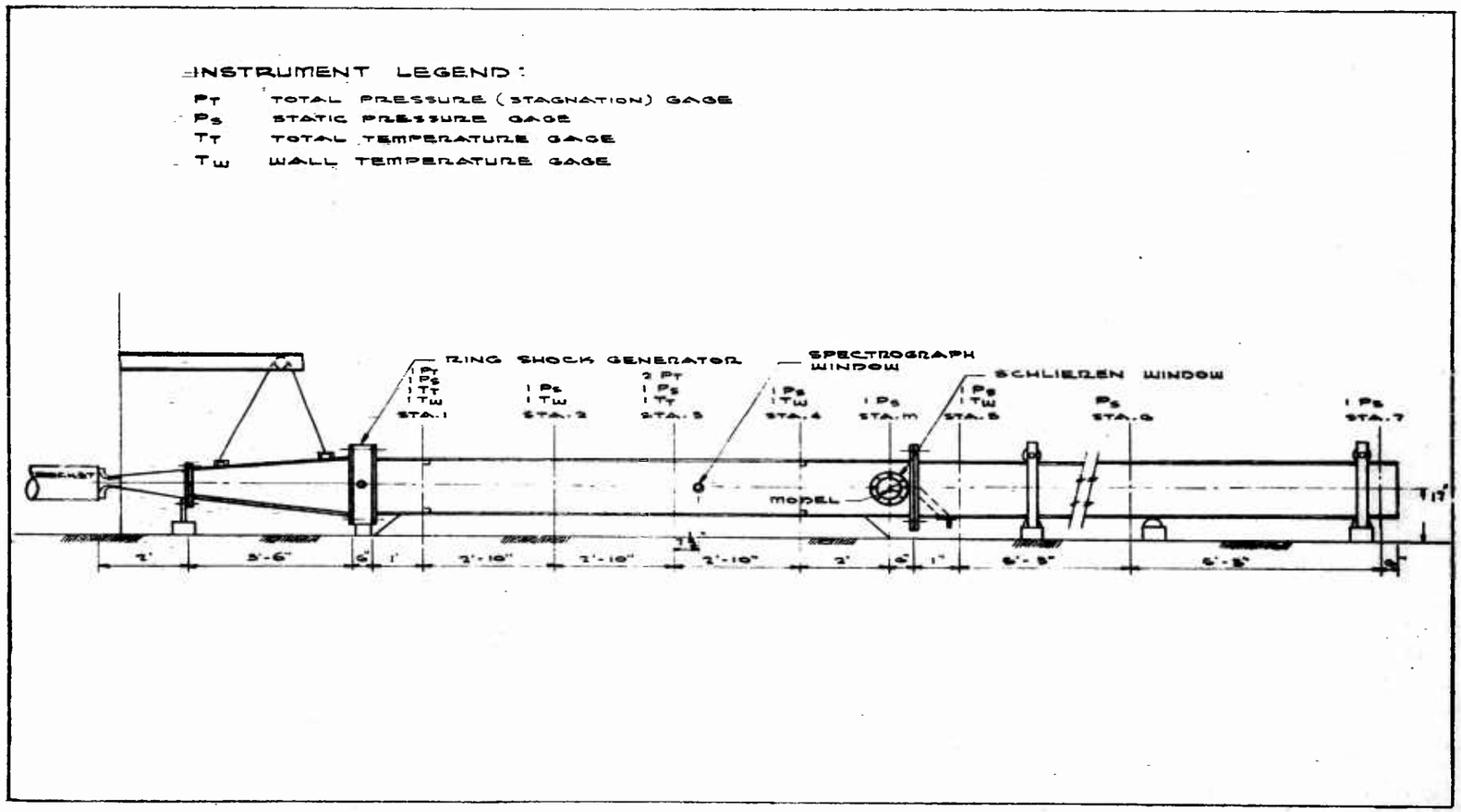

FIGURE 2.3. INSTRUMENT STATIONS, 17-IN. TUNNEL, ELEVATION

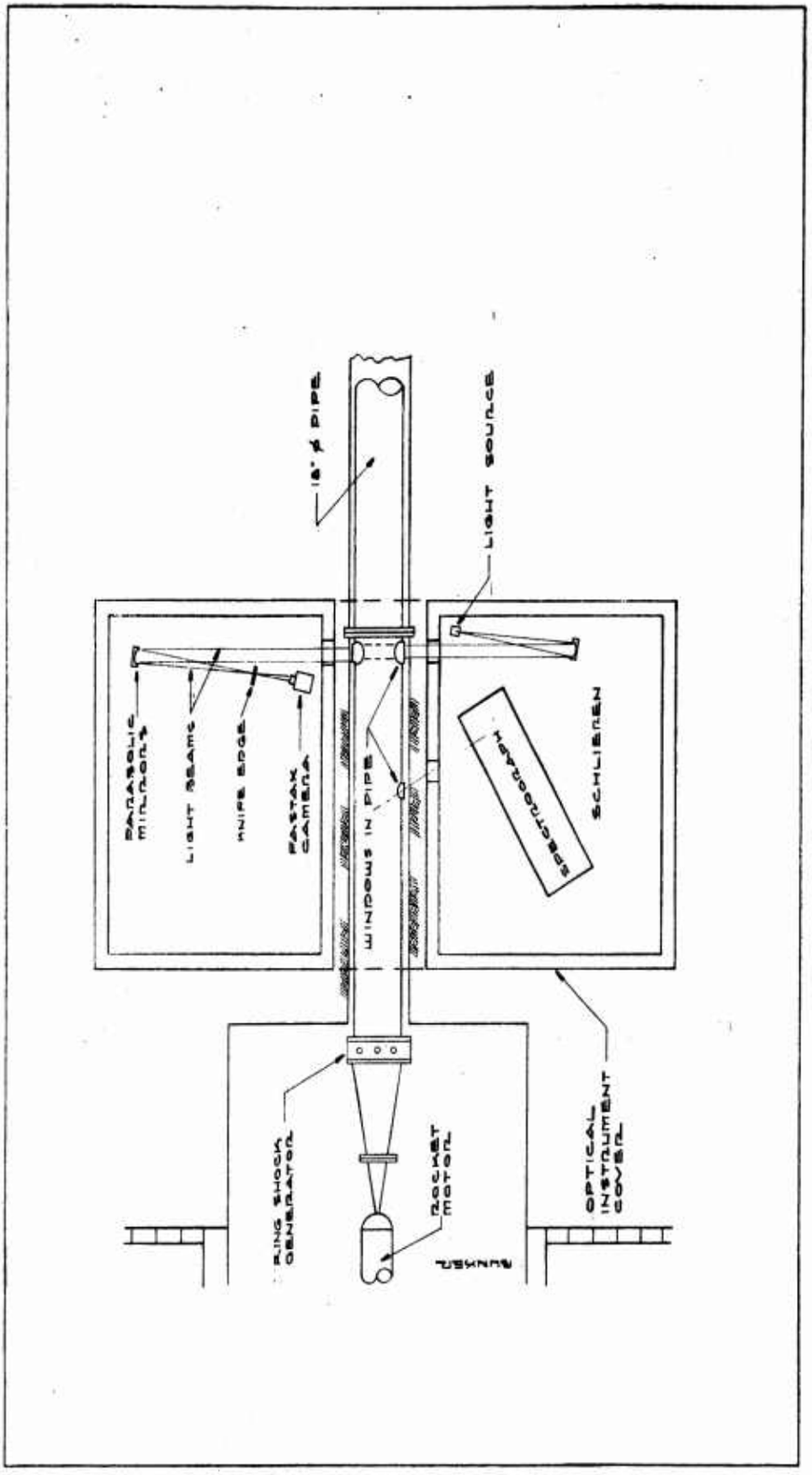

FIGURE 2.4. OPTICAL INSTRUMENT LAYOUT, 17-IN. TUNNEL, PLAN

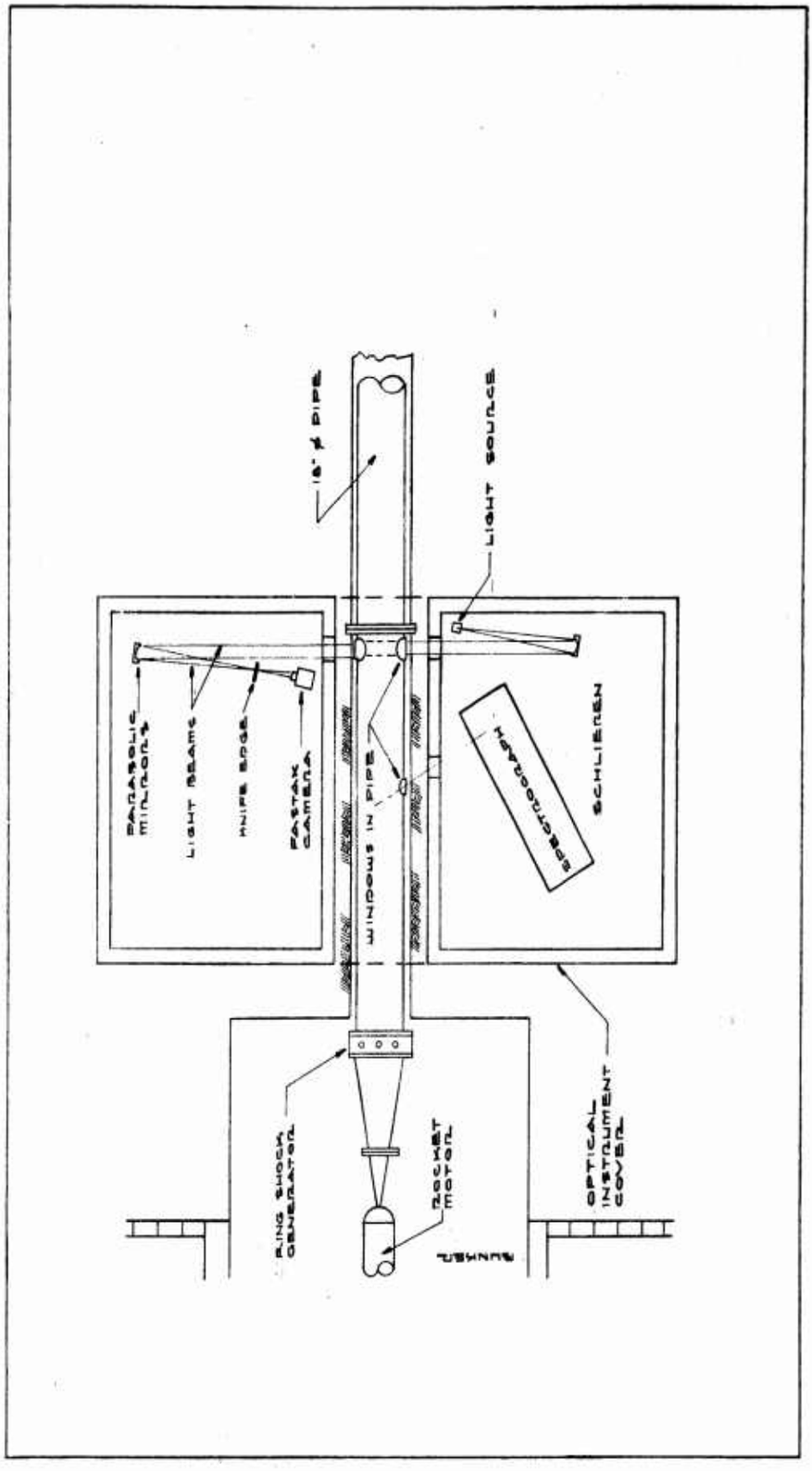

FIGURE 2.4. OPTICAL INSTRUMENT LAYOUT, 17-IN. TUNNEL, PLAN

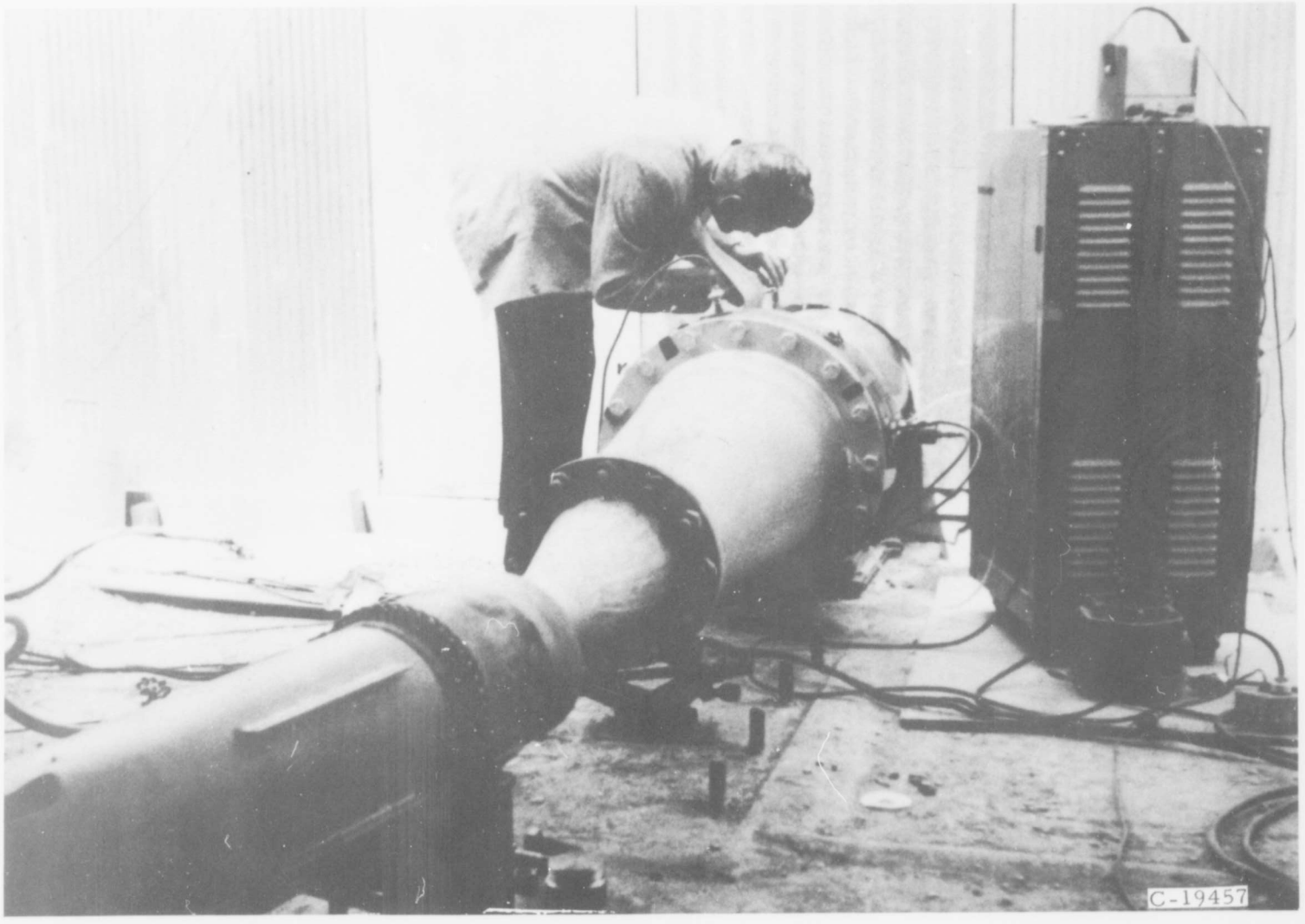

FIGURE 2.5. VIEW OF 17-IN. TUBE LOOKING DOWNSTREAM TOWARD INSTRUMENT HOUSE

Note: High voltage system and shock generator ring at joint of tube and nozzle

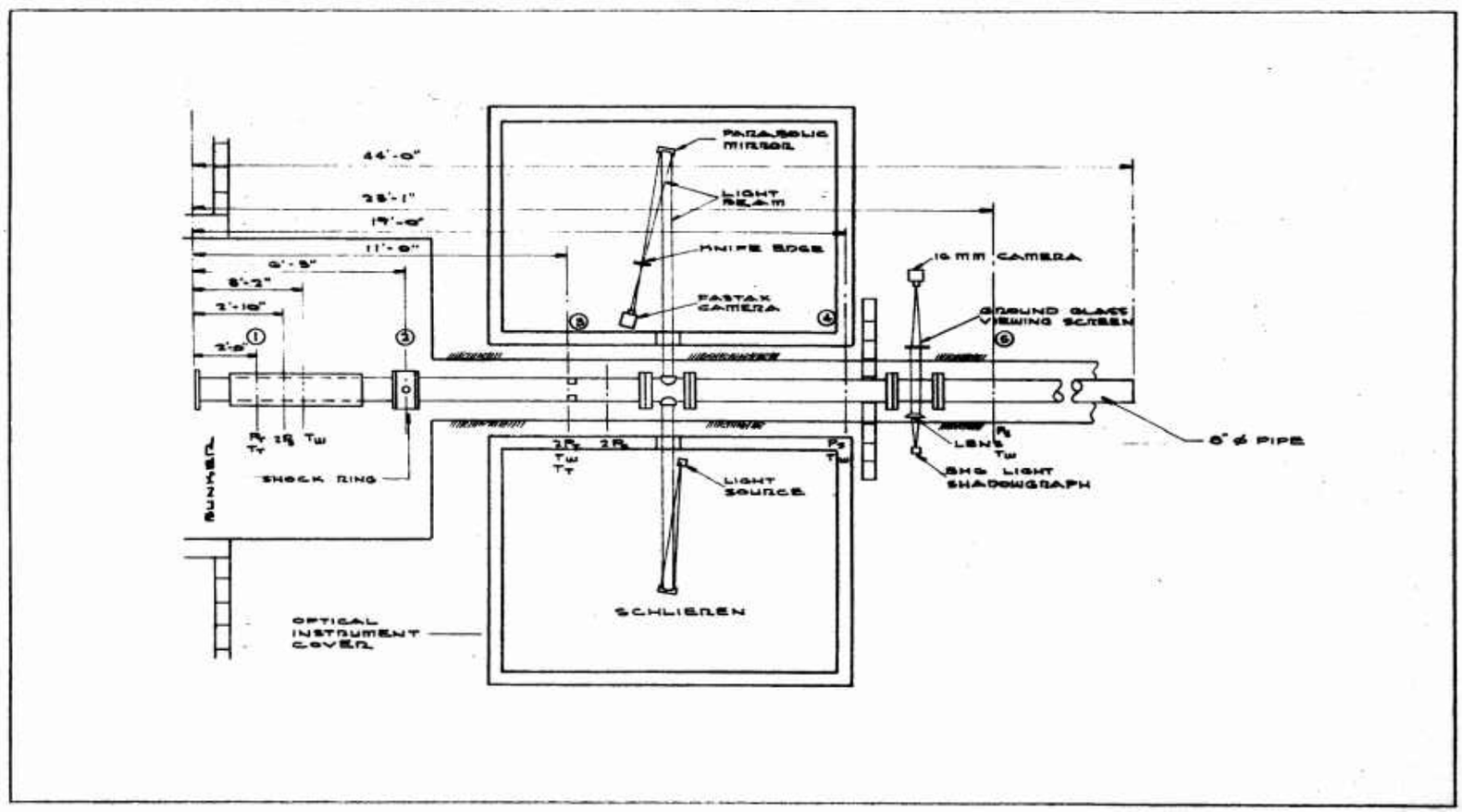

FIGURE 2.6. OPTICAL INSTRUMENT LAYOUT, 8-IN. TUNNEL, PLAN

2.3.2 Pressure Measurement

Static and dynamic pressure measurements were made in order to define the flow conditions in the tube.

The combustion pressure, as well as combustion temperature and γ, had been furnished by the rocket motor manufacturer (see Table 2.1), and this was accepted; however, it developed later that variations of the combustion pressure do occur which are important to have recorded for each test.

2.3.2.1 Static Pressure

The measure of static pressure in a tunnel presented no fundamental difficulty. A flush mounted sensing element in the wall was generally reliable. Temperatures at the wall were low enough and brief enough that nonpiezoelectric transducers worked well. Water cooling was even effective on piezoelectric type transducers.

2.3.2.2 Dynamic Pressure

A direct measure of dynamic pressure, "q," required simultaneous sensing of stagnation pressure, P_t, minus static pressure, P_s, at or near the same point in the flow. While this was attempted with the Broadview dynamic pressure gage[3], there were inherent mechanical difficulties in such an approach, as discussed later. Separate measurements of stagnation pressure and static pressure were more easily achieved; however, care had to be taken so that one measurement did not interfere with the other. The stagnation pressure measurement is described in the next section.

Since dynamic pressure is defined as

$$q \equiv \frac{1}{2} \rho V^2 \qquad (1)$$

a separate approach was to measure flow velocity and density. Density was calculated with sufficient accuracy from the pressure and temperature measurements. Velocity measurements are described in Section 2.3.4.

Spectrographic techniques can be used to measure velocity as well as temperature. Although some of the problems described above are avoided, new ones arise with the use of high speed, high resolution photographic equipment. A Bausch & Lomb Dual Grating Spectrograph was employed; however, its resolution capacity was insufficient, and no useful data were obtained.

In the Broadview dynamic pressure gage, a direct measure of dynamic pressure is obtained with a transducer immersed in the flow such that one side sensed the stagnation pressure while the other side sensed the static pressure. This is done with a small piezoelectric cylindrical tube crystal mounted in a thin, flat strut. A stagnation baffle stagnates the flow adjacent to one side of the crystal. Since the two pressures opposed each other, the crystal output is relatable to dynamic pressure. The crystal was protected from temperature effects by water cooling and thin diaphragms; however, no cooling for the strut structure was provided. Consequently, the hot flow from the Cajun motor eroded the leading edge and piled molten stainless steel on the stagnation baffle which in turn plugged the pressure port (see Fig. 2.7). While the principle of the Broadview Gage seemed to be sound, the cooling capacity was not sufficient for withstanding the rocket tunnel environment. Of course, other instrumentation components suffered also, see Figures 2.8 and 2.9.

Pressures were also measured in a midstream sting mounted model (17-in. tunnel only), see Figure 2.10, which also served as the model for the schlieren equipment described in Section 2.3.4.2. The model pressure measurements were taken for the purpose of determining shock loading for the research in Reference 2.

2.3.2.3 Stagnation Pressure

In supersonic flow, the relation between P_t and M becomes complicated by the existence of a shock formed in front of the impact probe (Fig. 2.11). To decelerate the flow isentropically to 0 at the probe mouth requires crossing the shock front so that the stagnation pressure is measured at subsonic velocities. A relation between P_t, or total pressure before the shock, and P_t' or total pressure after the shock, is given by the Rayleigh formula.

Using x to denote the region in front of the shock and y to denote the region behind the shock as in Figure 2.11

$$\frac{P_y}{P_x} = \frac{1 + \gamma M_x^2}{1 + \gamma M_y^2} \tag{2}$$

from momentum and continuity and solving for T_x and T_y adiabatically (eliminating by ratio the temperature), we get

$$\frac{P_y}{P_x} = \frac{M_x}{M_y} \frac{\sqrt{1 + \frac{\gamma - 1}{2} M_x^2}}{\sqrt{1 + \frac{\gamma - 1}{2} M_y^2}} \tag{3}$$

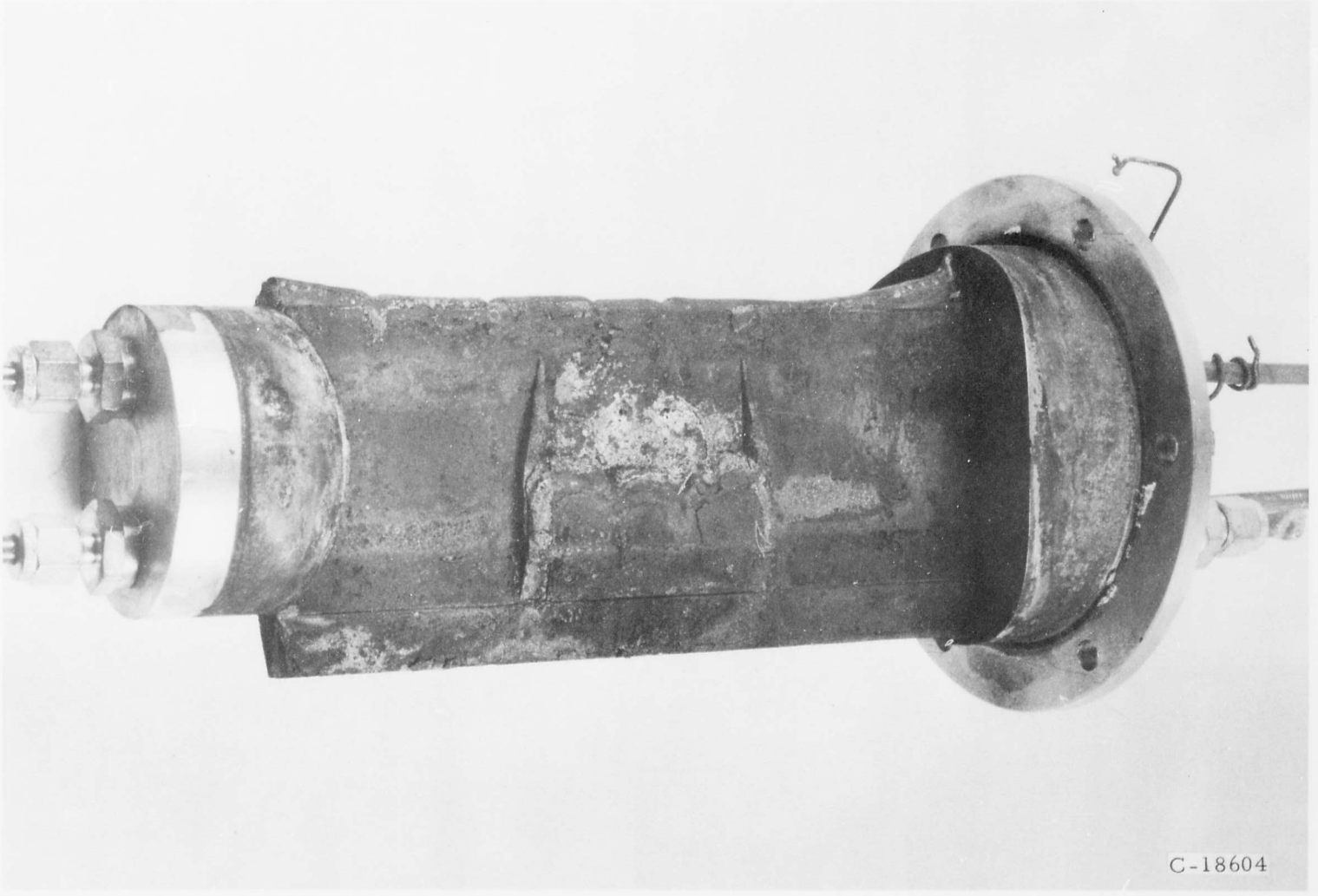

FIGURE 2.7. PLAN VIEW OF STAGNATION SIDE OF BROADVIEW GAGE AFTER FIRING IN TEST 2

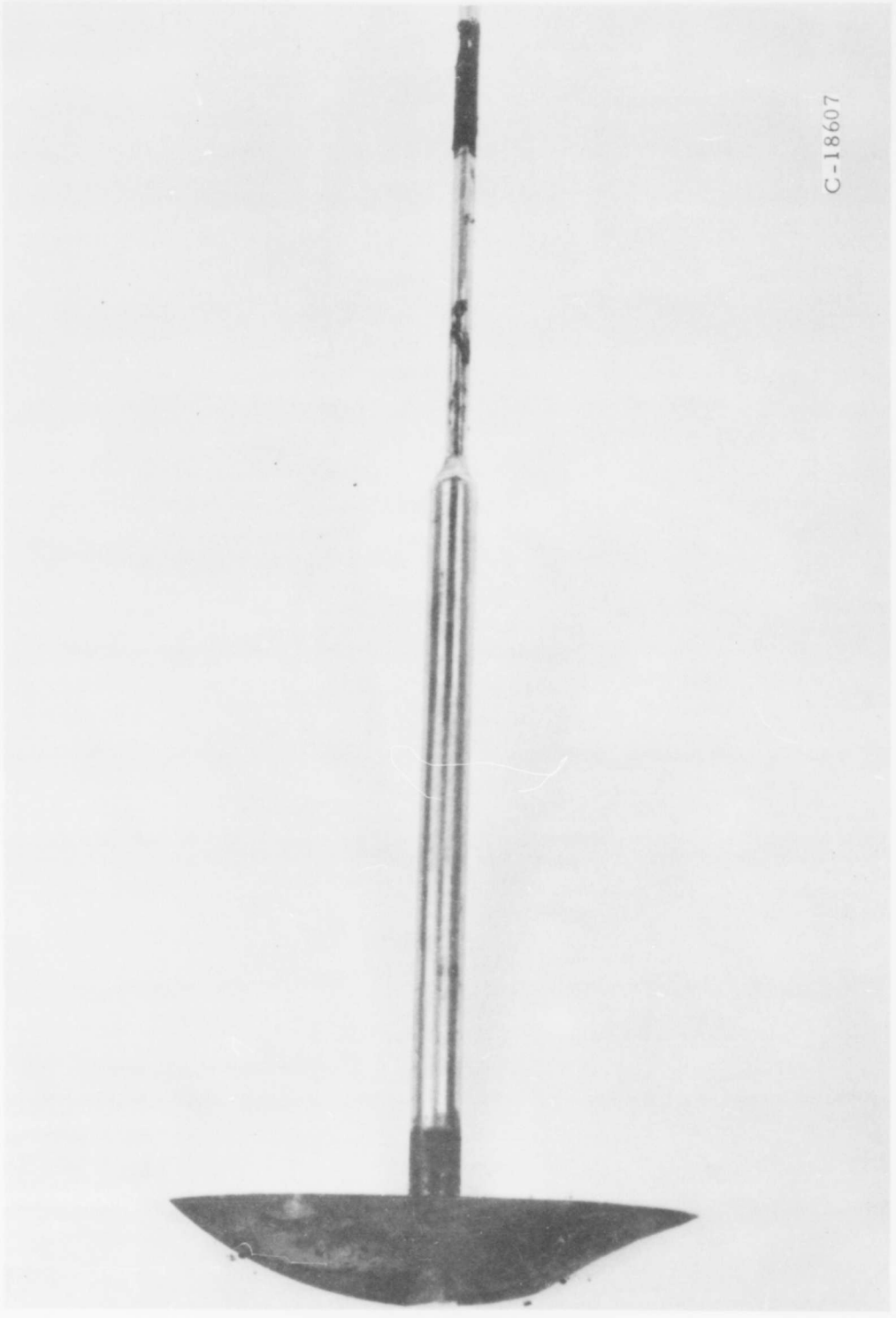

FIGURE 2.8. THERMOCOUPLE 1/2-IN. WAFER AFTER TEST 2

FIGURE 2.9. STING AND MODEL AFTER TEST

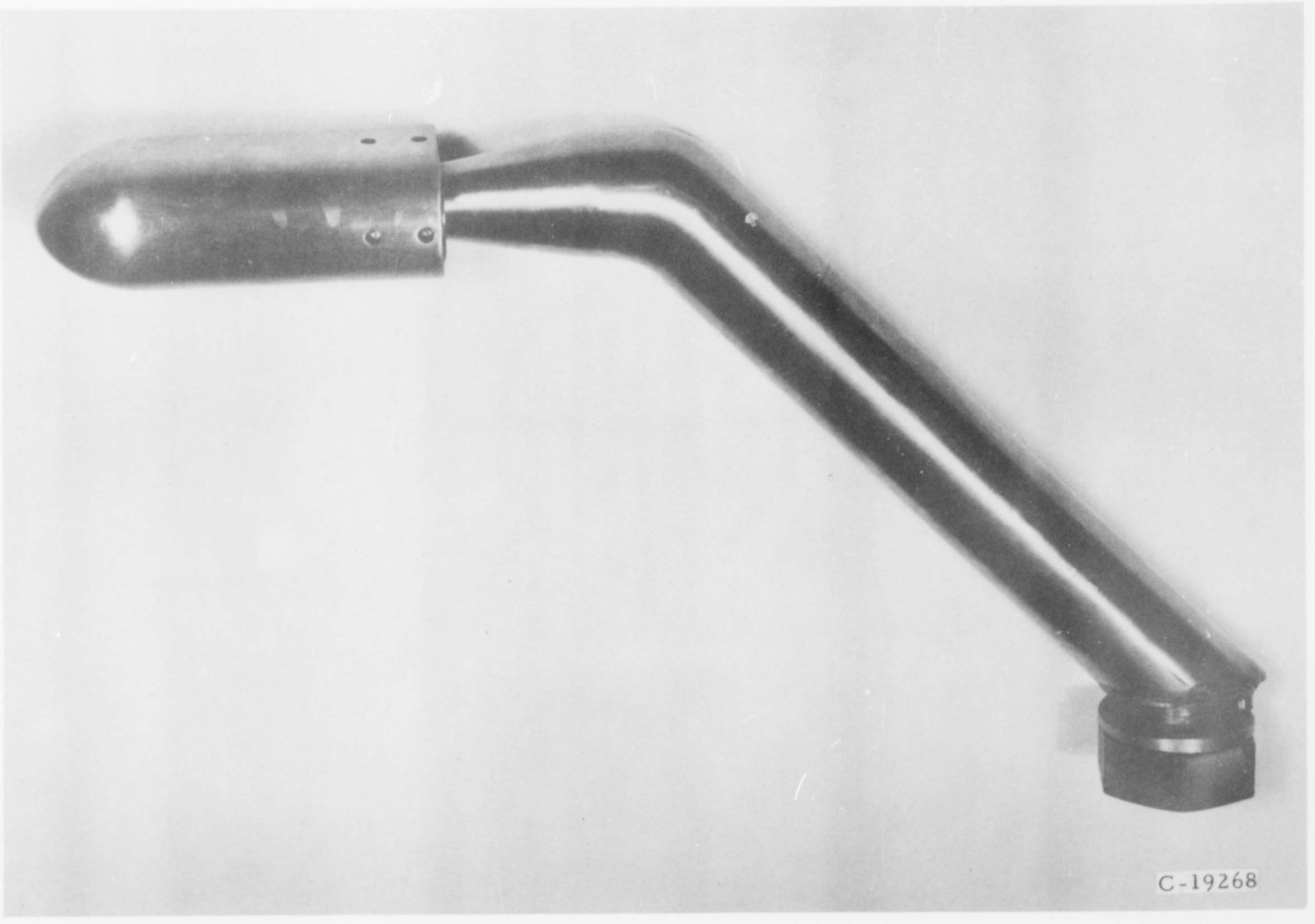

FIGURE 2.10. MODEL AND STING

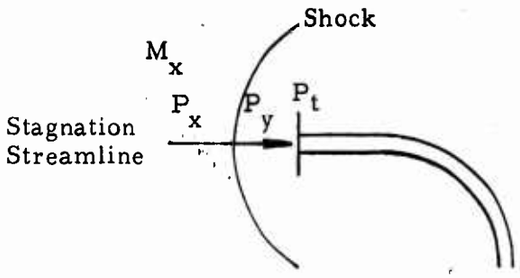

FIGURE 2.11. STAGNATION PRESSURE PROBE

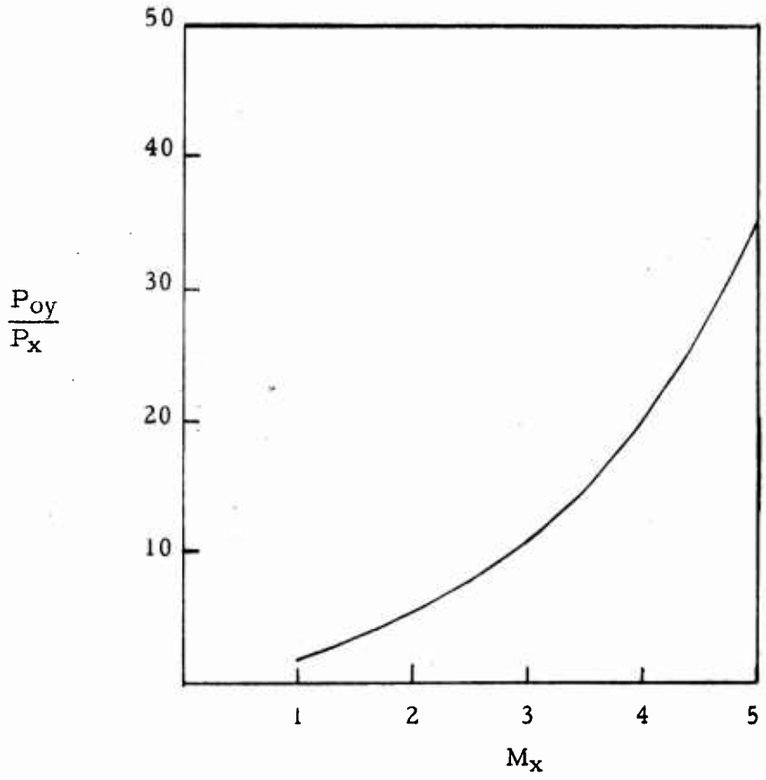

FIGURE 2.12. TYPICAL CORRECTION FOR SUPERSONIC PITOT TUBE

but obviously

$$M_x = M_y$$

or, substituting

$$\frac{P_x}{P_y} = \frac{2\gamma}{\gamma + 1} M_x^2 - \frac{\gamma - 1}{\gamma + 1} \tag{4}$$

Letting 0 denote stagnation pressure, we get the identity

$$\frac{P_{oy}}{P_{ox}} \equiv \frac{P_{oy}}{P_y} \frac{P_y}{P_x} \frac{P_x}{P_{ox}}$$

therefore

$$\frac{P_{oy}}{P_x} = \left[\frac{\gamma + 1}{2} M_x^2\right]^{\frac{\gamma}{\gamma - 1}} \Big/ \left[\frac{2\gamma}{\gamma + 1} M_x^2 \quad \frac{\gamma - 1}{\gamma + 1}\right]^{\frac{1}{\gamma - 1}} \tag{5}$$

P_x is now the static pressure ahead of the probe. In Figure 2.12, a plot of P_{oy}/P_x vs M, it can be seen that for high Mach numbers, P_{oy}/P_x becomes very large.[4] The probe used is shown in Figure 2.13.

2.3.2.4 Pressure Transducers

The three different types of pressure transducers used in the rocket tunnel were: a bourdon tube gage, a capacitance diaphragm gage, and a piezoelectric crystal gage. These gages were used to measure static pressure, stagnation pressure and model pressure.

Static or side-on pressure, P_s, was measured by a Wiancko bourdon tube gage. These gages employ a short section of twisted tube, which tends to untwist when pressure is applied to the inside. Attached to the end of the tube is a variable reluctance element acting in a push-pull arrangement with two coils in a bridge circuit driven by a suitable AC power supply. The output amplitude from the bridge is a measure of pressure.

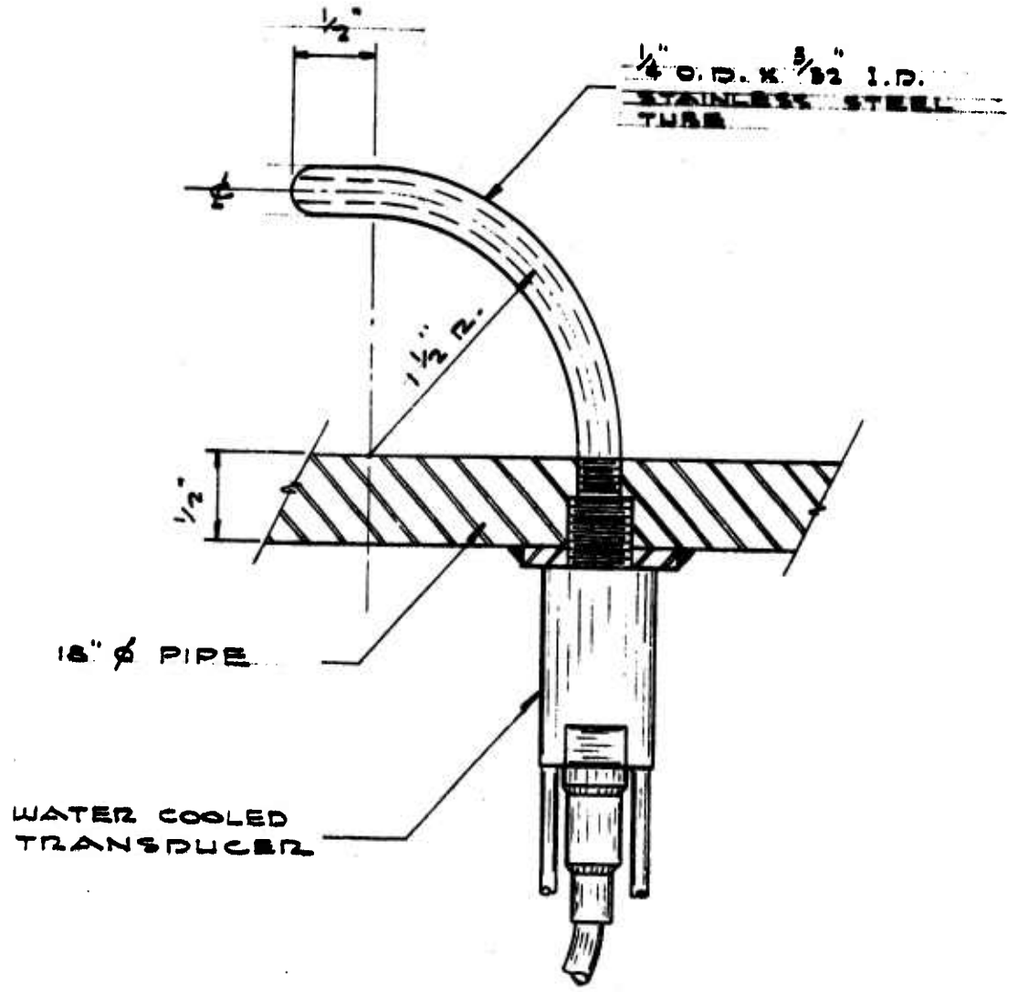

FIGURE 2.13. STAGNATION PRESSURE PROBE

Kistler piezoelectric gages were also used for static pressure measurements. Kistler gages consist of two semicylindrical natural quartz crystal transducer elements. Because crystalline quartz is almost unaffected by time or high temperature, they are excellent gages for not only measuring static pressure but also for recording the passage of a shock, the rise time for the gage being 3 microseconds as compared to the Wiancko's 300 microseconds. These gages were laboratory tested by SwRI to check linearity at high temperature and 3-sec duration. They are convenient to use, since they can be calibrated using a dead-weight tester.

Stagnation pressure was measured by Photocon and Kistler transducers. In the Photocon gage, the diaphragm in conjunction with an insulated electrode forms an electrical capacitor. Deflection of the diaphragm produces small changes in capacitance, which is connected to an inductance forming a tuned radio frequency circuit detected in an oscillator detector. The output is proportional to the pressure applied to the transducer diaphragm. The Photocon gage was chosen for stagnation pressure measurement because the diaphragm can be water cooled to allow pressure measurement in mediums of up to 6000°R. The rise time for the Photocon gage is 50 microseconds.

2.3.3 Temperature Measurement

Temperature measurement in a hot gas stream moving at supersonic speeds is a complex and difficult task. Stream temperature, T_∞, is the temperature of a particle moving with the stream in the absence of radiation. This cannot be measured per se. If the stream is brought to rest adiabatically, stagnation temperature T_o is reached. The relation between stagnation and free stream temperatures is

$$T_o - T_\infty = \frac{V}{2q\,Cp_s}\,\frac{Cp_s}{Cp_a} \qquad (6)$$

If a probe temperature element is used, it will measure a value between T_o and T_∞. The difference between T_o and T_p is due to conduction and radiation of the probe and surrounding elements and shear in the probe boundary layer.[4] When the heat flows to and from the probe reach a balance, the probe reaches its adiabatic temperature Tp_a.

$$Tp_a - T_\infty = r\,\frac{V^2}{2q\,Cp_a} \qquad (7)$$

Combining Equations (6) and (7), we get

$$r = \frac{T_{p_a} - T_\infty}{T_o - T_\infty} \tag{8}$$

Experimentally, r is between 0.83 and 0.90.[4, 5] Therefore, r is seen as a correction factor for a given probe.

A Nanmac pencil probe was used to measure T_p. This probe has a sensing tip in two dimensions formed with thermocouple wires flattened to a thickness of 0.001 in., insulated by 0.002 in. of mica and fused at the ends. The platinum-platinum 10% rhodium thermocouple is surrounded by insulation of magnesium silicate potting inside a cylinder of stainless steel. With a probe of this kind, stem conduction should be at a minimum. If $(\Delta T_p)_c$ is stem conduction, then

$$(\Delta T_p)_c = \frac{T_p - T_w}{\cosh \left[\left(\frac{hA_p}{kA_\ell} \right) L \right]^{1/2}} \tag{9}$$

Because of the depth of immersion, low thermal conductivity and heat transferred to the walls, stem conduction was minimized. The gas will be stagnated against the probe, causing heat to be radiated to the surrounding area. The radiant heat transfer $(\Delta T_p)_r$ is

$$(\Delta T_p)_r = \frac{\sigma \epsilon}{h} \left[\left(\frac{T_p}{100} \right)^4 - \left(\frac{T_r}{100} \right)^4 \right] \tag{10}$$

The pencil probe (Fig. 2.8) used was quite small, the immersion deep, and the thermal conductivity of the shield low, so as to reduce this error.[4] Other errors in the probe were made small by the fast response time of 10 microseconds.

The Rosemount 103-3 gage is one of the recently developed total temperature gages which is feasible for use in the environment of a rocket tunnel. Two of these were installed in the tunnel, see Figure 2.14. This

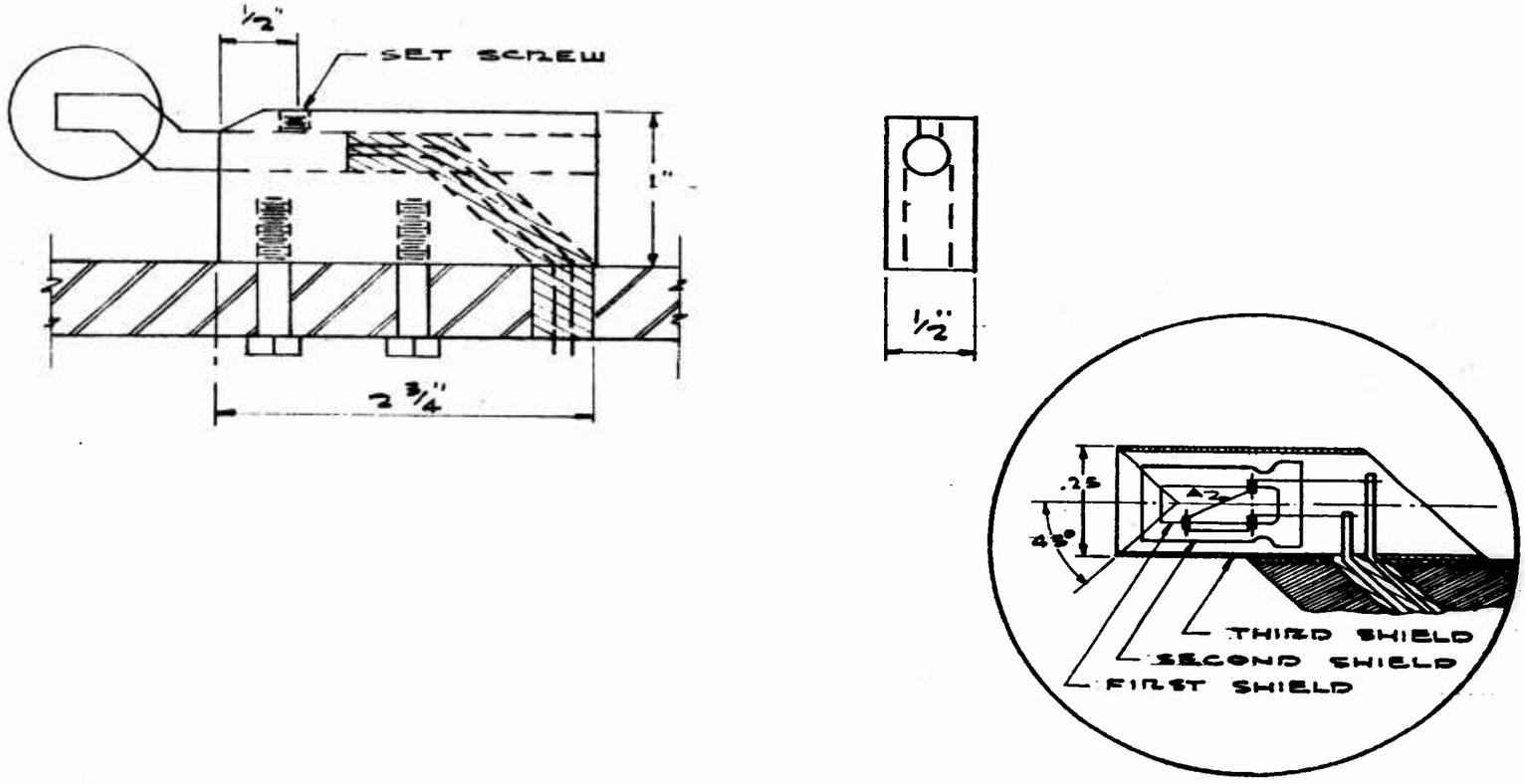

FIGURE 2.14. TEMPERATURE GAGE MOUNT, ROSEMOUNT, T_t

gage was triple shielded with platinum ceramic shields to reduce radiation as shown in Figure 2.14. The thermocouple is platinum-platinum 10% rhodium. These gages are designed for Mach 5 flow and 3000°R temperature; however, no useful data were obtained.

An attempt was made to measure stream temperature by means of a spectrograph. This instrument measures stream temperature, T_∞, without the difficulties of conduction and radiant heat losses. As mentioned in Section 2.3.2.2, useful data were not obtained by spectrographic means.

2.3.4 Velocity Measurement

An independent approach to the measurement of dynamic pressure is to measure the velocity of the gas and compute $q = 1/2\ \rho V^2$. Such an approach is the ultrasonic technique described below in Section 2.3.4.1 and in detail in Appendix B.

Since velocities of the magnitude of 7000 fps proved difficult to measure, an optical measure of the Mach angle of the bow wave standing on a model was employed. The schlieren measuring technique used for measuring velocities is described in Section 2.3.4.2

2.3.4.1 Ultrasonic Technique

An ultrasonic acoustic wave propagating across a supersonic flow expands at local sound velocity and is swept downstream at the velocity of the flow. The time-of-transit of this acoustic wave from its source to two separated receivers across the tube is relatable to these velocities, see Figure B.1.

The omnidirectional acoustic wave is generated by a high voltage source that is discharged as an arc. The pickup transducers are lead-zirconite piezoelectric crystals coupled to the stream through a monel bar.

Transit times between a transmitted pulse and the received pulses were measured by displaying the pulses on a dual beam oscilloscope and recording with a moving film camera. A complete report on the SwRI ultrasonic device is contained in Appendix B.

2.3.4.2 Schlieren Technique

The bow wave standing on a model immersed in supersonic flow can be optically recorded with a schlieren device, Figure 2.15. The Mach angle can then be measured and the velocity of the flow computed.

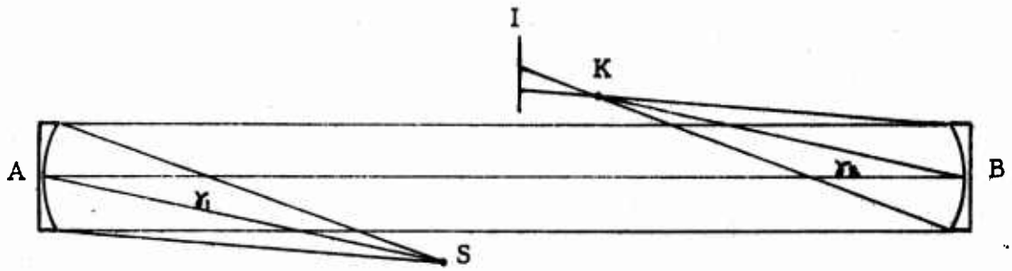

FIGURE 2.15. TWO-MIRROR SCHLIEREN

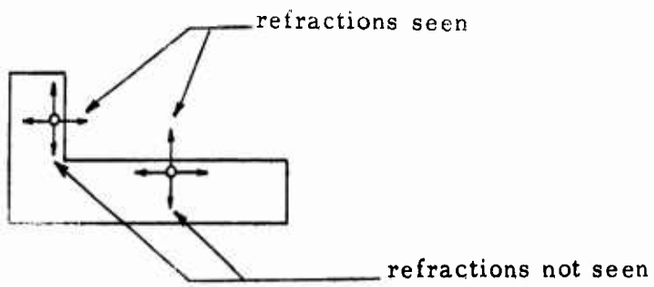

FIGURE 2.16. SCHLIEREN KNIFE EDGE

The schlieren device detects the sharp density gradient in the bow wave front because the refractive index of light is a function of density. As light rays pass through the bow wave they are deflected proportional to the refractive index which is imaged on the viewing screen. The density gradient is conically shaped so the knife edge screens all gradients not perpendicular to the knife edge such that only the density profile normal to the axis of the light beam is viewed and recorded, Figure 2.16.

For the schlieren device to function, light had to penetrate the relatively opaque rocket exhaust. To achieve penetration, an ultra bright, point light source had to be used. The light used by NASA with marginal results in a liquid rocket tunnel had an intrinisic brightness rating of 30,000 stilbs whereas the selected Pek-109 super hypressure mercury vapor lamp could be briefly pulsed to 420,000 stilbs by increasing the amperage. With this, penetration was achieved, Figure 2.17.

For maximum viewing area, the schlieren chosen for the rocket tunnel was a 6-in. diameter parallel light Toepler system with f8 parabolic mirrors ground to 1/4 the wave length of light and with a six-way adjustable knife edge.

As shown schematically in Figure 2.15, the schlieren device consisted of two identical parabolic mirrors, a light source, a knife edge, and a viewing device. The light source, S, was placed at the focal point of the parabolic mirror, A, and the knife edge, K, was placed at the focal point of mirror, B. The "f" factor of the mirrors had to be kept small to conserve light but large enough so that a distortions were minimized.

2.3.5 Recording

A CEC 114 oscillograph was used to record the various data, Figure 2.18. A bank of carrier amplifiers, CEC System D, was available; however, the 600-cps carrier had response limitations. Because of this slow response and because the galvanometers required so much transducer output to drive them, some data were recorded on dual beam oscilloscopes, which were triggered by a cam timer that programmed all the events that were timing-critical.

2.4 Shock Wave Generator

2.4.1 Ring Housing

The pressure rise upon ignition for nondiaphragmed motors was so slow (50 ms) that a separate shock generator was developed. Multiple explosive charges housed circumferentially in a massive steel ring were

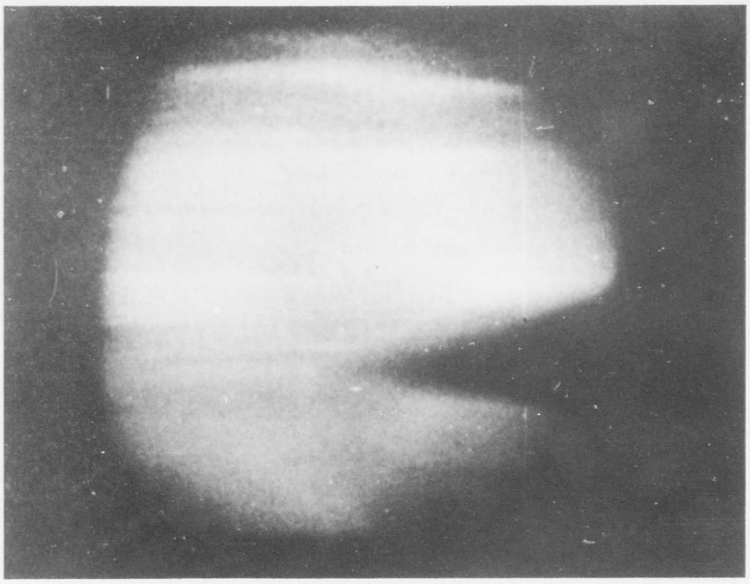

(a) Shot 5 (Schlieren Windows Were Not Parallel)
Note Faint Bow Wave

(b) Shot 9 (Picture Is Both Over and Underexposed)

FIGURE 2.17. SCHLIEREN PICTURES

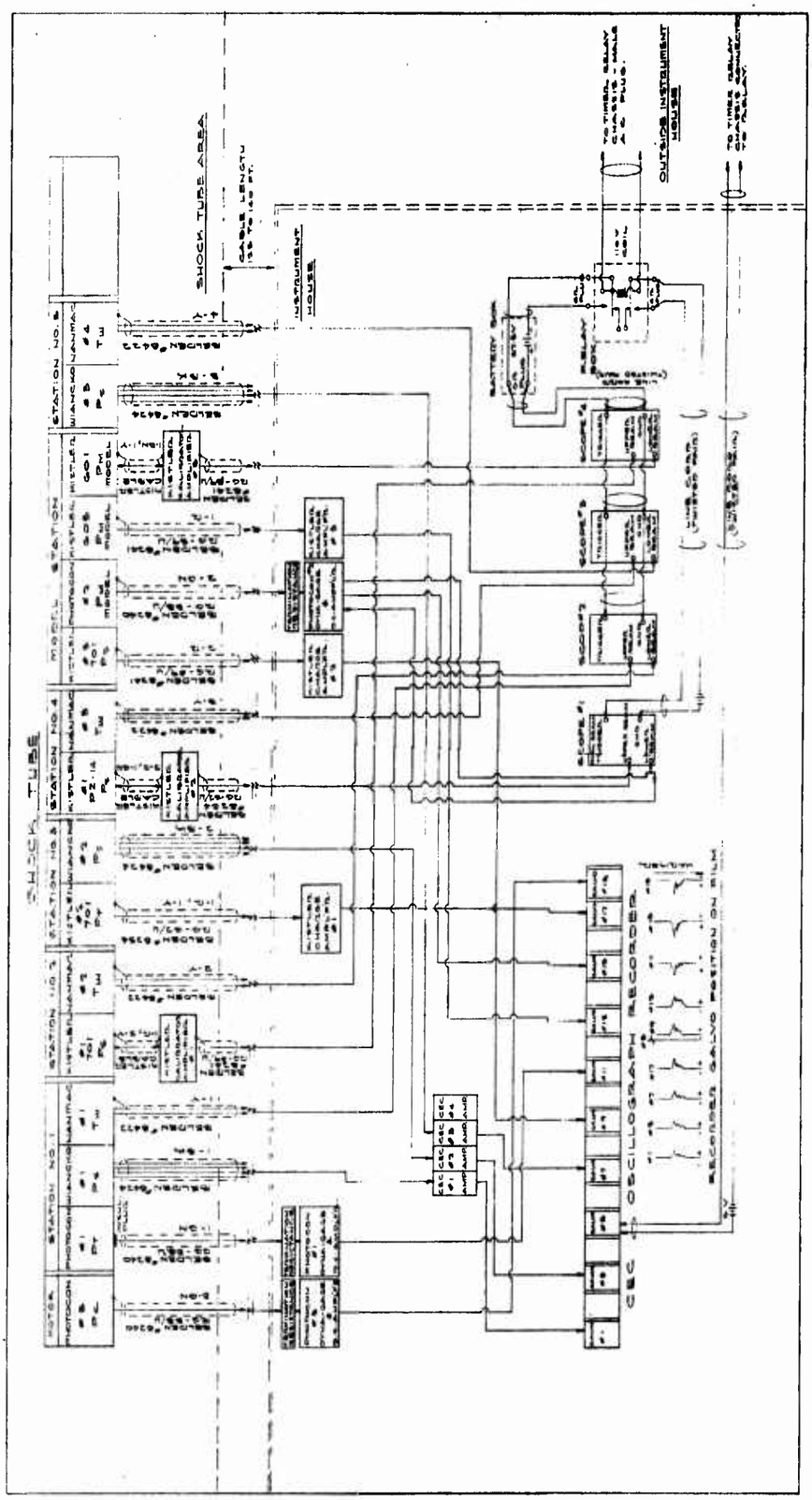

FIGURE 2.18. SCHEMATIC DIAGRAM FOR INSTRUMENTATION, TESTS - 7, 8, 9

simultaneously detonated into the rocket flow at a preselected time. As shown in Figure 2.19, the ring inside diameter was flush with that of the tunnel so as to minimize disruption of the supersonic flow. In the wall of the ring, 8 cavities were machined for 8 cylindrical charges of 8 grams of pentolite each. The charges were protected from the hot gases by a teflon cup with a thin "face" that would blow off upon detonation. Based on preliminary tests, the thin teflon face had to be less than 50 mils to prevent containment of the explosive shock pressure.

2.4.2 High Voltage System

The multiple charges must detonate simultaneously so that a strong clean shock front is generated. Detonation times at the usual detonation voltages vary so much that a high voltage firing circuit was developed. The system developed had a 3-microfarad storage capacity charged to 20 KV giving 600 joules of energy which could be discharged at any preselected time.

This shock ring generator technique was employed in shots 5 and thereafter for both the 8-in. and 17-in. tunnels, as can be seen in Figures 2.2 and 2.5.

3. EXPERIMENTAL PROGRAM

3.1 General

Experiments with rocket motors had been planned to include only 4 shots under the initial phase of the contract. Although the 8 shots that followed were primarily under the broadened scope to study the re-entry environment, the tunnel flow characteristics were very similar to the environment desired, therefore valuable data can be derived for evaluation of the objectives of the initial scope of the contract. Consequently all 12 experiments are described in this section. An outline of each test is presented in Table 3.1.

Since there existed very little information in the literature on which performance of the motor exhaust flow could be predicted or treated theoretically, each test constituted a stepping stone to probe for data as well as to improve the results obtained from the previous test. Many problems did not become evident until after a test run. This manner of testing naturally subjected the program to apparent failures when, in fact, negative or poor data may have been extremely valuable in planning the following test. Flexibility in making changes was exercised throughout the program.

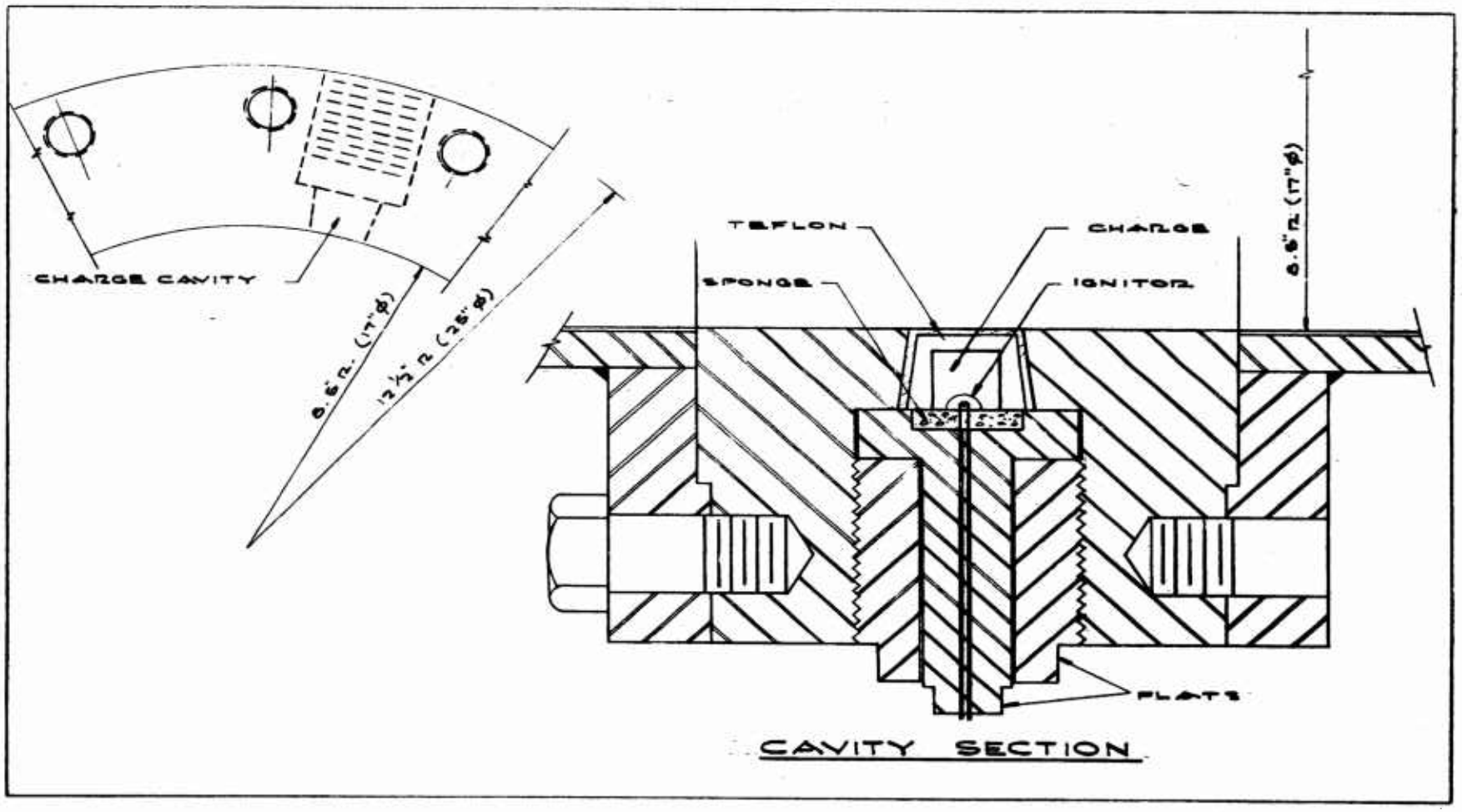

FIGURE 2.19. 18-IN. RING SHOCK GENERATOR

TABLE 3.1. EXPERIMENTAL PROGRAM

Test No.	Tunnel Size I. D. (in.)	Motor	Duration of Burning (sec)	Types of Instrumentation or Measurements	Objective of Test
1	7-5/8	Turbine-Spinner-1	0.7	P_s, T_s, Ultrasonic Velocity	To check the firing circuit and operation of all gages and recorders.
2	7-5/8	Cajun-1	2.8	P_s, T_s, Ultrasonic Velocity, Q-Gage	To obtain a high dynamic pressure in the tunnel. To determine chokeage effects in the flow.
3	7-5/8	Turbine-Spinner-2	0.7	P_s, T_s, Ultrasonic Velocity, Q-Gage, r-f shift doppler	To determine if the BRC-Q-Gage would take a lower temperature level. To provide an additional test at low velocity for the ultrasonic measurement. To verify a very low tunnel static pressure measurement recorded in the tunnel with the first T-S motor.
4	7-5/8	Cajun-2	2.8	P_s, T_s, Ultrasonic Velocity, Q-Gage	To test shock input on flow using Y section. To attempt a dynamic pressure measurement using the second BRC-Q-Gage. To correlate with the results of Test 2.
5	7-5/8	Turbine-Spinner-3	0.7	P_s, P_t, T_s, T_t, Schlieren, Shadowgraph	To check operation of the shock generator rings. To observe the flow over a cone shape using a Schlieren and shadowgraph. To observe the luminosity of the flow through a glass section. To check the operation of new gages and recorders.
6	7-5/8	Redhead/ Roadrunner-1	1.8	P_s, P_t, T_s, T_t, Shadowgraph Spectrograph	To obtain a high dynamic pressure in the tunnel using a different propellant than in Tests 2 and 4. To measure the flow velocity using a Mach angle measurement or spectrograph data. To measure a shock input on a supersonic flow.
7	17	Redhead/ Roadrunner-2	1.8	P_s, P_t, T_s, Schlieren Spectrograph, Model	To obtain Mach 5 flow. To determine the shock loading on a model. To measure the flow velocity.
8	17	Redhead/ Roadrunner-3	1.8	Same as Test No. 7	Same as Test No. 7
9	17	Redhead/ Roadrunner-4	1.8	Same as Test No. 7	Same as Test No. 7
10	17	T.S.-4	0.7	Same as Test No. 7	To check operation of all tunnel components. First test with new model.
11	17	Redhead/ Roadrunner-5	1.8	Same as Test No. 7	Same as Test No. 7 with additional checks on H.V. system.
12	17	Redhead-Roadrunner-6	2.2	Same as Test No. 7	Same as Test No. 7.

3.2 Test Procedures

3.2.1 Preliminary Preparations

Calibration of all transducers was conducted with the complete systems. Pressure transducers were dead weight and vacuum calibrated with their full lead length and with serialized amplifiers. Temperature effects on pressure transducers were evaluated.

Thermocouples were checked; however, there was no facility to calibrate conductance and radiant heat losses.

Mountings for transducers were prepared and water cooling provided. Connections and circuits were checked. Electrical isolation, shielding and grounds were installed as required.

The rocket motors were checked for fit to the tube, for proper diaphragms and for proper igniter. Firing circuits were checked for integrity of safety interlocks and continuity and for sufficient firing voltage.

The program timer was preset so that it would prestart the cameras, pretrigger the oscilloscope sweeps, fire the rocket motor and trigger the high voltage explosive detonation system in sequence. This unit was rechecked many times and again just prior to countdown to insure its proper functioning. A typical time sequence is shown in Table 3.2.

As a preliminary check of the functioning of all complete systems, high explosive shots were conducted and data were taken as in rocket firings. This also confirmed the adequacy of timing sequences and the time response of instrumentation.

After pressing the firing button, there was an approximate 50-millisecond delay as the igniter started the motor. The peak pressure and flow were not attained until about 100 milliseconds. Adequate tunnel conditions were usually not established until 200 milliseconds, and the explosive charge was always fired after 250 milliseconds. The records indicated that the best flow for the 2-second motors was usually after 1.2 sec.

After each test the tunnel was broken down, cleaned and repairs made. All gages and instruments were recalibrated and, when necessary, modifications made to improve their performance.

3.2.2 Safety Procedure

The procedure of each test, to insure maximum safety of personnel, was to prepare everything possible before the explosives were

TABLE 3.2. TYPICAL TIMING SEQUENCE

-15 min	Water supply to water-cooled gages turned on.
-10 min	Spectrograph shutter opened.
-3 min	Nitrogen for cooling model turned on. Pek light turned on under low amperage. High voltage discharge capacitors charged.
-2 min	Motor and explosive firing leads connected.
-5 sec	Documentary camera started.
-500 msec	Timer sequence started, CEC Oscillograph started. Pek light amperage increased from 5 to 30 amps. Salt water injector started.
-50 msec	Oscilloscope sweep initiated.
0 msec	Motor firing pulse initiated. Schlieren and Shadowgraph high speed cameras started.
+500 msec	Explosive charge fired from HV capacitors.
+2 sec	High speed cameras stopped.
+3 sec	Pek light turned off. Salt water injection stopped. Timer sequence completed.
+10 sec	CEC Oscillograph stopped.
+ 15 min	Nitrogen and water supply turned off.

inserted and the rocket motor was attached, see Figures 2.2 and 2.5, then make fine adjustments and last minute preparations, arm and fire. A typical procedure was as follows:

(1) prepare all instrumentation and equipment,

(2) insert explosives and attach rocket motor, and connect firing lines,

(3) adjust schlieren equipment, charge high voltage capacitors, adjust zero, expose grids, check triggers and open camera shutters of all the oscilloscopes, etc., and

(4) close safety interlocks of firing circuits and fire.

3.3 Chronological Discussion of Test Results

3.3.1 General

Much of this discussion will be directed towards conditions existing at the tunnel entrance (nozzle exit), for it is here that theory will most likely correspond with the measured values. This should not be construed as stating that the state of the flow cannot be reasonably determined for downstream points, but only that a rigorous treatment cannot be applied due to the effect of friction, heat transfer to the walls, etc. Test results for each test are shown in Table 3.1.

3.3.2 Test 1

Upon completion of the calibration and installation of pressure and temperature transducers (4 each) and recording equipment, the first motor, a Rocketdyne 6-1/2-lb gas generator, was mounted in the 8-in. tunnel and fired. Data were recorded with complete success except for the ultrasonic system which malfunctioned.

The pressure and temperature records are shown in Figures A.1 and A.2, respectively. This motor had a specially designed igniting diaphragm located just upstream from the throat. A shock was observed to precede the flow in the tunnel propagating at an average velocity comparable to the free air value. A peak shock overpressure of more than 38 psig was recorded 2.9 ft down the 8-in. tunnel. The shock wave intensity decreased exponentially in a fashion similar to a classical shape reaching zero gage pressure after approximately 250 milliseconds. The peak pressure of the

initial shock had decayed to 18 psig by the time it had reached station 4 (99.7 ft) which was 3 ft from the end of the pipe. The duration of this shock pulse at station 4 was 200 milliseconds. A comparison of the shock attenuation to that predicted by BRL[6] in their studies of shock in tunnels indicates a slightly greater rate in this case; however, the difference is only 8 percent between the first two stations. Transfer of heat from the boundary layer to the wall could account for this difference. After several milliseconds, the sustained gas generation within the motor caused an expansion wave to propagate part way down the tube (until the flow was choked by friction). Flow behind this wave is supersonic; however, no factual measure of velocity was achieved to validate this. A surprising negative pressure of -11 psig was measured at station 1 and -12 psig at station 2 after passage of the first shock and lasted until motor burnout. The pressures recorded in this test represent conditions associated with overexpansion of the gas flow. Without a measurement of the change in stagnation pressure and temperature, it is difficult to predict theoretical gas behavior under the boundary conditions imposed. Also, the propagation of high strength initial shock down the tunnel changes the steady-state flow conditions based on isentropic flow through a nozzle into a tube at ambient pressure. Instead of a pressure ratio of 136 between the motor and the back pressure on the nozzle, the shock wave decay could have introduced a ratio as high as 1000. The velocity obtained is a function of the pressure ratio and temperature. Thus, the low absolute pressures recorded on the first and second gages indicated a very high velocity. Somewhere down the tunnel, diffusion or choking occurred with the velocity passing from supersonic to subsonic. That this occurred is substantiated by an approximate calculation using an estimated density and measured pressures and temperature for the time 0.5 sec at gage 3. This computation yielded a Mach No. of about Mach 0.7. The sonic transition of flow would have occurred between gages 2 and 3. Early analysis of the data led to the opinion that the flow had not filled the tunnel during the early times, resulting in a nonuniform velocity profile. However, the initial shock would have progressed as a plane wave with the exception of the boundary layer thickness and could have established conditions under which the tunnel would have been filled. The pressure at stations 3 and 4 was about ambient with some oscillation noted at station 3. There was evidence of shocked separation during expansion in the nozzle. If this happened the first station could have been within the exhaust diamonds formed by rocket exhausts when overexpanded. This would have explained the 1-psi difference in negative pressure between stations 1 and 2. The flow must have filled the tunnel at station 2 with some loss in theoretical velocity. The best flow conditions can be deduced as occurring at station 2 with chokeage at or near station 3. Thermocouple records reflected a slow rise to about 500°F at burnout. It is believed that these readings represent a value between the flow temperature and the stagnation temperature.

It is interesting to observe that the temperature at station 4 only rose to 290°F. Theory would dictate that the temperature increase as the velocity decayed down the tunnel. The fact that this did not occur shows heavy loss of flow temperature to the tunnel walls which acted as a heat sink.

The Broadview Gage, DQ-1, was installed at a location of 13 ft from the entrance of the tube for the second test and was checked by the Broadview representative.[3]

3.3.3 Test 2

The second motor, Thiokol's Cajun, was fired after recalibration of the gages. Again data were successfully recorded; however, ultrasonic records were completely masked by the high background noises present in the tunnel. The Broadview Gage initial signal was strong (extrapolated to be about 73 psi) but dropped off so rapidly that the temperature effect on the crystal must be earlier than anticipated. Pressure and temperature recordings again indicate combustion gas generation up to expansion conditions and an expansion wave moving down the tube followed by supersonic flow. The Broadview Gage initial signal of 73 psi substantiates the existence of supersonic flow (Fig. A.3). Computations based on a dynamic pressure of 73 psi and the average measured temperature and pressure level at 0.25 indicate a Mach 2.4 flow.

The pressure and temperature records are shown in Figures A.4 and A.5, respectively. The presence of an initial shock is again observed even though a diaphragm was not used. This shock did not follow the classical waveform as in the first test. Chokeage of the high velocity flow indicated by the pressure record at station 3 appeared to cross the gage at station 2 (34.3 ft) after 1.55 sec. The thermocouple at station 1 did not record distinctly after 250 milliseconds; however, a trace could be estimated to reach about 2700°F after 2 sec. No temperature reading was recorded at station 4.

The hot, high velocity gases severely eroded all components protruding into the flow near the entrance of the pipe. The stainless steel wafers protecting the temperature probes had their leading edges blown completely off as was a portion of the shank of the probe, Figure 2.8. The Broadview Gage, DQ-1, sustained severe damage to all exposed surfaces, especially the leading edges, Figure 2.7. The gage was returned to Broadview for inspection.

initial shock had decayed to 18 psig by the time it had reached station 4 (99.7 ft) which was 3 ft from the end of the pipe. The duration of this shock pulse at station 4 was 200 milliseconds. A comparison of the shock attenuation to that predicted by BRL[6] in their studies of shock in tunnels indicates a slightly greater rate in this case; however, the difference is only 8 percent between the first two stations. Transfer of heat from the boundary layer to the wall could account for this difference. After several milliseconds, the sustained gas generation within the motor caused an expansion wave to propagate part way down the tube (until the flow was choked by friction). Flow behind this wave is supersonic; however, no factual measure of velocity was achieved to validate this. A surprising negative pressure of -11 psig was measured at station 1 and -12 psig at station 2 after passage of the first shock and lasted until motor burnout. The pressures recorded in this test represent conditions associated with overexpansion of the gas flow. Without a measurement of the change in stagnation pressure and temperature, it is difficult to predict theoretical gas behavior under the boundary conditions imposed. Also, the propagation of high strength initial shock down the tunnel changes the steady-state flow conditions based on isentropic flow through a nozzle into a tube at ambient pressure. Instead of a pressure ratio of 136 between the motor and the back pressure on the nozzle, the shock wave decay could have introduced a ratio as high as 1000. The velocity obtained is a function of the pressure ratio and temperature. Thus, the low absolute pressures recorded on the first and second gages indicated a very high velocity. Somewhere down the tunnel, diffusion or choking occurred with the velocity passing from supersonic to subsonic. That this occurred is substantiated by an approximate calculation using an estimated density and measured pressures and temperature for the time 0.5 sec at gage 3. This computation yielded a Mach No. of about Mach 0.7. The sonic transition of flow would have occurred between gages 2 and 3. Early analysis of the data led to the opinion that the flow had not filled the tunnel during the early times, resulting in a nonuniform velocity profile. However, the initial shock would have progressed as a plane wave with the exception of the boundary layer thickness and could have established conditions under which the tunnel would have been filled. The pressure at stations 3 and 4 was about ambient with some oscillation noted at station 3. There was evidence of shocked separation during expansion in the nozzle. If this happened the first station could have been within the exhaust diamonds formed by rocket exhausts when overexpanded. This would have explained the 1-psi difference in negative pressure between stations 1 and 2. The flow must have filled the tunnel at station 2 with some loss in theoretical velocity. The best flow conditions can be deduced as occurring at station 2 with chokeage at or near station 3. Thermocouple records reflected a slow rise to about 500°F at burnout. It is believed that these readings represent a value between the flow temperature and the stagnation temperature.

initial shock had decayed to 18 psig by the time it had reached station 4 (99.7 ft) which was 3 ft from the end of the pipe. The duration of this shock pulse at station 4 was 200 milliseconds. A comparison of the shock attenuation to that predicted by BRL[6] in their studies of shock in tunnels indicates a slightly greater rate in this case; however, the difference is only 8 percent between the first two stations. Transfer of heat from the boundary layer to the wall could account for this difference. After several milliseconds, the sustained gas generation within the motor caused an expansion wave to propagate part way down the tube (until the flow was choked by friction). Flow behind this wave is supersonic; however, no factual measure of velocity was achieved to validate this. A surprising negative pressure of -11 psig was measured at station 1 and -12 psig at station 2 after passage of the first shock and lasted until motor burnout. The pressures recorded in this test represent conditions associated with overexpansion of the gas flow. Without a measurement of the change in stagnation pressure and temperature, it is difficult to predict theoretical gas behavior under the boundary conditions imposed. Also, the propagation of high strength initial shock down the tunnel changes the steady-state flow conditions based on isentropic flow through a nozzle into a tube at ambient pressure. Instead of a pressure ratio of 136 between the motor and the back pressure on the nozzle, the shock wave decay could have introduced a ratio as high as 1000. The velocity obtained is a function of the pressure ratio and temperature. Thus, the low absolute pressures recorded on the first and second gages indicated a very high velocity. Somewhere down the tunnel, diffusion or choking occurred with the velocity passing from supersonic to subsonic. That this occurred is substantiated by an approximate calculation using an estimated density and measured pressures and temperature for the time 0.5 sec at gage 3. This computation yielded a Mach No. of about Mach 0.7. The sonic transition of flow would have occurred between gages 2 and 3. Early analysis of the data led to the opinion that the flow had not filled the tunnel during the early times, resulting in a nonuniform velocity profile. However, the initial shock would have progressed as a plane wave with the exception of the boundary layer thickness and could have established conditions under which the tunnel would have been filled. The pressure at stations 3 and 4 was about ambient with some oscillation noted at station 3. There was evidence of shocked separation during expansion in the nozzle. If this happened the first station could have been within the exhaust diamonds formed by rocket exhausts when overexpanded. This would have explained the 1-psi difference in negative pressure between stations 1 and 2. The flow must have filled the tunnel at station 2 with some loss in theoretical velocity. The best flow conditions can be deduced as occurring at station 2 with chokeage at or near station 3. Thermocouple records reflected a slow rise to about 500°F at burnout. It is believed that these readings represent a value between the flow temperature and the stagnation temperature.

TABLE 3.3. LOCATION OF INSTRUMENTS ON DRAG FACILITY FOR TEST NO. 4

	Gage	Distance from Station 0
No. 1	Pressure Gage	2 ft 10-1/2 in.
No. 1	Thermocouple	3 ft 2-1/2 in.
No. 2	Pressure Gage	16 ft 4 in.
No. 3	Pressure Gage	28 ft 4 in.
No. 2	Thermocouple Ultrasonic Section	28 ft 8 in. 30 ft 6 in.
No. 4	Pressure Gage	43 ft 6 in.
No. 5	Pressure Gage	60 ft 5-1/2 in.
No. 3	Thermocouple BRC Gage	60 ft 9-1/2 in. 82 ft 3-1/2 in.
No. 6	Pressure Gage	103 ft 3-1/2 in.
No. 4	Thermocouple	103 ft 7-1/2 in.

junction of sufficient strength could have caused the signal. The shock applied from the lateral had been precalibrated to equal 70 psi at gage No. 2. This is more than was actually recorded in this test; however, the ambient pressure was much higher.

The records from Tests No. 2 and 4 in which the hot burning perchlorate motor with a mass flow of 42 lb/sec was used reflect a closer approach to theoretical flow behavior. However, the environment in which the measurements had to be taken makes the reduction of data very difficult. The greatest source of error is in the temperature measurements. This is particularly true for Test 4 when the gages appeared to short out or pick up a negative ion charge from the ionized flow.

At this point in the program the scope of work was revised and a more sophisticated program undertaken. Efforts to improve the tunnel and instrumentation would enable higher flow velocities and better shock wave inputs to be examined.

3.3.6 Test 5

The fifth test consisted of the firing of a third Rocketdyne Turbine-Spinner. Many additional measurements such as stagnation pressure and temperature and a Mach angle measurement of velocity were attempted. A new type of shock generator was designed (Fig. 2.19) and installed. Also, a spectrograph was installed to assist in pressure and temperature measurements.

Pressure measurements are given in Figures A.11, A.12, A.13, A.14 and A.15. The location of the gages is shown in Figure 2.6 and Table 3.4. The explosive charge in the shock ring generator was timed to fire at approximately 0.5 sec after motor ignition.

The motor was ignited as planned and the charge fired at about 0.49 sec. Two 8-gram charges were used. As observed in Tests 1 and 3, an initial shock was present; however, the duration appeared shorter. This was possibly due to the shorter tunnel used in this test. A shock input in excess of 35 psi lasting for about 10 milliseconds was recorded on the Wiancko gages.

All of the oscilloscope records were of such poor quality as to be unacceptable. Investigation revealed a ground loop was set up between one of the Photocon gage amplifiers and the ground circuit on the oscilloscopes.

TABLE 3 4. INSTRUMENT LOCATIONS FOR TESTS 5 AND 6

Station	Quantity Measured	Gage	Distance from Tunnel Entrance
1	T_t	Rosemount No. 1	2' - 0"
1	P_s	Photocon No. 1	2' - 0"
1	P_s	Wiancko No. 1	2' - 10"
1	T_w	Nanmac No. 1	3' - 2"
1	P_t	Photocon No. 2	2' - 10"
2		Shock Ring	6' - 3"
3	T_t	Rosemount No. 2	11' - 0"
3	T_w	Nanmac No. 2	11' - 0"
3	P_t	Kistler No. 1*	11' - 0"
3	P_s	Wiancko No. 2	12' - 6"
3	P_s	Kistler No. 2	12' - 6"
		Schlieren	14' - 0"
4	P_s	Wiancko No. 3	19' - 0"
4	T_w	Nanmac No. 3**	19' - 0"
		Shadowgraph	20' - 6"

*Not used on Test 6
**Not used on Test 5

A Photocon and a Wiancko static gage were paired at station 1. The Photocon only measured 20 psi initial shock whereas the Wiancko showed 61 psi. The response of the Photocon being better than the Wiancko, this variation cannot be explained. Correlation with the other measurements indicates that the Photocon was in error.

The high flow rate blew out the shielded thermocouple (see Fig. 2.14) in the Rosemount No. 1 stagnation temperature gage even though the manufacturer had felt sure that it would perform properly. The other thermocouple appeared to record a reasonable level; however, the ground loop oscillations previously described prevented an accurate reading.

The glass section used in conjunction with the shadowgraph was photographed in color. The flow appeared as a brilliant orange plasma followed at burnout by a dense, black smoke which coated the entire interior of the tube with black particles. No record was obtained from the shadowgraph.

The schlieren was successful in penetrating the flow; however, no density gradients were apparent in the picture, Figure 2.17. The problem of knowing in advance just how much light would pass through made any prospect of a clear picture very marginal. Also, the film was developed commercially; therefore, no flexibility in development time was possible. The light was pulsed at the rate of 15 times a second to an amperage of 11 amps over the normal 5. This was not entirely satisfactory. The operation of the schlieren equipment was considered to be partially successful under these handicaps.

3.3.7 Test 6

Test No. 6 utilized the "Readhead/Roadrunner" motor with the 8-in. tunnel. The instrumentation used was basically the same as in Test No. 5 (see Table 3.4). Again a shock was imparted on the main flow after about 260 milliseconds using two 8-gram charges from Maryland Assemblies. The charges were fired using a 12-KV capacitance discharge. The pressure and temperature records are given in Figures A.16, A.17, A.18, A.19, A.20, and A.21. An initial shock of about 30 psi preceded the flow. The shock generator produced a shock of more than 40 psi at the first gage station. Stagnation pressures of over 100 psi were measured; however, the stagnation probe failed after about 1.2 sec. The leading edge near the base was completely eroded on one side allowing the probe to fold back in the direction of the flow.

High static pressures were measured at station 3. These decreased to about 20 psi after 600 milliseconds. The Kistler gage used to measure the static pressure drifted as a result of a zero line shift after about 300 milliseconds. One thermocouple failed to respond after 1.5 sec. The apparent flow temperature was about 1100°R.

A dynamic pressure of 140 psi was predicted at the first gage station. Using the measured stagnation and static pressure, a dynamic pressure of 150 was computed. A Mach of 3.7 was predicted for this point, and a measured value of Mach 3.5 was computed using the pressure and temperature measurements.

A Vang tube was used to provide 45 amps to the schlieren light. Again it was possible to see through the flow with the schlieren system; however, the Pek light failed after the first few milliseconds. No information was gained from the few pictures recorded. Tests performed after the shot led to the belief that only about 30 amps would be required for the Pek light. The glass windows for the schlieren crazed from the heat after burnout. Cooling was then designed for the windows in the larger tunnel. The glass section failed after about 1 sec due to the high overpressures sustained in the tunnel. No usable data resulted from the shadowgraph connected to this section. The loss of the glass section was not unexpected.

All the experience gained in the previous tests was used in the design of the 17-in. tunnel. As discussed in Reference 2, the larger tunnel was constructed in order to study the feasibility of using a rocket tunnel as a means of obtaining shock loading data for vehicles travelling at hypersonic speeds and which are struck by a shock wave. Certain modifications were made just before the 7th test. These consisted of altering four of the eight charge holders in the shock ring generator so that a sodium solution could be injected, porting the schlieren windows for nitrogen cooling, removal of the wafer support from the pencil thermocouples and reinforcement of the leading edge of the stagnation pressure probe with titanium. The location and purpose of the instrumentation are given in Table 3.5 and Figure 2.18.

3.3.8 Test 7

In Test 7 a nitrate propellant motor, Rocketdyne's modified "Redhead/Roadrunner," was used. This motor was the same as the one previously fired in Test 6 using the small tunnel. The automatic timer did not function properly, and all systems depending upon it failed to operate. These included the oscilloscope trigger, camera runs, and charge detonation.

TABLE 3.5. INSTRUMENT LOCATION FOR TESTS 7, 8 AND 9

Station	Quantity Measured	Gage	Distance from Entrance
1	P_t	Photocon No. 1 ****	12"
1	P_s	Wiancko No. 1	12"
1	T_t	Rosemount No. 1 *	12"
1	T_w	Nanmac No. 1	12"
2	P_s	Kistler 701 No. 1	46"
2	T_w	Nanmac No. 2	46"
3	P_t	Photocon No. 3**	80"
3	P_t	Kistler 701 No. 2	80"
3	P_s	Wiancko No. 2	80"
3	T_t	Rosemount No. 2 *	80"
	T_∞ & V	B & L Spectrograph	87-1/2"
4	P_s	Kistler P_z14 No. 1 ***	114"
4	T_w	Nanmac No. 3	114"
M	P_s	Kistler 701 No. 3	138"
M	$P_{0°m}$	Photocon No. 2 ****	138"
M	$P_{45°m}$	Kistler 605	138"
M	$P_{90°m}$	Kistler 601	138"
	Mach number	Aerolab Supply Schlieren	138"
5	P_s	Wiancko No. 3	154"
5	T_w	Nanmac No. 4	154"

* Gages destroyed before Test
** Gage placed in motor for Test 8
*** Replaced with Kistler 601 for Shot 9
**** Photocon No. 2 moved to P_t at Station 1 and Photocon No. 1 placed in model for Test 9

The pressure records shown in Figures A.22, A.23, A.24, A.25, and A.26, which were recorded on the oscillograph (not connected to the timer), gave highly satisfactory results. Expansion of the flow occurred in an almost ideal manner. The computed Mach number was only 5.8 percent less than the design value during most of the test. Pressures of 1.9 psi absolute were recorded at the first station.

Most of the piezoelectric Kistler gages drifted significantly due to temperature effects, and the data were considered unreliable after several milliseconds. It was decided that water-cooling jackets would be necessary for any future tests. Although it was impossible to use jackets in the model, a more efficient nitrogen gas supply was designed.

The spectrograph recorded a faint trace during the test; however, the base line taken before and after the test did not record. Without the base lines no reference shift could be measured.

3.3.9 Test 8

A Rocketdyne modified "Readhead/Roadrunner" was again fired for the eighth test. During the early part of the test the low absolute pressures obtained sucked one of the teflon cups and the charge from a shock ring generator port. This grounded the high voltage firing circuit and prevented the detonation of the other charges on schedule. The loose charge was swept downstream and detonated near the model station from the heat generated in the flow.

The Fastax camera used with the schlieren system was not in critical focus. No lens is used with the camera; therefore, the focus must be very precise. Apparently, the prism was slightly out of position during the time that the camera was brought into focus. The film was not sufficiently distinct to render any usable data. The collimated light penetrated the flow during most of the test.

The pressure data taken in this test were quite reproducible when compared to the previous test. The Mach number appeared to have increased above the theoretical value by about 6 percent using the measured temperatures and pressures. Plots of these records are given in Figures A.27 through A.34. It is interesting to note that the negative gage pressures recorded on the No. 3 Wiancko gage at station 5 beyond the model indicated little blockage of the flow by the model. Drifting was observed on some of the Kistler gages; however, they appeared stable up to about 0.5 sec. A further attempt was made to improve the stability of these gages.

An Osram spectrographic quality sodium light was used to record the base lines on the spectrograph. These appeared distinctly; however, no trace was recorded during the test.

The record of thermocouple TC No. 2 shows an unusually high reading when compared to TC No. 1 and TC No. 3.

3.3.10 Test 9

The ninth test consisted of a repeat of Tests 7 and 8 with improvements in instrumentation mounting. No nitrogen was used to cool the schlieren windows since the previous tests indicated that crazing would be no problem. No sodium water input was used for the spectrograph since studies had introduced the possibility of too much sodium in the flow.

The pressure and temperature measurements were again closely reproducible to those of Tests 7 and 8 and are given in Figures A.35 through A.45. The computed Mach numbers for Tests 7, 8, and 9 are compared in Table 3.6. The Kistler piezoelectric gages performed far more satisfactorily on this test than in the previous two tests. Cooling of the gage body appears mandatory for proper performance. The Photocon gage (No. 1) located face-on in the model appeared to fail after about 0.3 sec. Evidence of this appeared in Test 8; however, the possibility that the port had clogged led to the substitution of No. 1 for the No. 2 Photocon gage but not the replacement with a different type.

The thermocouple measurements were excellent. The agreement between the gages was the best of the tests conducted. The thermocouple No. 4 at station 5 dropped in value after about 0.2 sec but only by a small amount. The other readings reflected a slight increase in the temperature as the distance down the tube increased. This follows what would be predicted by theory.

The schlieren film showed a good picture across the model for the first 30 milliseconds, Figure 2.17 b. For an unknown reason, the film was obscured for the next 0.5 sec after which the picture phased back in and was clear again at approximately 1.1 sec. The latter portion of the film was the best of any test; however, no density gradients emulating a bow shock wave were visible. The model edges were fuzzy possibly due to a temperature corona as the flow passed around the model. The blurred image could also be caused by fluctuations in the flow due to the slow frame exposure time of the camera. This same phenomenon would tend to wash out the definition of the bow wave.

TABLE 3.6 COMPARISON OF MACH NUMBERS IN TESTS 7, 8, AND 9 AS A FUNCTION OF TIME (RAYLEIGH CALCULATIONS)

Test Number	Measurements	Time (sec) 0.2	0.4	0.6	0.8	1.0	1.2	1.4	1.6	1.8
7	Static Pressure, psia	5	5	4.5	4	4	3.5	2.2	2.2	2.2
	Stagnation Pressure, psia	39	39	36	35	37	35	38	38	38
	Mach Number	4.4	4.4	4.5	4.6	4.6	4.7	4.9	4.9	4.9
8	Static Pressure, psia	2	0.8	0.8	0.8	2.0	0.8	1.8	1.0	0.8
	Stagnation Pressure, psia	54	50	51	51	61	54	61	56	54
	Mach Number	5.0	5.5	5.5	5.5	5.0	5.5	5.1	5.4	5.5
9	Static Pressure, psia	2	2	1.5	1.5	1.5	0.8	0.8	0.8	0.8
	Stagnation Pressure, psia	62	64	64	64	64	64	64	64	64
	Mach Number	5.0	5.0	5.3	5.3	5.3	5.5	5.5	5.5	5.5

No record was obtained from the spectrograph. Consultation with experts in the field of combustion spectrography lead to the conclusion that the sodium D lines could have reversed due to an overabundance of sodium.(7)

3.3.11 Test 10

Test number 10 was conducted in the 17-in. tunnel with a turbine spinner for purposes of determining the reliability of the overall functioning of the system. The same nozzle adapter block used for attaching the turbine spinner to the 8-in. pipe was used in assembling the 17-in. tunnel. The nozzle passage from the throat of the turbine spinner to the beginning of the tunnel contained two geometric discontinuities: one between the turbine spinner and the adapter block and one between the adapter block and the 17-in. nozzle. These geometric inadequacies were of little concern, however, since the test was primarily a facility check. During the test all instruments functioned and the two 8-gram charges exploded on schedule.

No theoretical determinations of the flow could be made due to the discontinuities in the nozzle. The pressure results were inconclusive as to the nature of the flow, i.e., $P_s \approx 14.7$.

Test 10 was also the first test in which the model shown in Figures 3.1 and 3.2 was used. Instruments mounted on the model indicated a shock struck the model with a peak overpressure of about 8 psi.

3.3.12 Test 11

In Test No. 11, conducted in the same manner as Test 10, a RH/RR was used as a driver and the nozzle contained no geometric discontinuities. All recorded data agreed closely with data from the previous firing of RH/RR in the 17-in. tunnel. The shock ring was loaded with 6 charges, none of which exploded. Consequently, the high voltage system was redesigned to operate at a greatly increased (9 times) output energy level.

3.3.13 Test 12

Test number 12 was a duplication of the previous test, except for the use of the improved high voltage system for high explosive detonation. Also, the spectrograph was not used because of disappointing results from the other tests. All six charges exploded satisfactorily at the appropriate time during the test.

The pressure gage positioned at 0° on the model showed considerable drift, which is attributed to extreme temperature effects. Only the

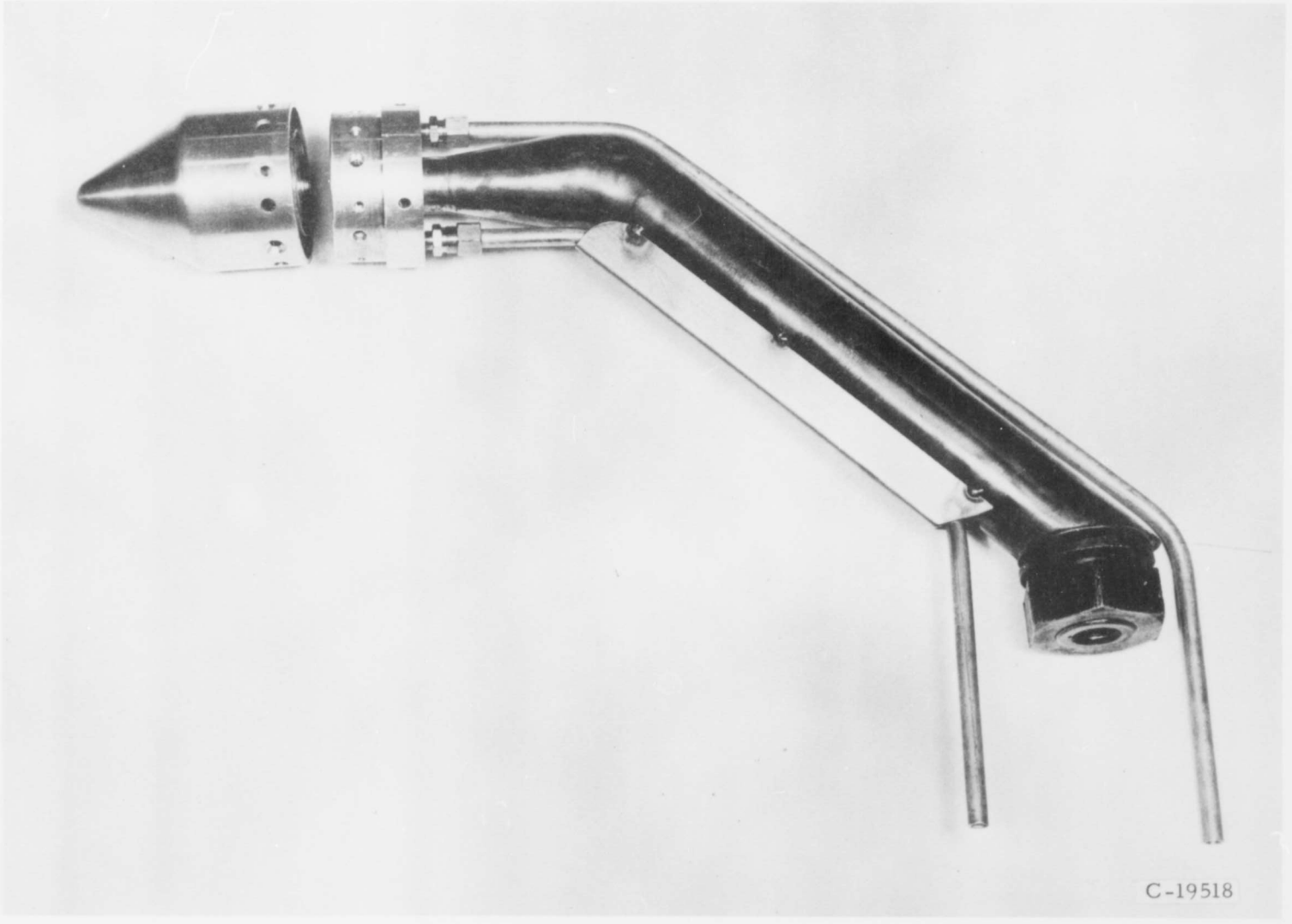

FIGURE 3.1. IMPROVED MODEL ASSEMBLY

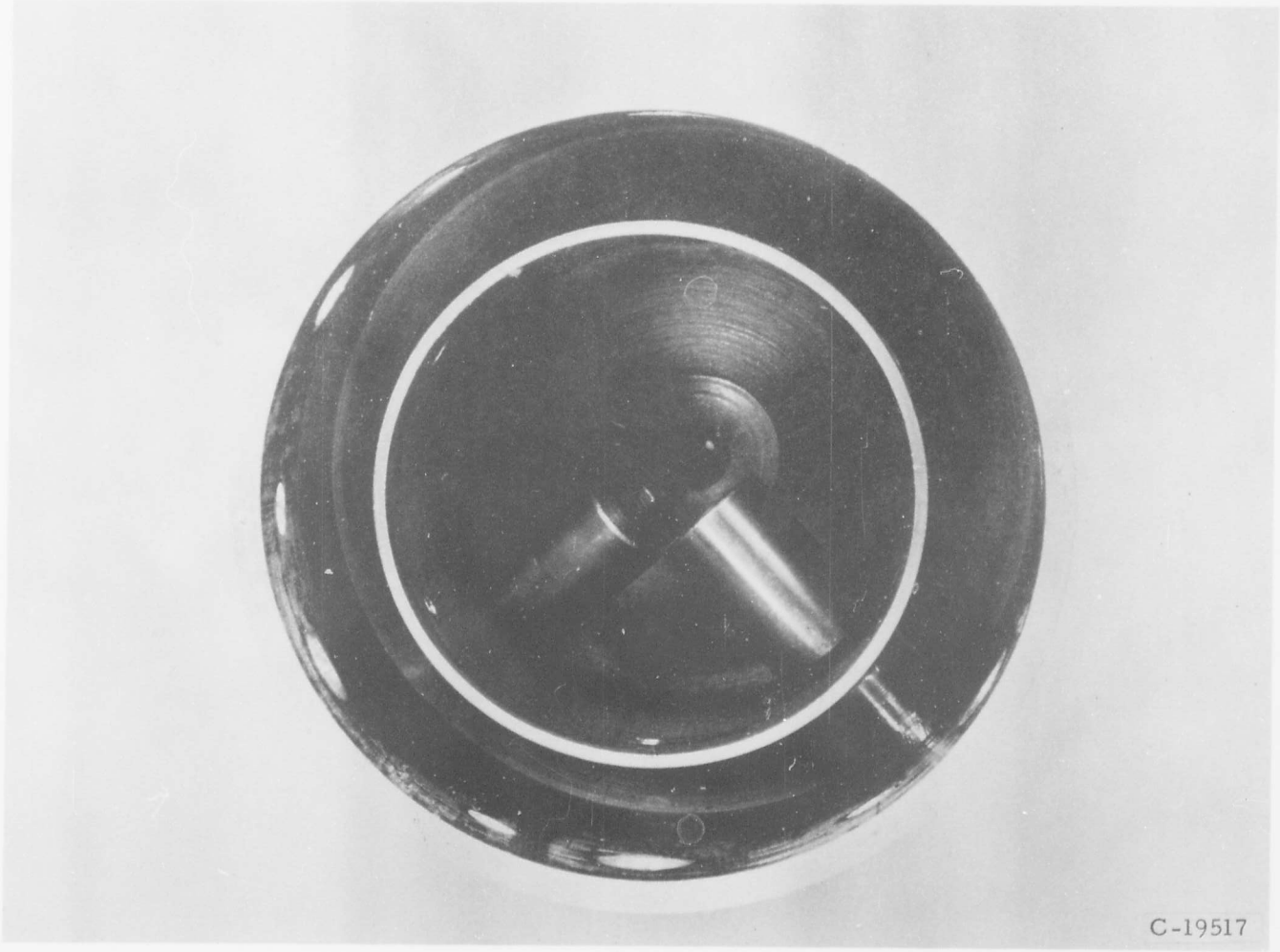

FIGURE 3.2. IMPROVED MODEL SHOWING WATER-COOLING CAVITY

peak value and duration of the shock could be determined from this data. The pressure gage at 45° on the model gave an excellent classical record, showing clearly the peak shock pressure. The low shock pressure recorded on the 90° pressure gage was attributed to masking the peak shock pressure on the gage by the presence of an expansion fan, caused by the discontinuity at the edge of the cone on the model as shown in Figure A. 46.

By measuring the duration of flow from the rocket and calculating the rate of flow, it was possible to compute that the chamber pressure was 2050 psia. From this, the Mach number, M, after expansion was found to be 4. 4 as compared with the design M of 5. 18. With M = 4. 4 and a new computed area ratio it was found that the radius of flow was about 6 in.; that is, the effective boundary layer at station 1 was close to 2-1/2 in. in depth. Under such conditions, it was impossible to measure accurately flowing pressures and shock pressures with side wall gages as shown in Figure A. 47. Data from instruments on the model, however, gave reasonable values for the shock pressure.

The slow burning of the motor may be attributed to a ruptured diaphragm on the rocket motor prior to Test 12. This failure allowed the motor to be exposed to moisture for several weeks. The solid propellant rocket fuel, being highly hygroscopic, absorbed moisture into the grain. This reduced the burning rate of the propellant in Test 12 and resulted in a 20% longer burning time for the motor. Pressure in the motor chamber was reduced, and incomplete expansion with a thick boundary layer resulted in the tunnel.

4. RECOMMENDATIONS

The variety of environments possible in the solid propellant tunnel allow not only for simulation of nuclear blasts but also for creation of a re-entry environment.[2] Furthermore, theories of frozen exhaust, two-phase flow and related subjects might readily be evaluated in a solid propellant tunnel. Applied research studies that would be possible involve shock interaction, structural dynamics, re-entry communications, material performance and solid propellant evaluations. For such research the solid propellant tunnel has the advantage of being a device in which high temperatures, high pressures, high gas velocities and Mach number, controlled flow duration, and the shock superposition on high velocity gas flow can be produced. Such versatility in a single test facility combined with its unique features is believed to warrant continued effort toward elimination of difficulties experienced in initial tests and the improvement of instrumentation.

It is recommended that a program be initiated to:

(1) Improve operational characteristics and control in the existing solid propellant driven tunnel

(2) Refine techniques for cooling the instrumentation

(3) Refine techniques for mounting transducers to reduce accelerations

(4) Refine and/or develop temperature measurement so as to improve its accuracy and reliability

(5) Develop **and evaluate special propellant formulations** and grain configurations suitable for rocket tunnel research

(6) Study the effect of very high combustion pressures on the solid propellant tunnel operation

(7) Refine the schlieren techniques so as to provide a direct measure of Mach number

Based on the experience gained during the course of this research, a modification to the facility as shown in Figure 4.1 has been designed. Although preliminary, this design will eliminate difficulties caused by the turbulence of the flow and filter from the flow particles that cause optical opaqueness. Further, it will decrease the limitations standard rocket motor grain geometries place on chamber pressures and flow rates. In addition, improved instrumentation for measuring temperature, velocity and pressure has been incorporated into the new design.

The facility shown in Figure 4.1 was designed using hypersonic wind tunnel design criteria. The solid propellant driver would be attached to one end of the stilling chamber. The stilling chamber would be pressurized to greater than 60 percent of the operating pressures. Three mylar diaphragms would be located just before the minimum throat area. The volume of the stilling chamber would be as small as is practical. Honeycomb straighteners and fine screens would be used to remove turbulence according to standard wind tunnel practices and some provision would be made to remove solids from the flow. Because of the low velocities (10 fps in the stilling chamber), mechanical removal of some solids may be feasible. With these refinements, tunnel conditions would be varied as follows: P = 300 to less than 5 psia; T_s = 2800°R to 8500°R; M_∞ = 5 to 9; and velocity from 5000 to 14,000 fps. The dynamic pressure could be varied from a few psia to more than 300.

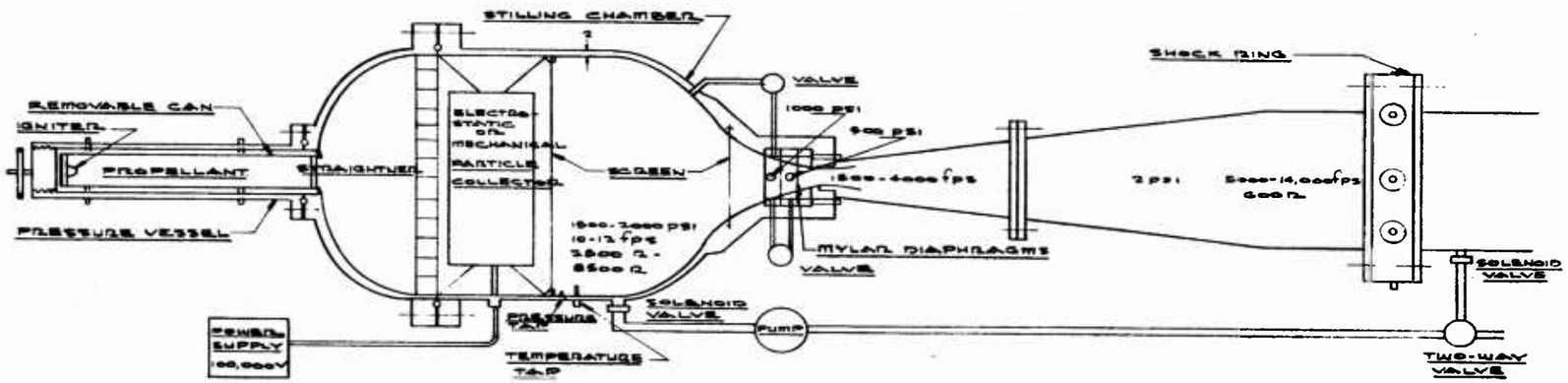

FIGURE 4.1. PROPOSED TUNNEL MODIFICATION

To measure such conditions, improved instrumentation has been studied. Developed hot-wire anemometer systems are available that have demonstrated capabilities in similarly severe environments up to 5000°R. Temperature and velocity could be measured with such an anemometer. For higher temperature environments, special spectrographic systems with high speed, high resolution capabilities would be required.

Improved pressure measuring techniques would require some development; however, it is believed that a NOL developed piston type strain gage transducer would have the required low temperature and acceleration sensitivities and still have adequate response.

LIST OF REFERENCES

1. "Research Concerning Feasibility of Producing Longer Duration Shock Waves in Existing Types of Shock Tubes," Final Report, Boynton Associates, La Canada, California, February 15, 1960, DASA 1172.

2. "Shock and Hypervelocity Studies in a Solid Propellant Driven Tunnel," by M. L. Whitfield, E. M. Briggs, R. K. Gregory, and R. C. DeHart, Preliminary Final Report to DASA, March 1963.

3. Kaplin, K., and Goodale, T. C., High Temperature Dynamic Pressure Gauge, Final Report, Broadview Research Corporation Burlingame, California, November 1961, DASA 1258.

4. Shapiro, A. H., Compressible Fluid Flow, The Ronald Press Co.

5. Volluz, R. J., "Wind Tunnel Instrumentation and Operation," Handbook of Supersonic Aerodynamics, Section 20, NAVORD Report 1488, Vol. 6.

6. Blast Patterns in Tunnels and Chambers, Ballistic Research Laboratories, Aberdeen Proving Ground, Maryland, March 1960, DASA 1171.

7. Bundy, F. F., Strong, H. M., and Bregg, A. B., "Measurement of Velocity and Pressure of Gases in Rocket by Spectroscopic Methods," General Electric Research Laboratory, Reprint 1849.

APPENDIX A

PRESSURE AND TEMPERATURE DATA

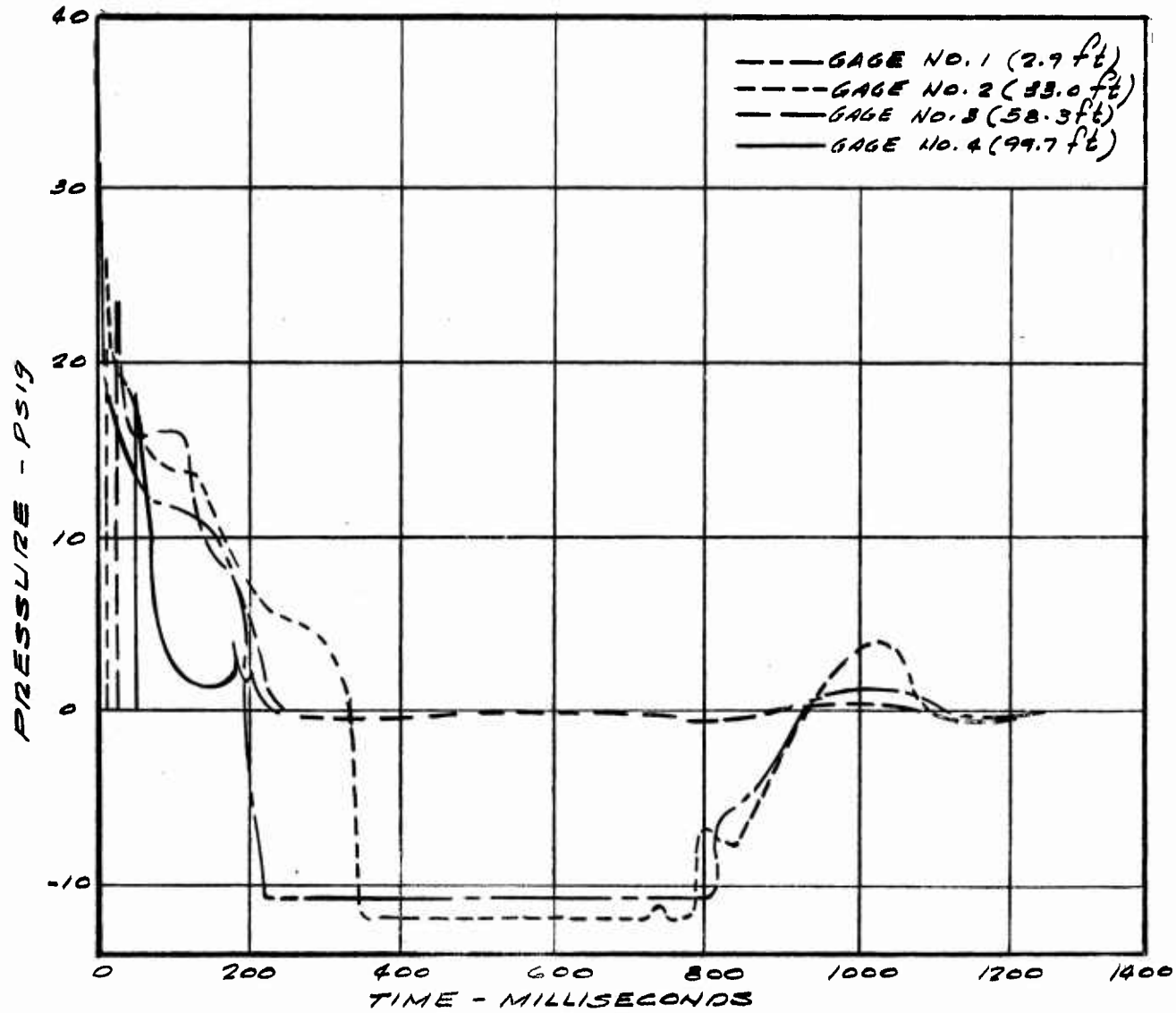

FIGURE A. 1. PRESSURE RECORDS, TEST 1, TURBINE SPINNER-1

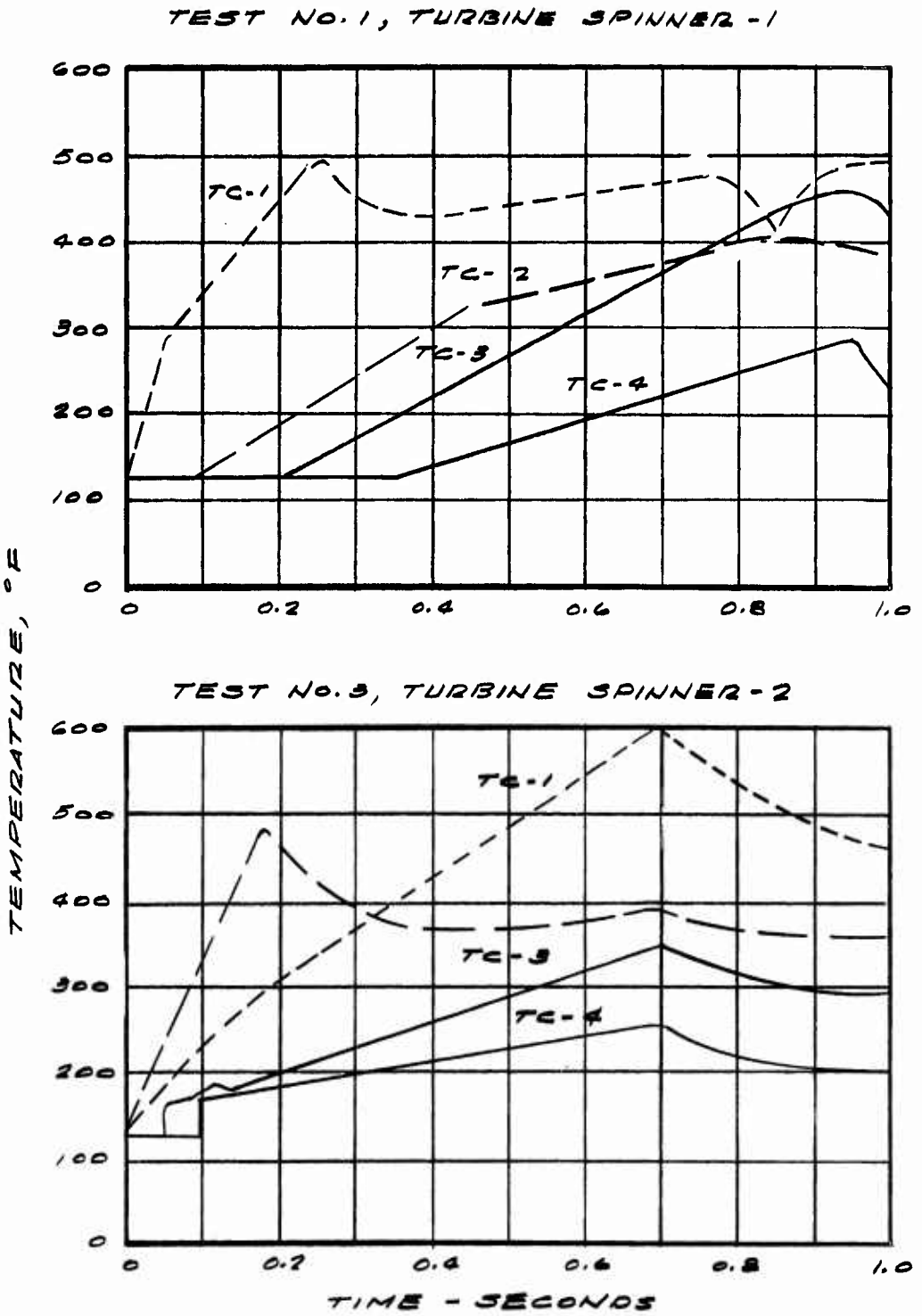

FIGURE A. 2. THERMOCOUPLE RECORDINGS FOR SHOTS 1 AND 3 (SEE FIG. A. 4 FOR GAGE LOCATIONS)

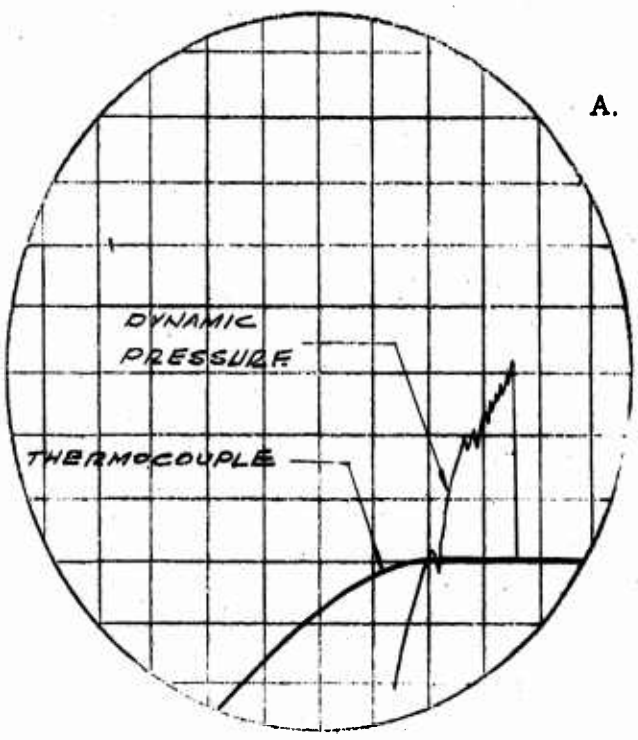

A. Test No. 2 DQ-1 (13 ft)

Charge Amplifier:
0.5 mv/pcb
Q Vertical Sensitivity:
1 v/div
Q Horizontal Sensitivity:
0.5 sec/div
Calibration approx.
80 pcb/psi at 1 mv/div

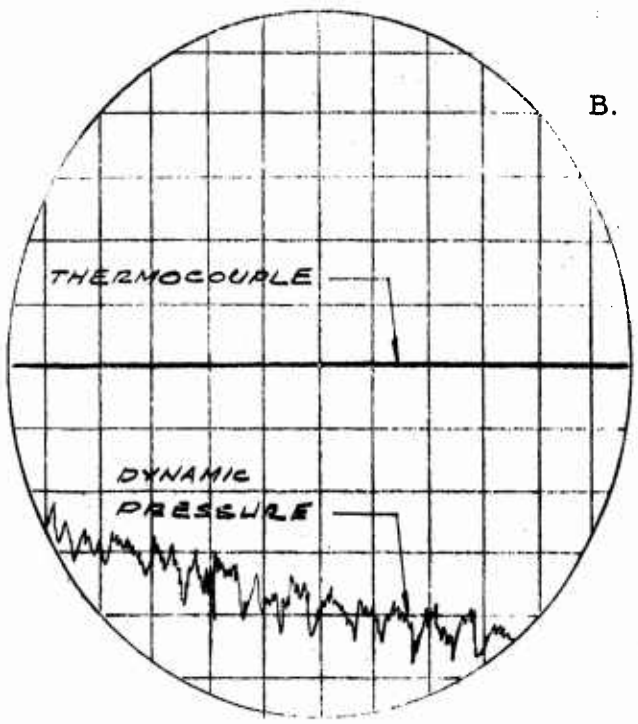

B. Test No. 3 DQ-2 (35 ft)

Charge Amplifier:
0.5 mv/pcb
Q Vertical Sensitivity:
2 v/div
Q Horizontal Sensitivity:
0.2 sec/div
Calibration approx.
87 pcb/psi at 1 mv/div

FIGURE A.3. BRC DYNAMIC PRESSURE GAGE RECORDS

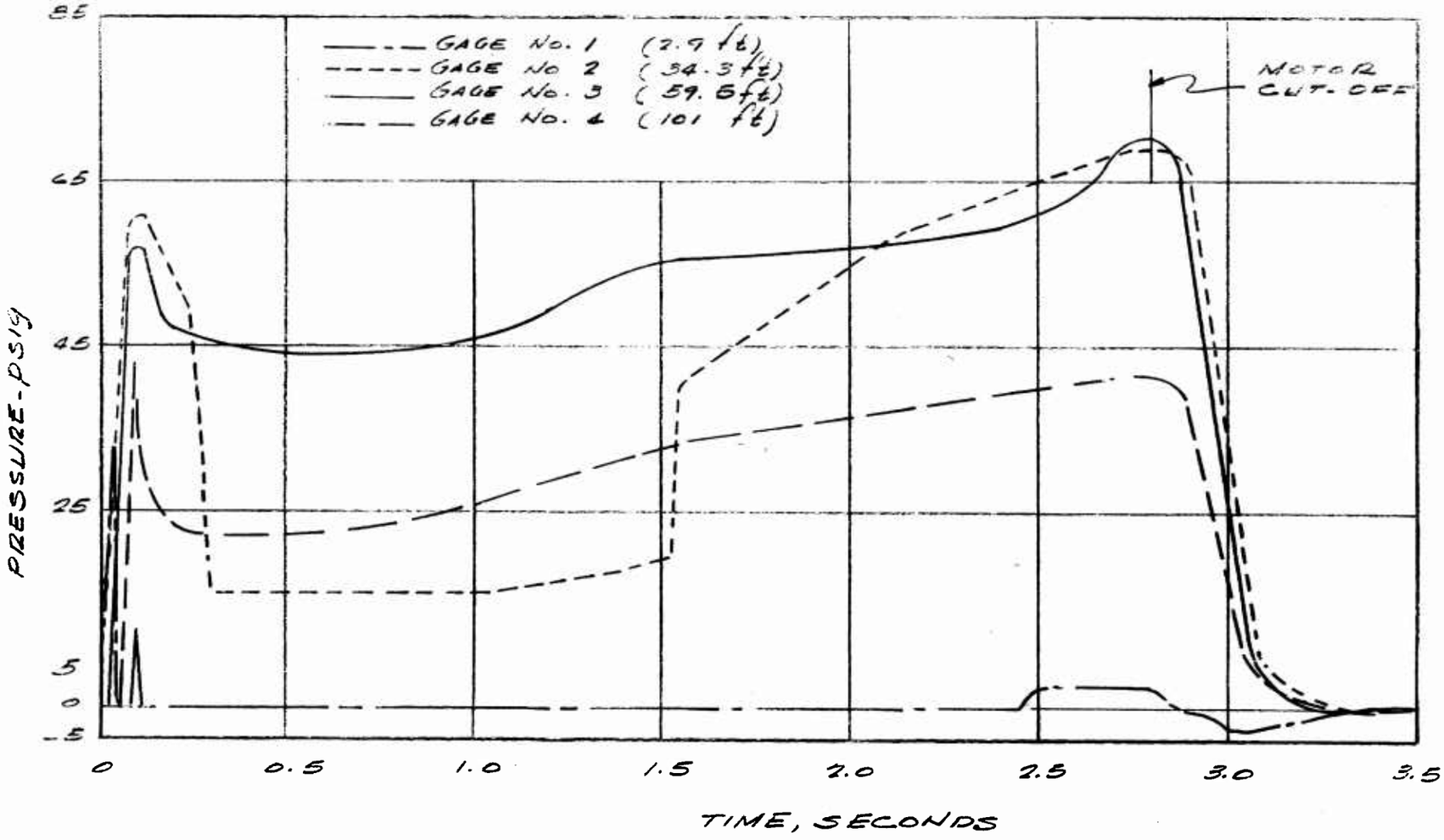

FIGURE A. 4. PRESSURE RECORDS, TEST 2, CAJUN-1

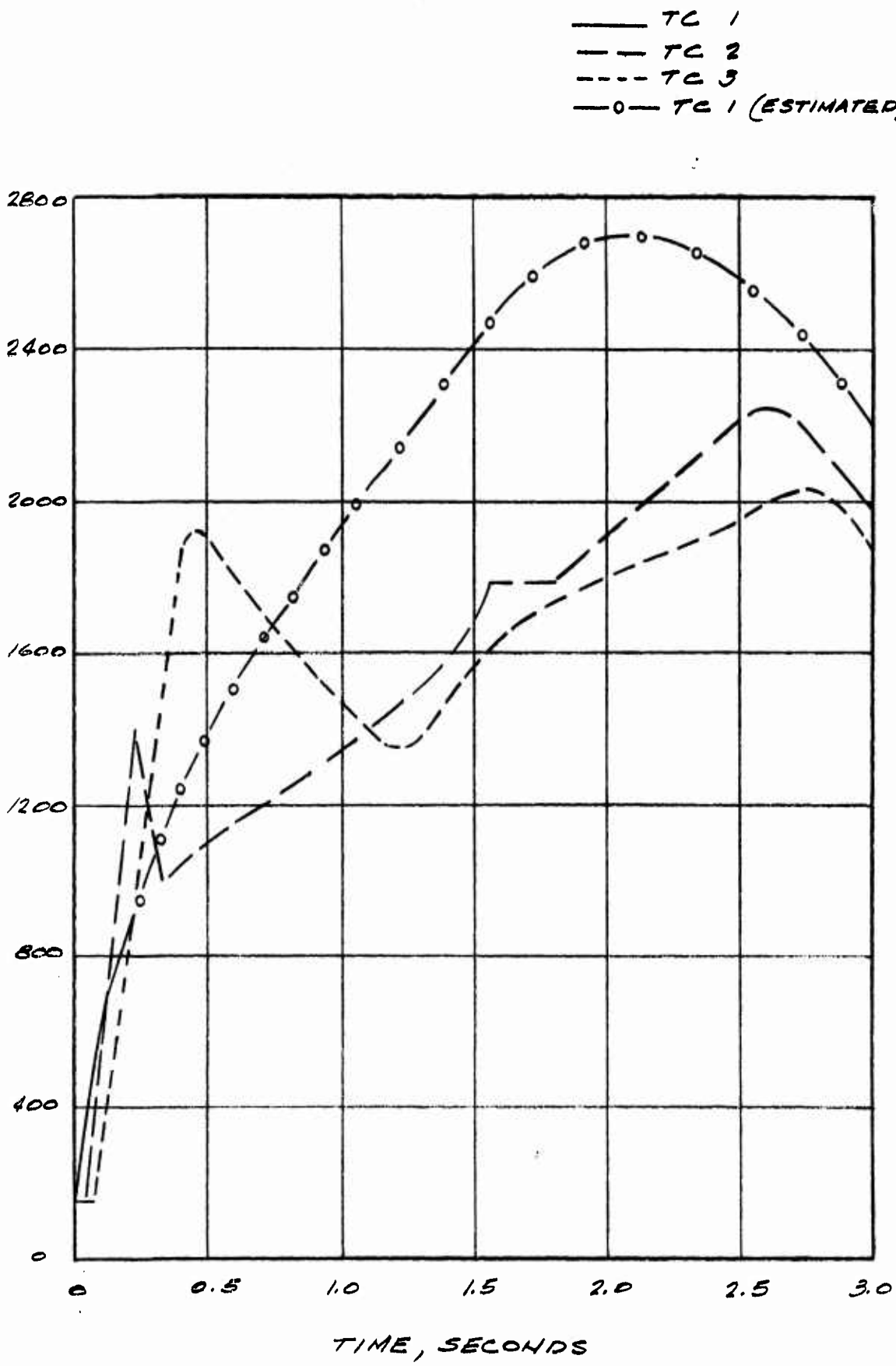

FIGURE A. 5. THERMOCOUPLE MEASUREMENTS, TEST 2 CAJUN-1

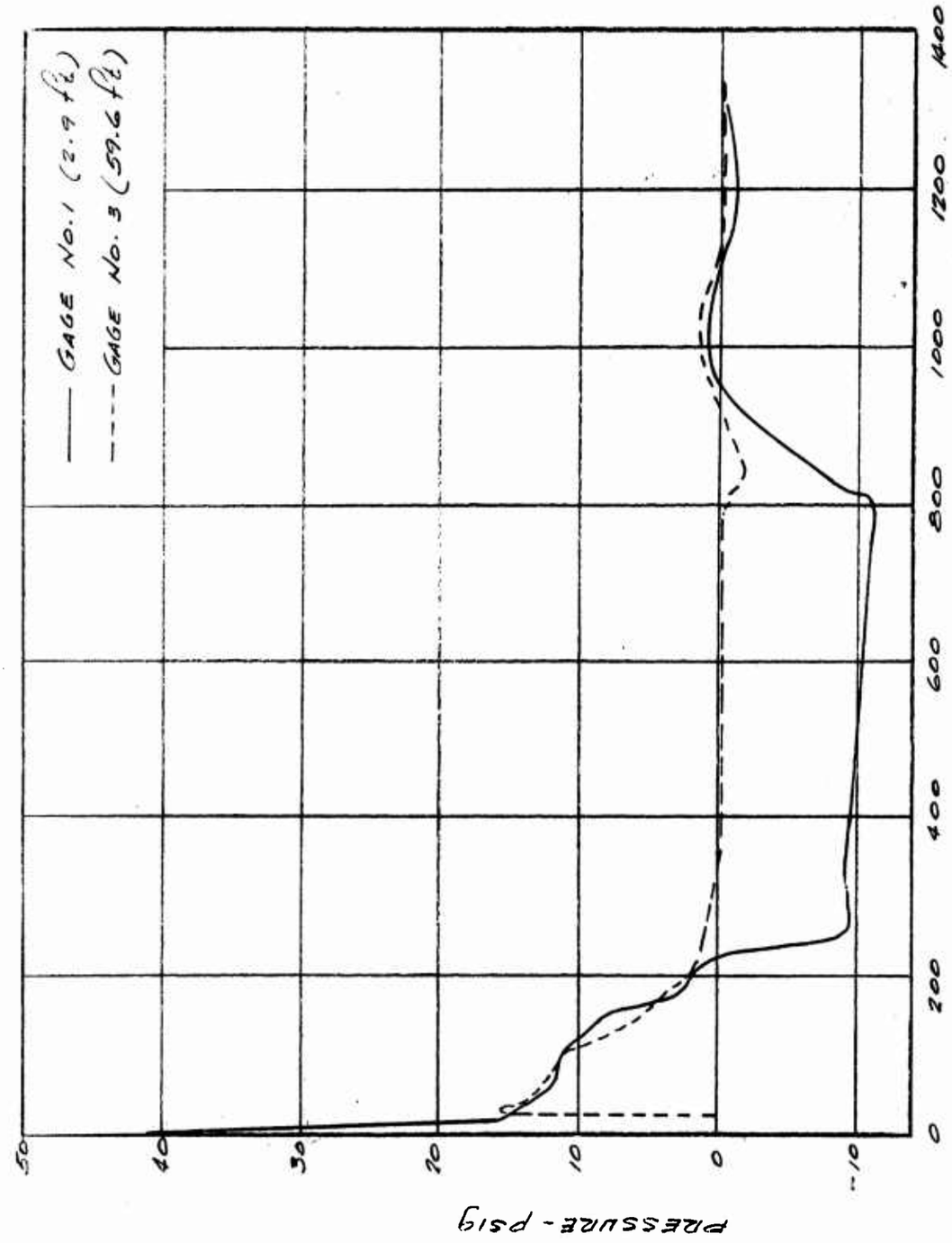

FIGURE A. 6. PRESSURE RECORDS, TEST 3, TURBINE SPINNER-2

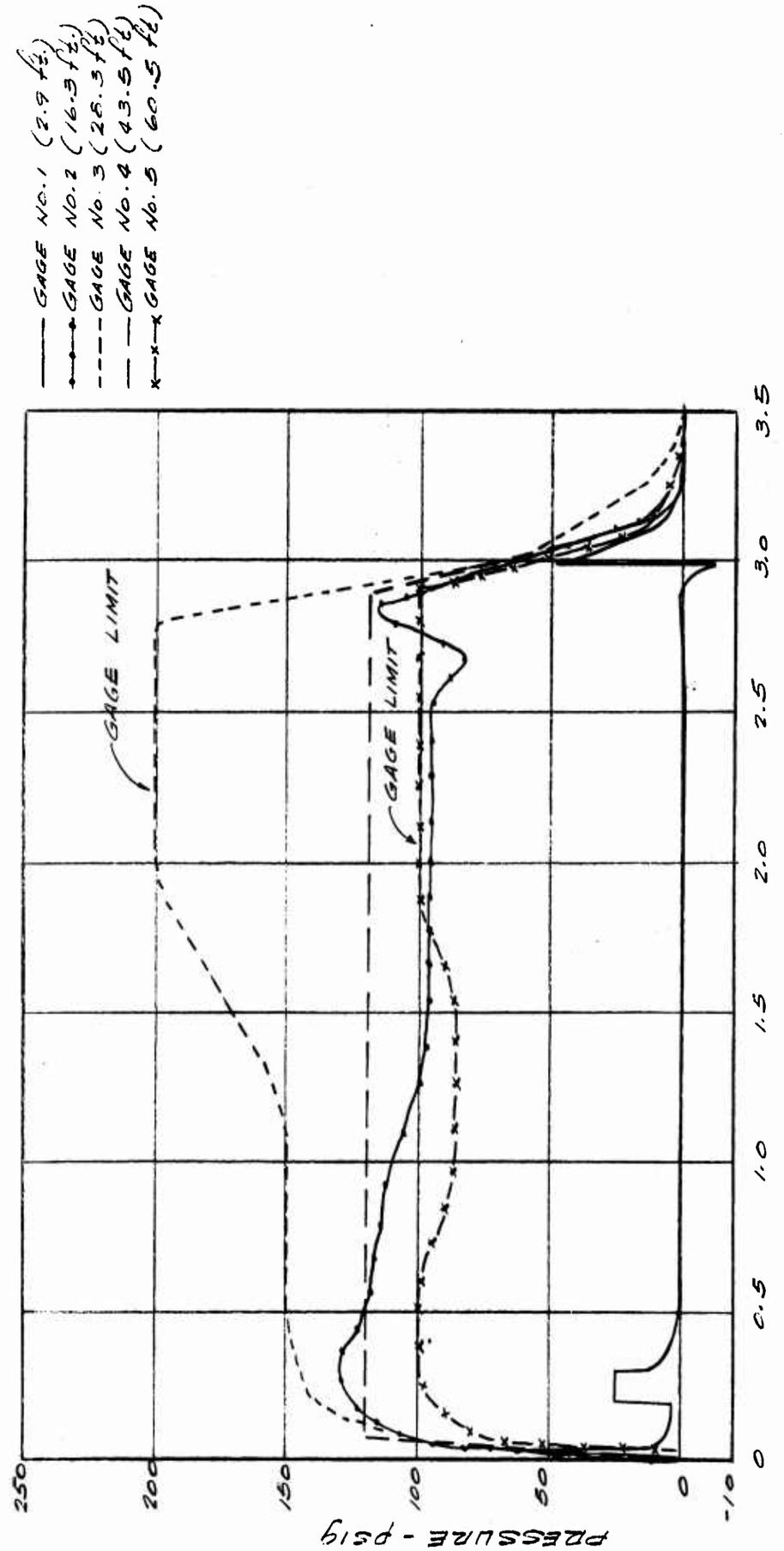

FIGURE A. 7. PRESSURE RECORDS, TEST 4, CAJUN-2.

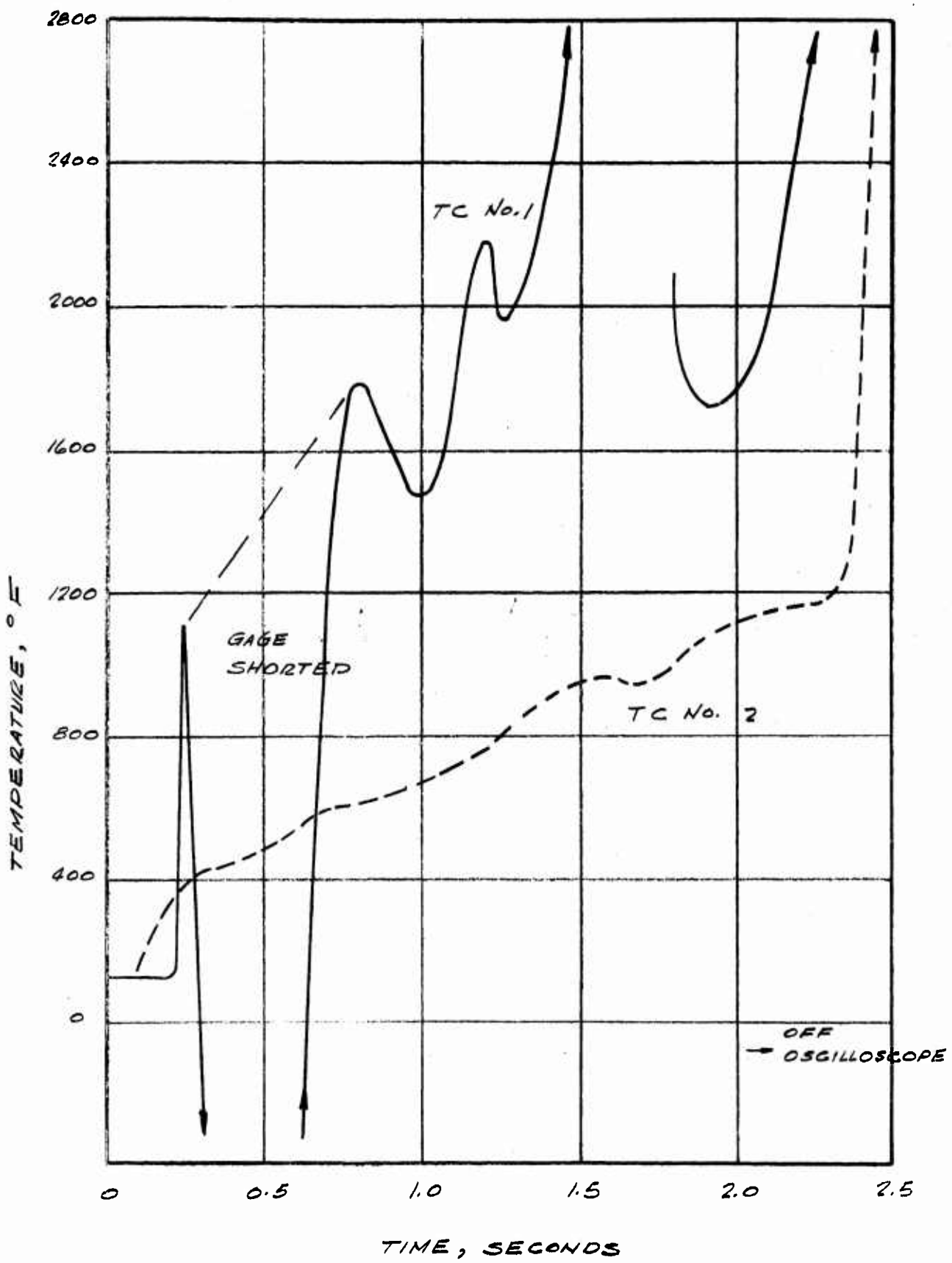

FIGURE A.8. THERMOCOUPLE MEASUREMENTS, TEST 4, CAJUN-2

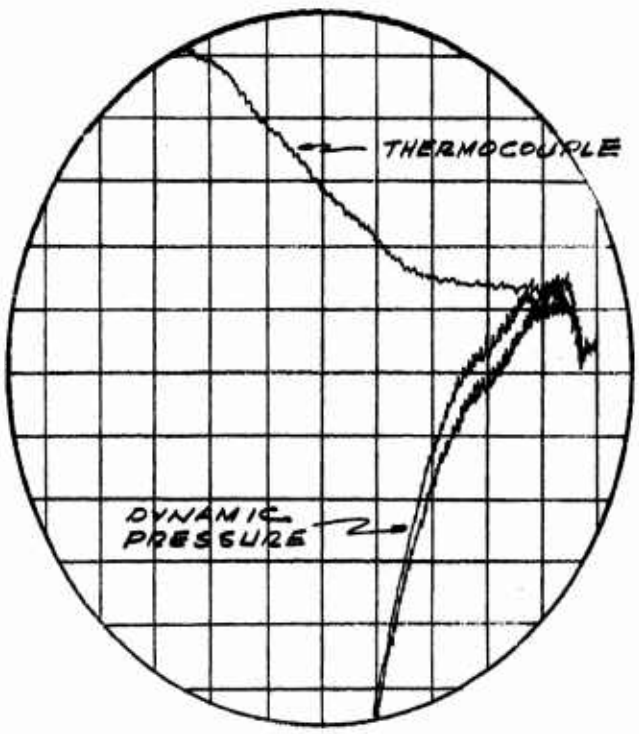

Test No. 4 DQ-2

Charge Amplifier:
0.5 mv/pcb
Q Vertical Sensitivity:
2 v/div
Q Horizontal Sensitivity:
0.2 sec/div
Calibration:
87 pcb/psi at 1 mc/div

FIGURE A.9. BRC DYNAMIC PRESSURE GAGE RECORD

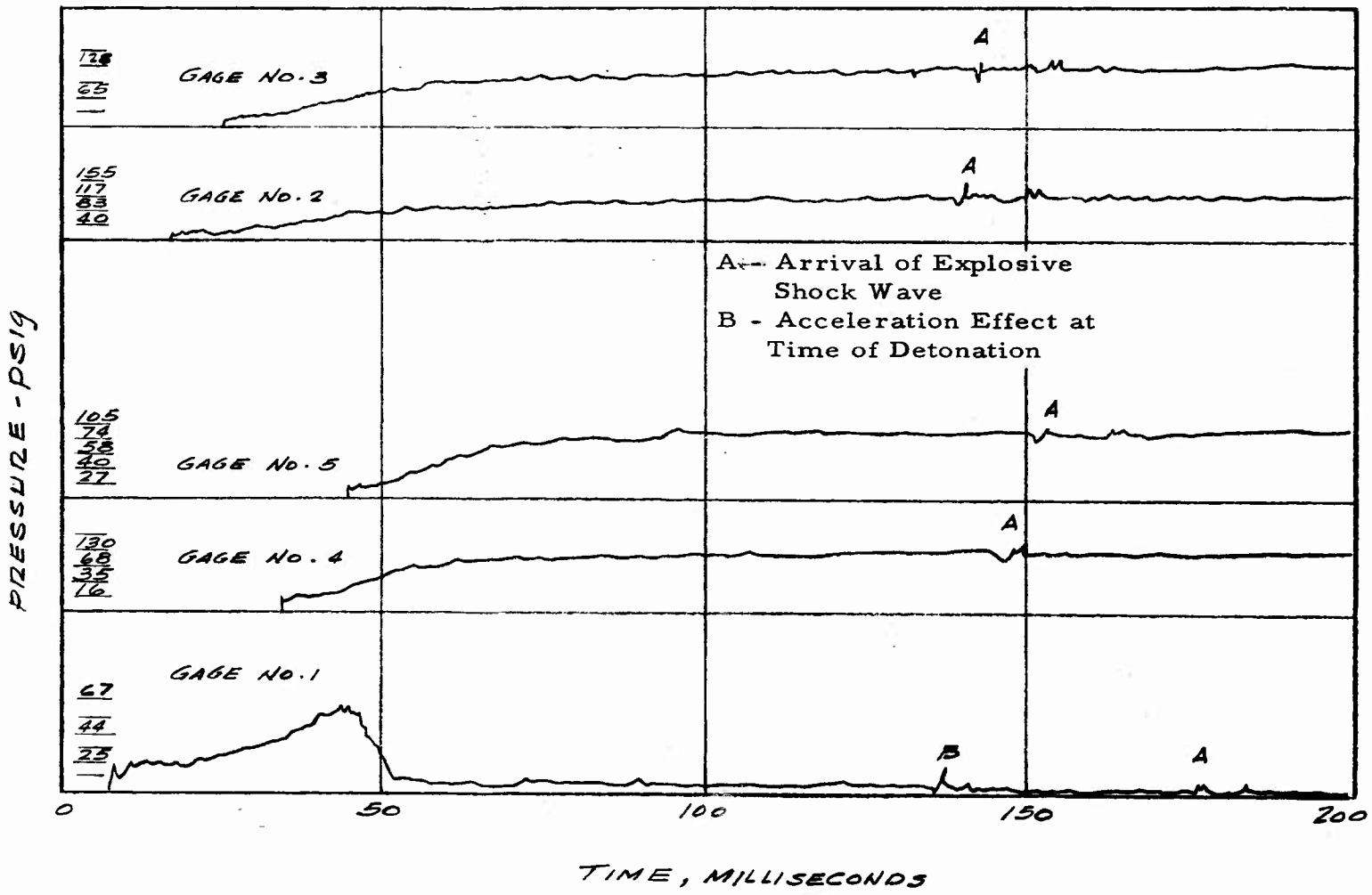

FIGURE A. 10. OSCILLOGRAPH RECORDS SHOWING DETONATION SHOCK WAVE

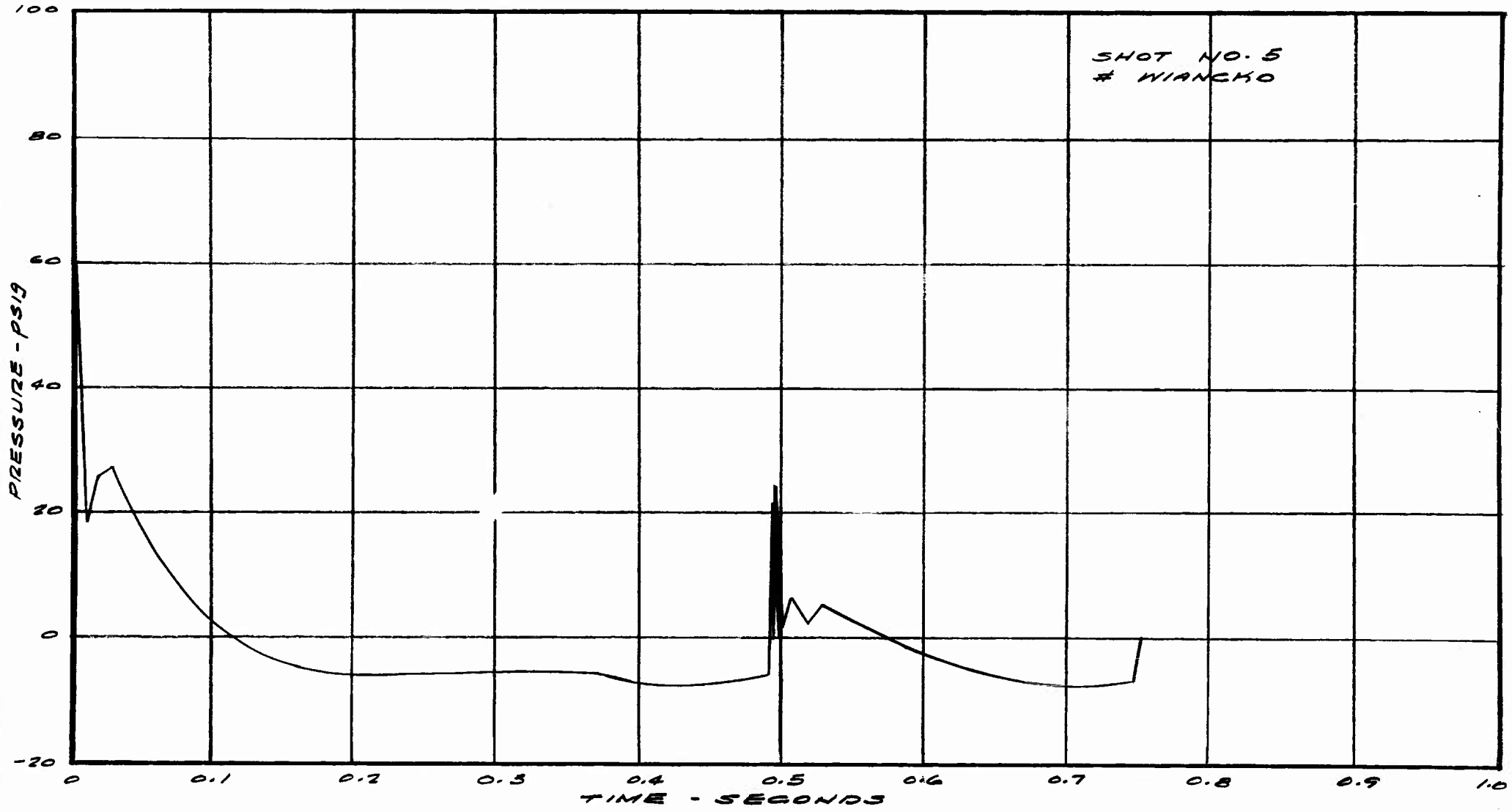

FIGURE A. 11. STATIC PRESSURE, STATION 1, TEST 5

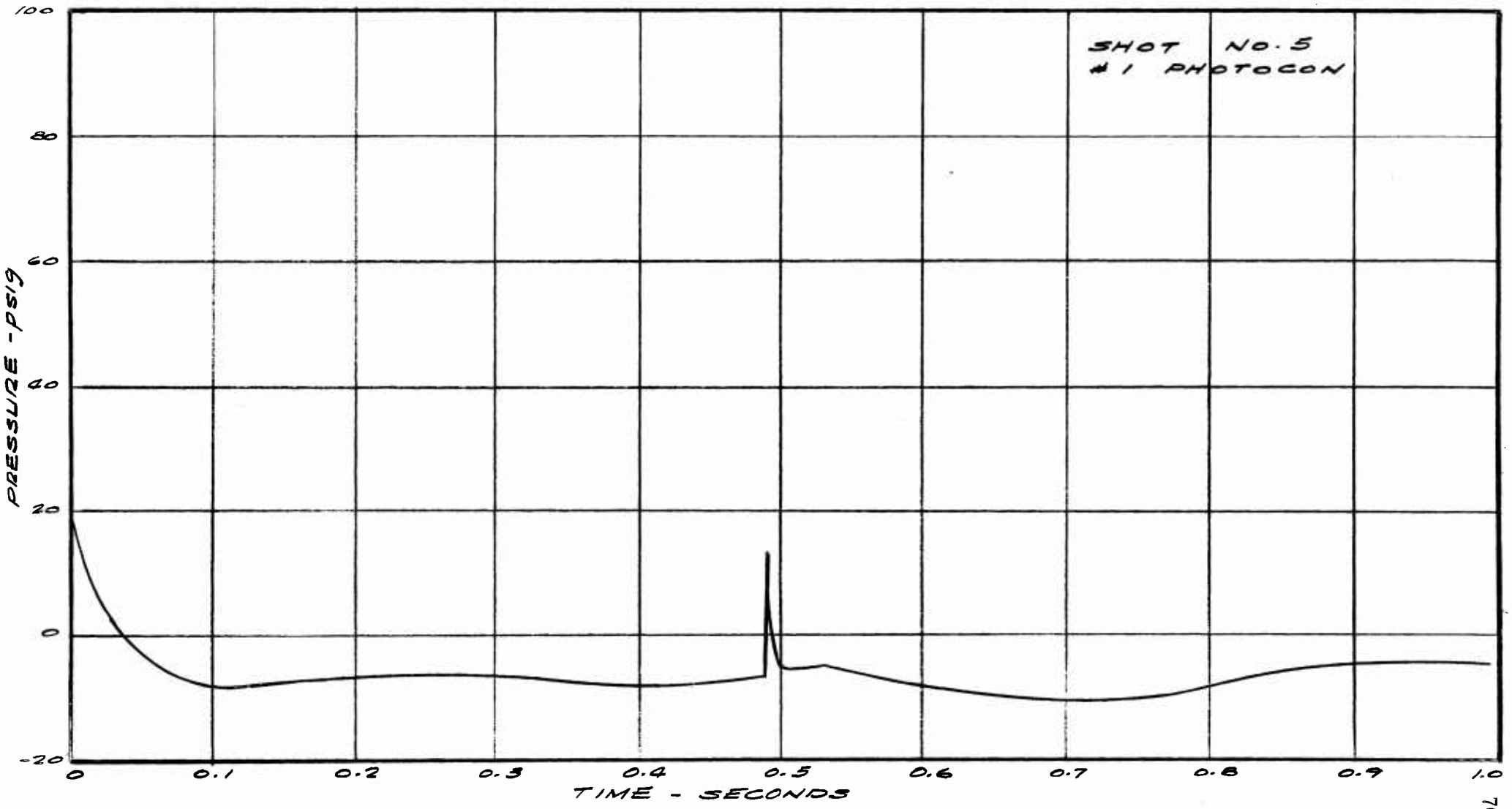

FIGURE A. 12. STATIC PRESSURE, STATION 1, TEST 5

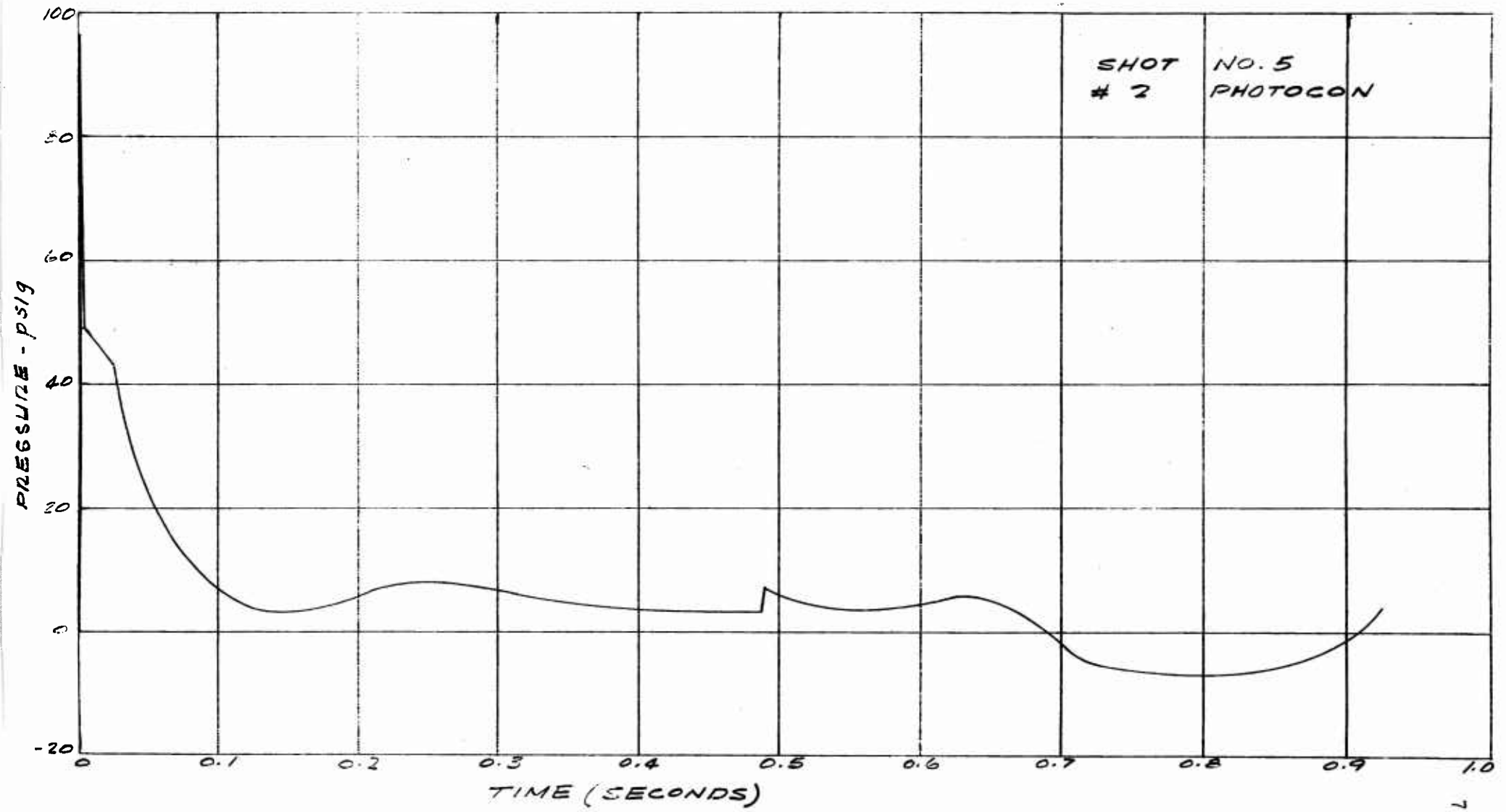

FIGURE A. 13 STAGNATION PRESSURE, STATION 1, TEST 5

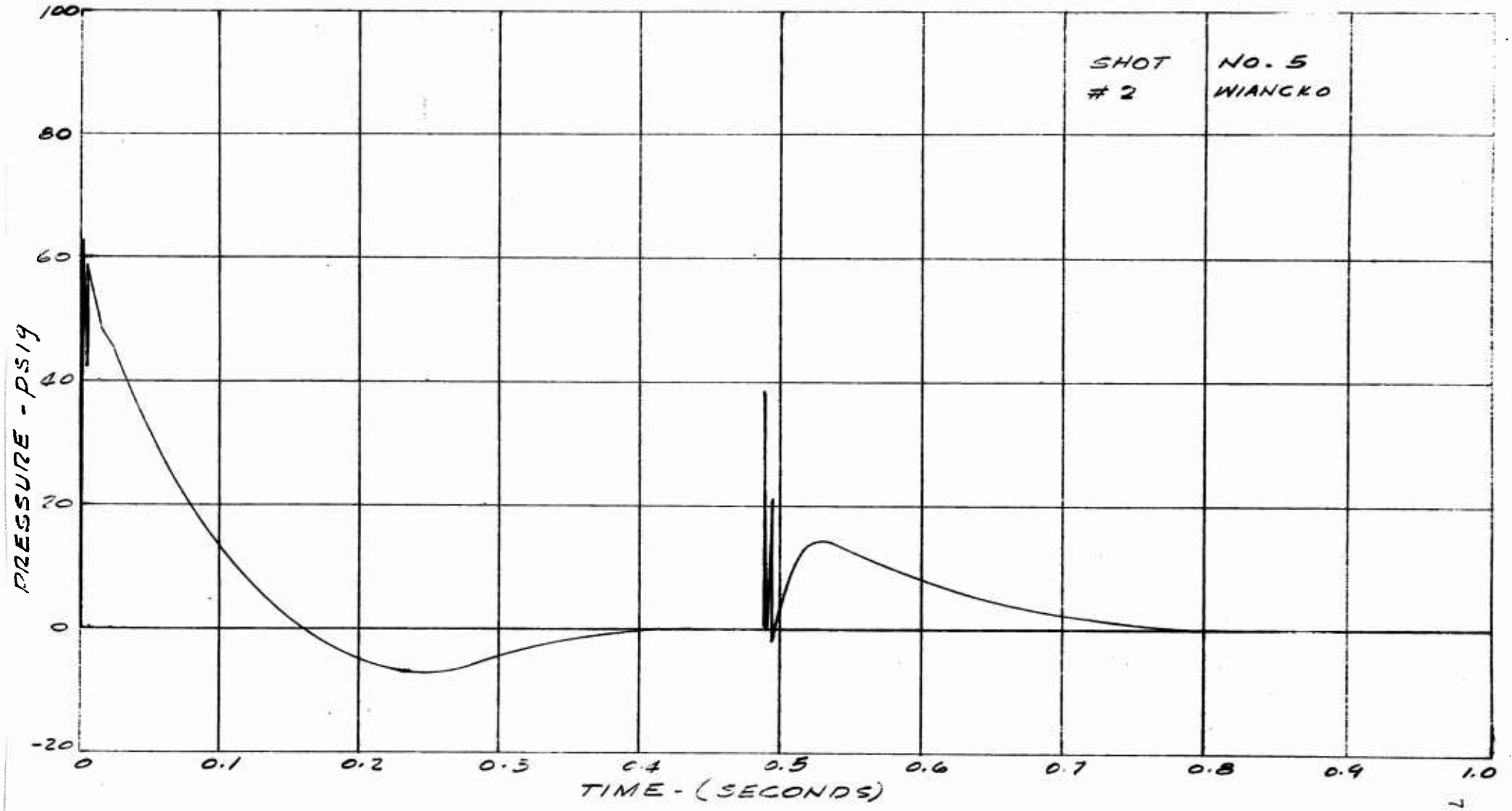

FIGURE A 14. STATIC PRESSURE, STATION 3, TEST 5

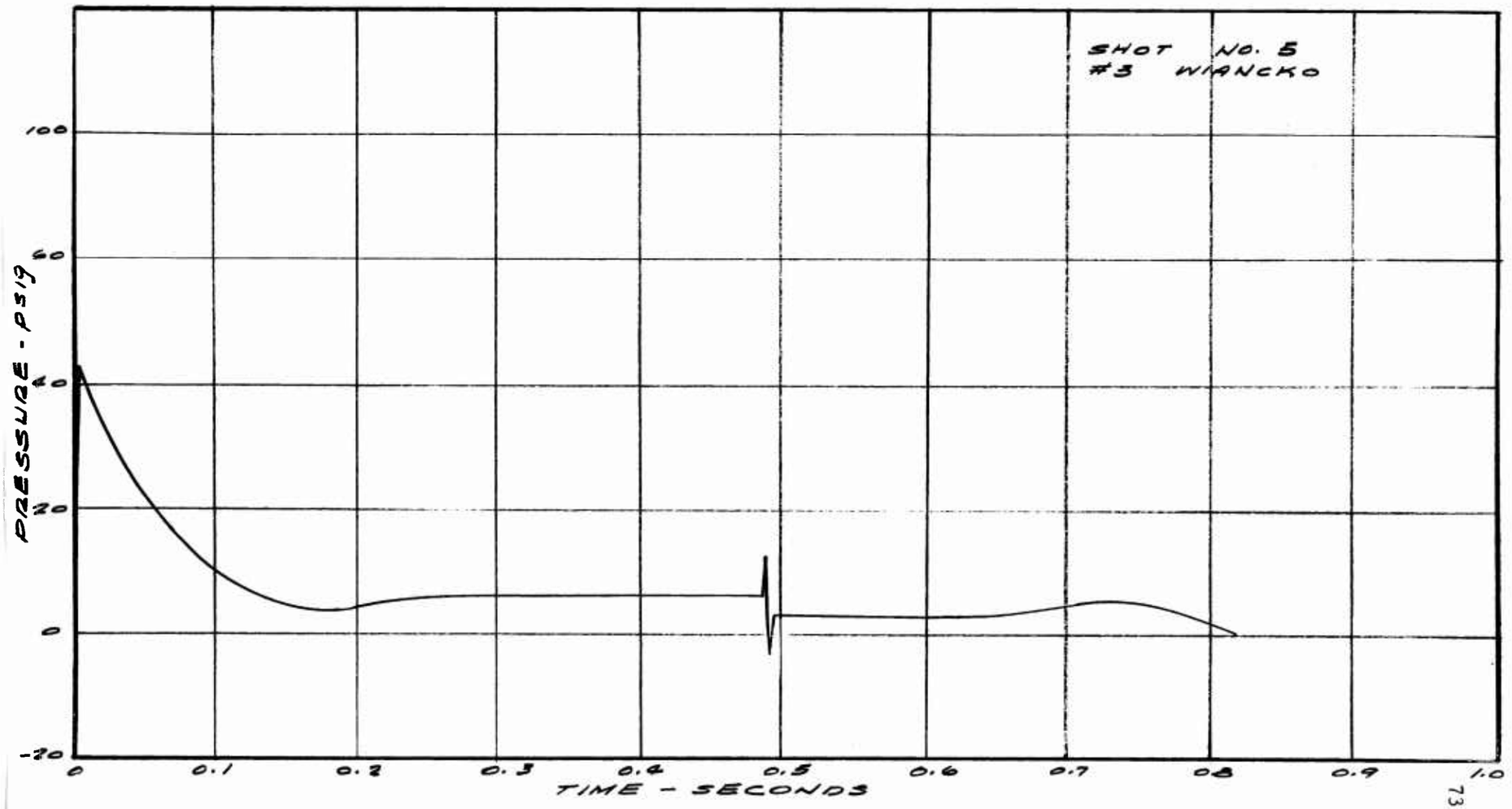

FIGURE A. 15. STATIC PRESSURE, STATION 4, TEST 5

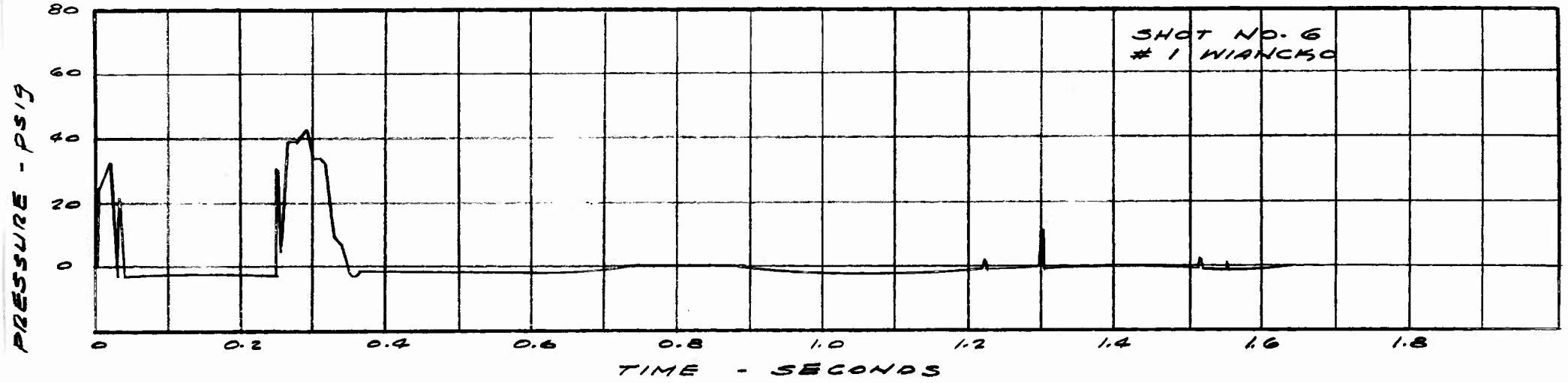

FIGURE A. 16. STATIC PRESSURE, STATION 1, TEST 6

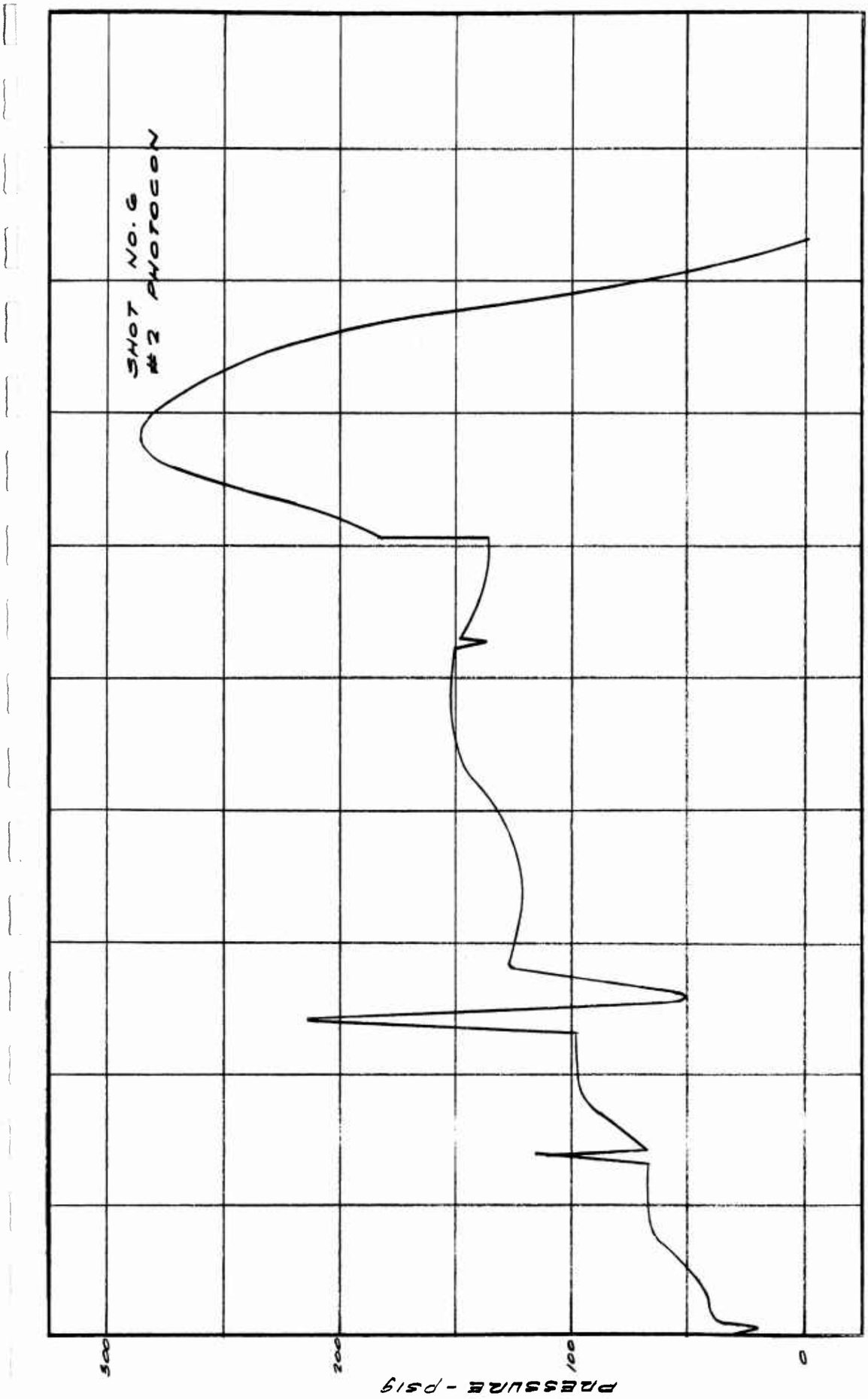

FIGURE A. 17. STAGNATION PRESSURE, STATION 1, TEST 6

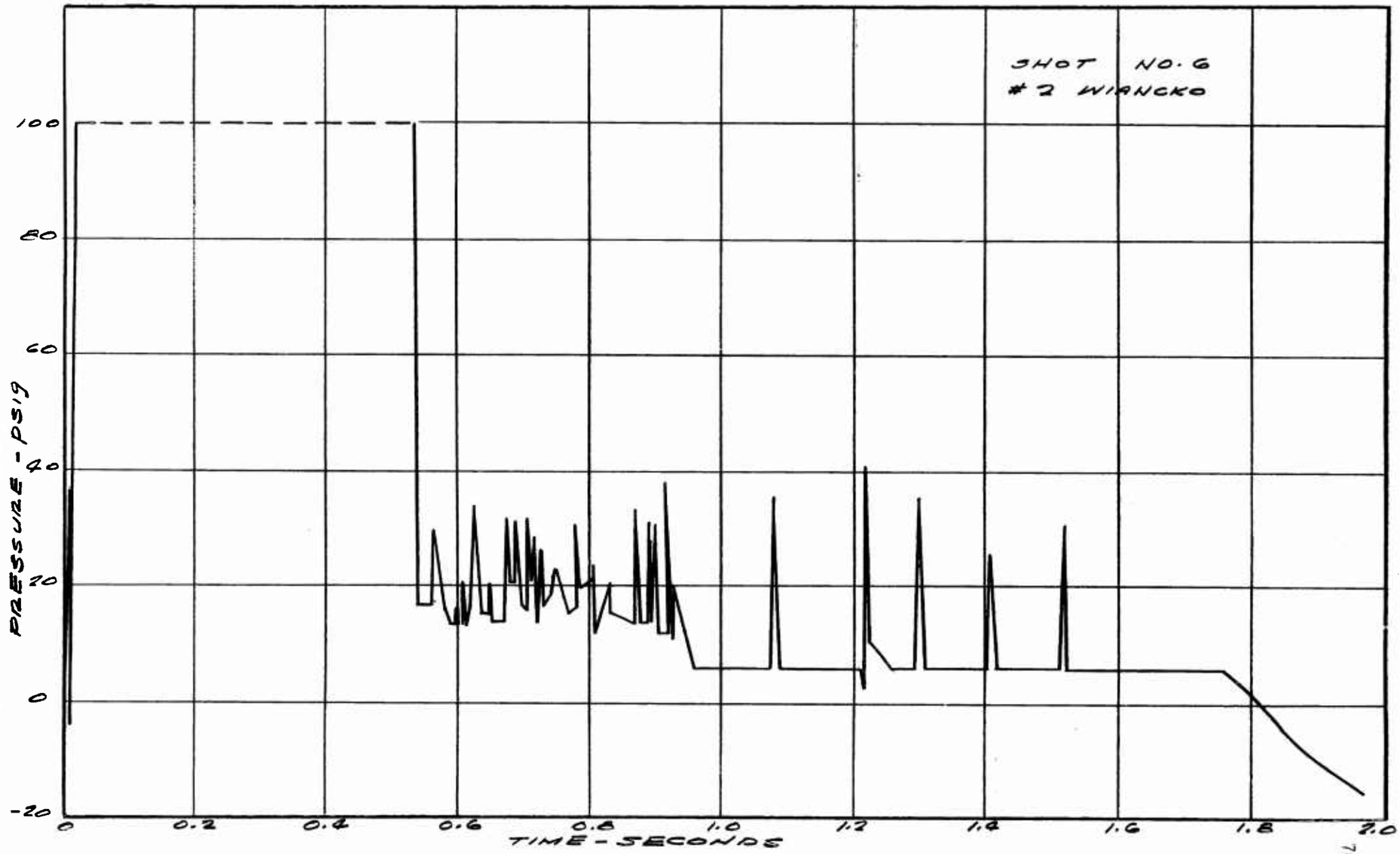

FIGURE A. 18. STATIC PRESSURE, STATION 3, TEST 6

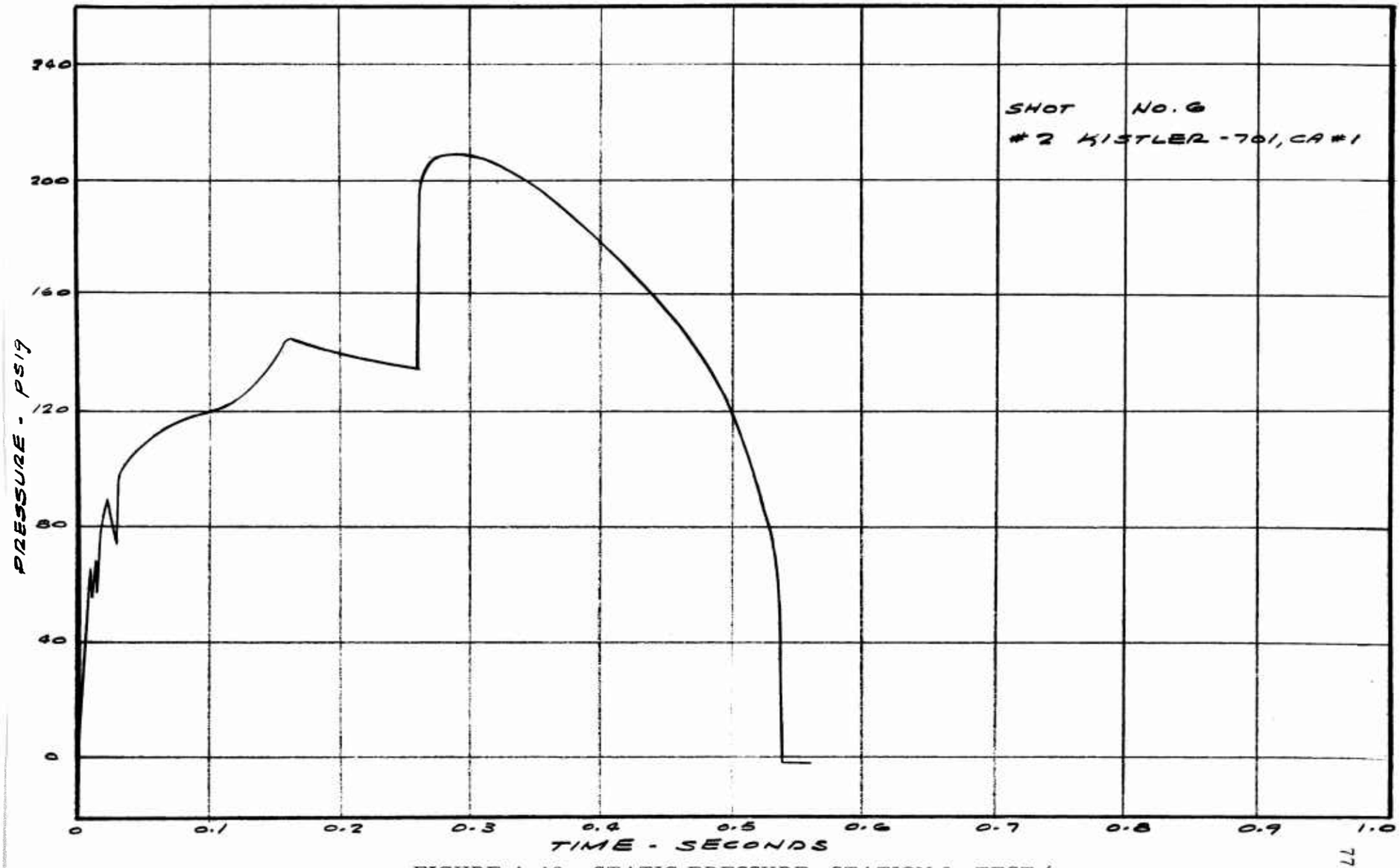

FIGURE A. 19. STATIC PRESSURE, STATION 3, TEST 6

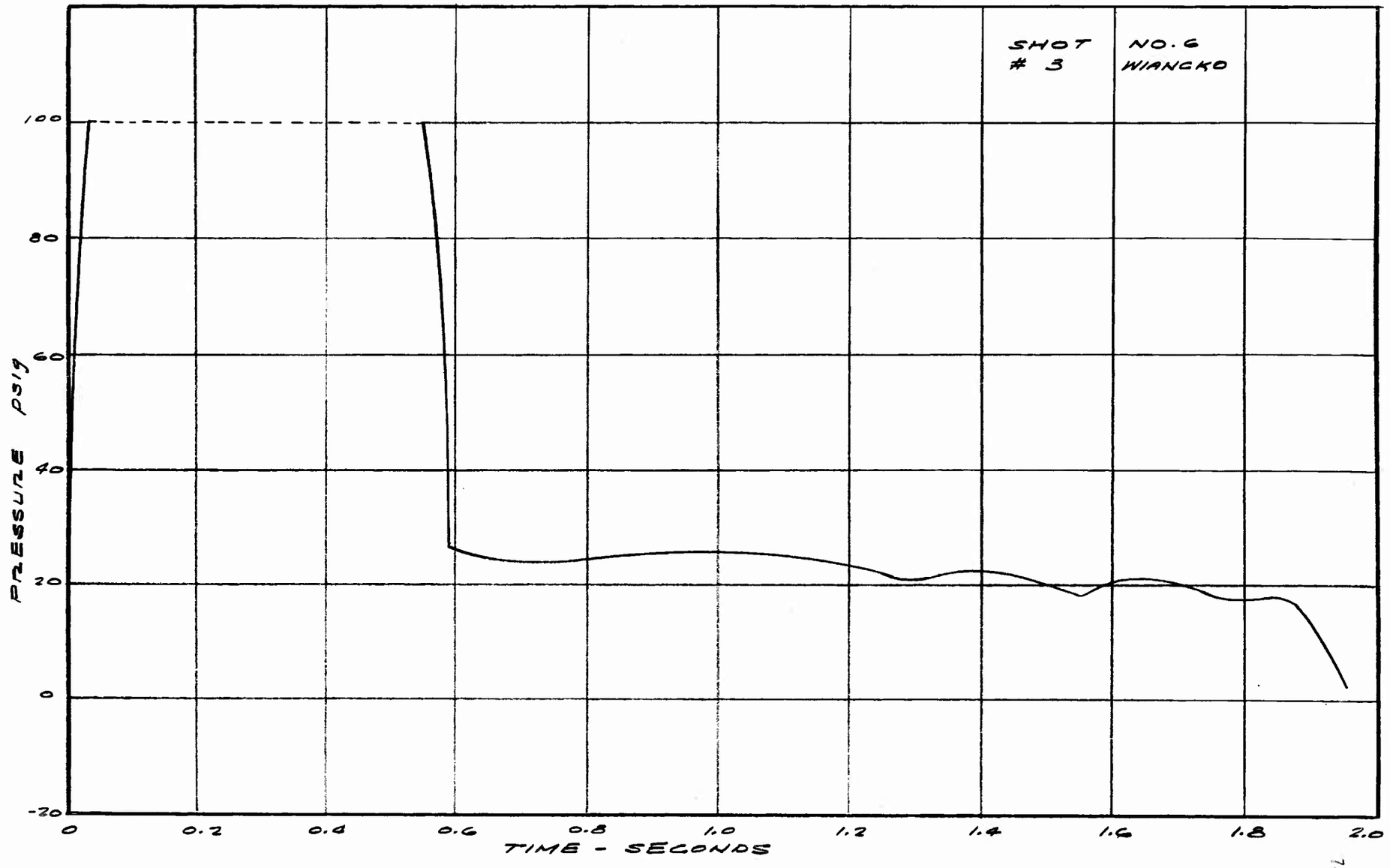

FIGURE A. 20. STATIC PRESSURE, STATION 4, TEST 6

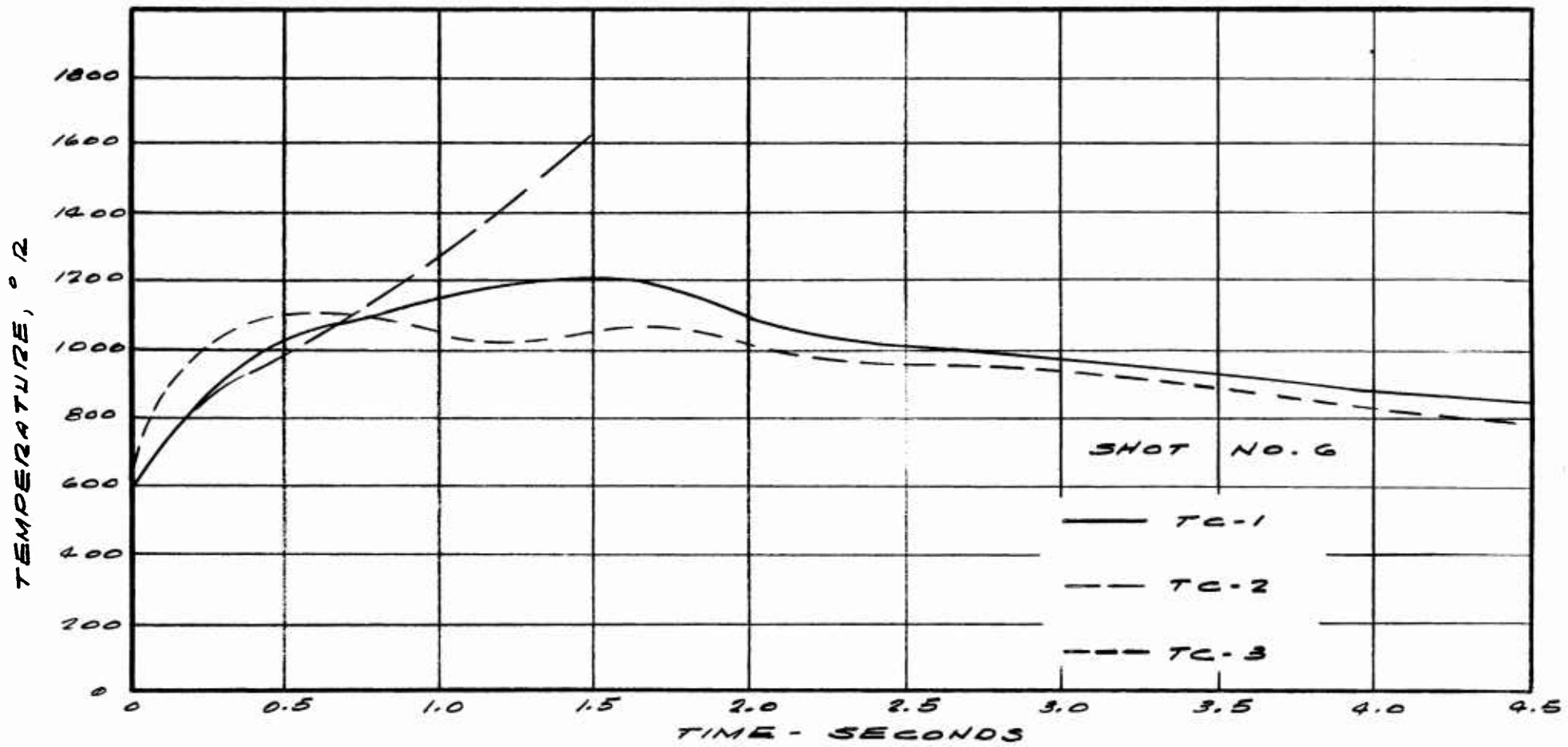

FIGURE A. 21. THERMOCOUPLE MEASUREMENTS, TEST 6 RH/RR-1

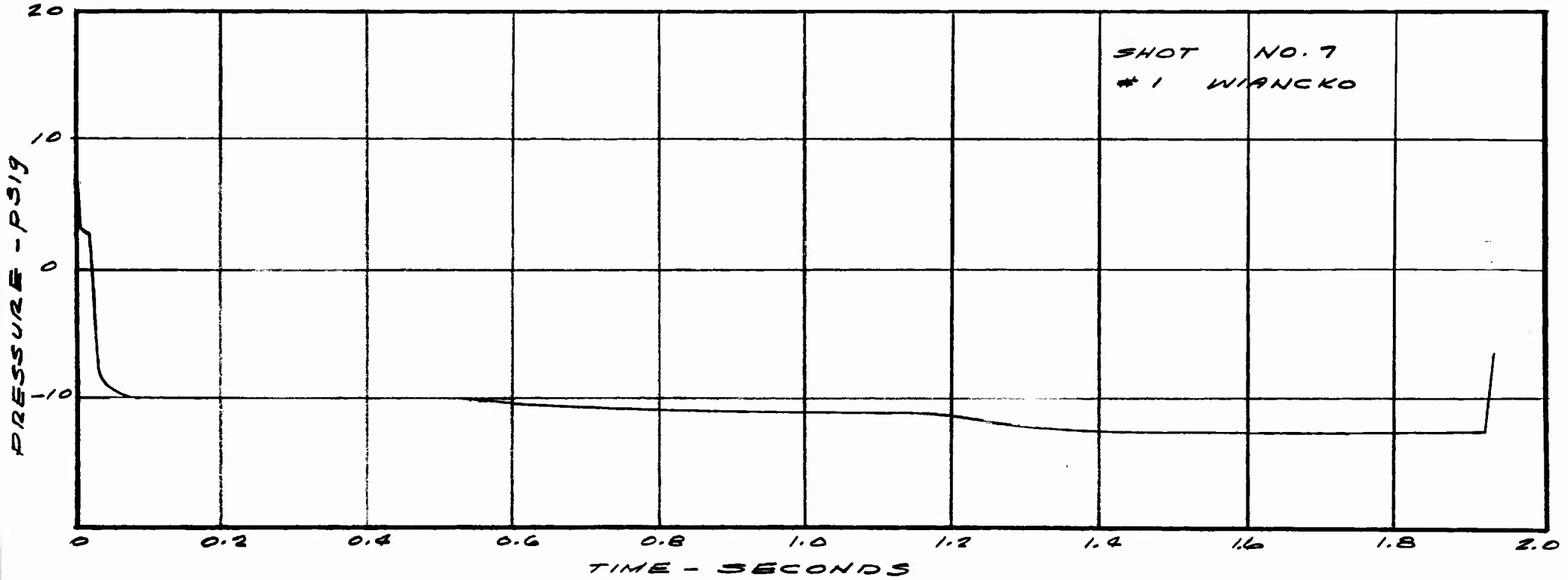

FIGURE A.22. STATIC PRESSURE, STATION 1, TEST 7

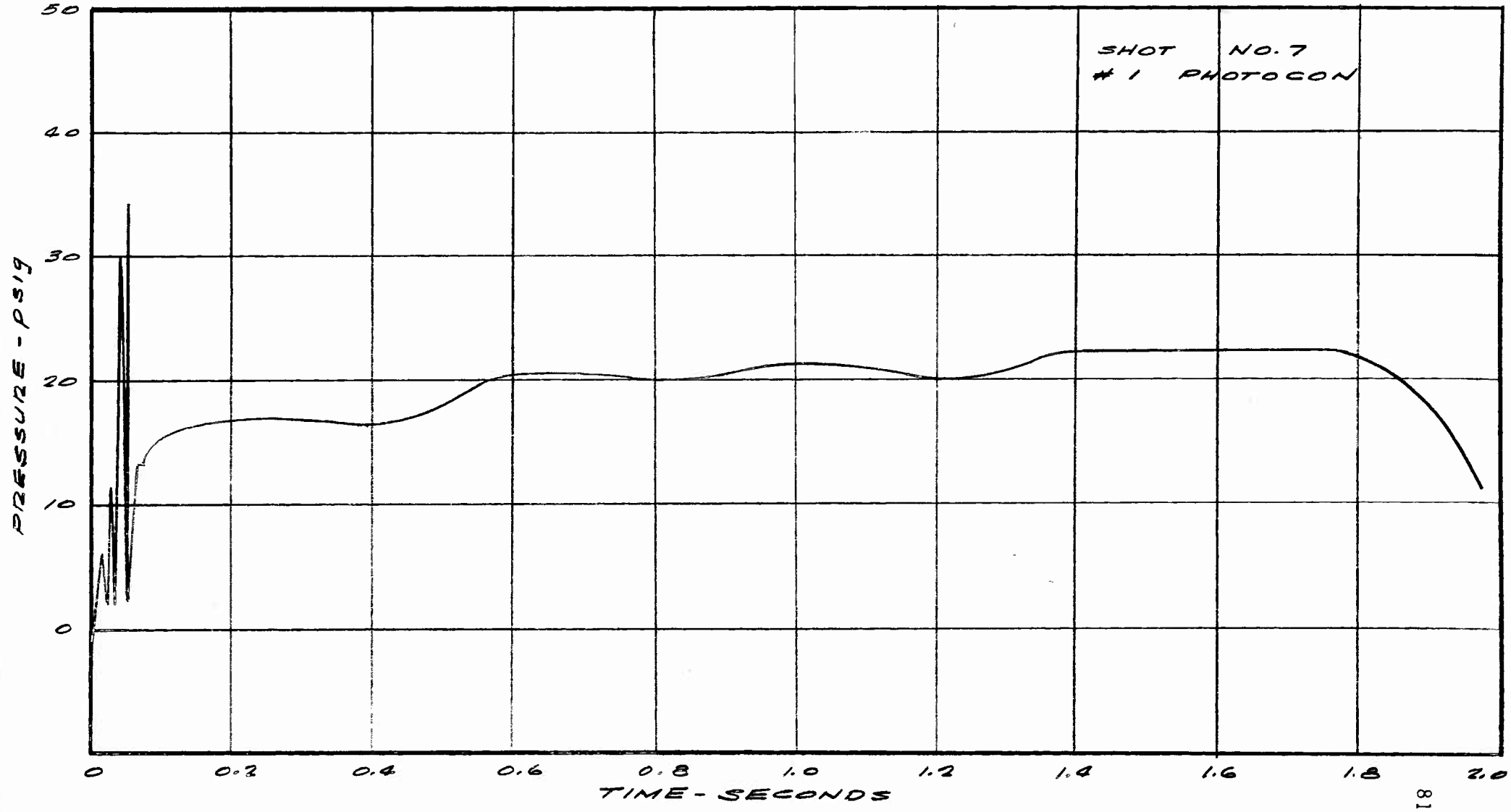

FIGURE A. 23. STAGNATION PRESSURE, STATION 1, TEST 7

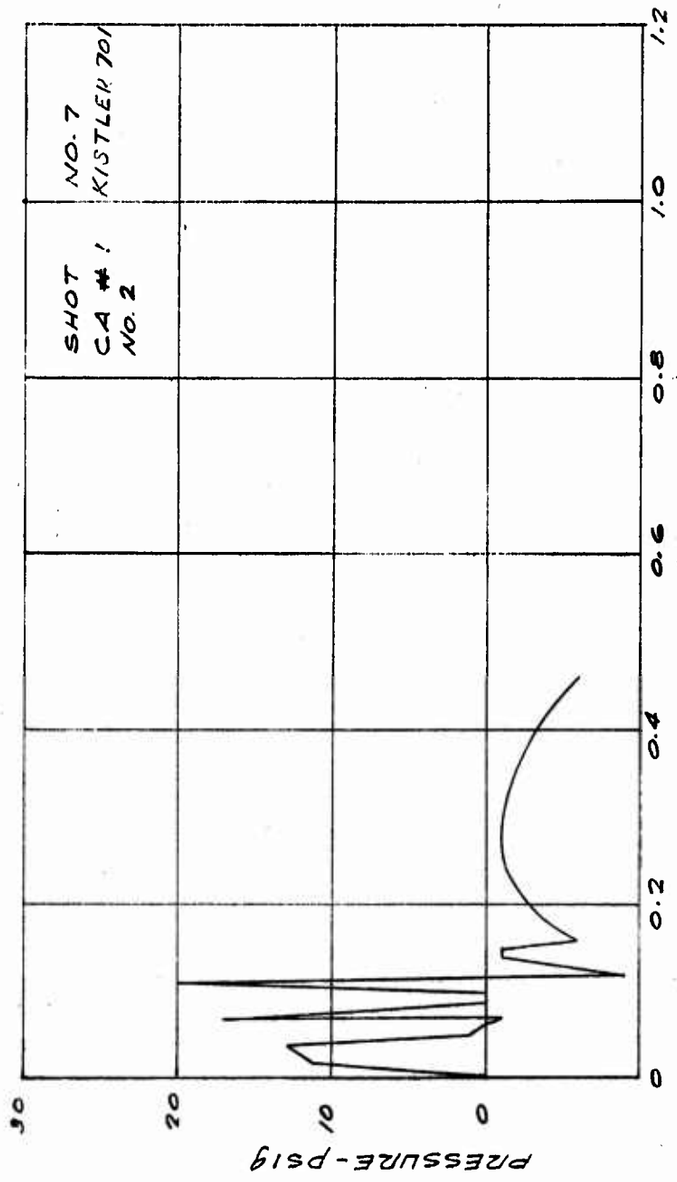

FIGURE A. 24. STAGNATION PRESSURE, STATION 2, TEST 7

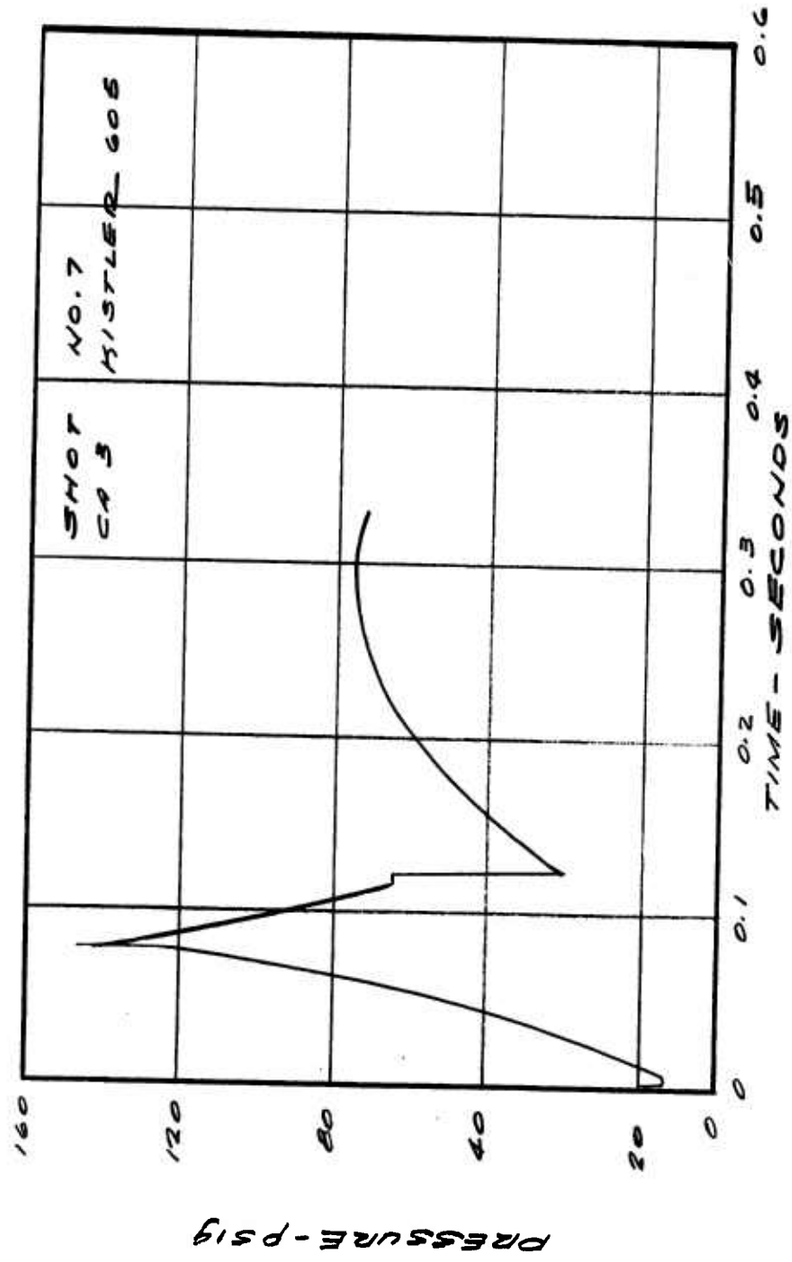

FIGURE A.25. 45° MODEL PRESSURE, TEST 7

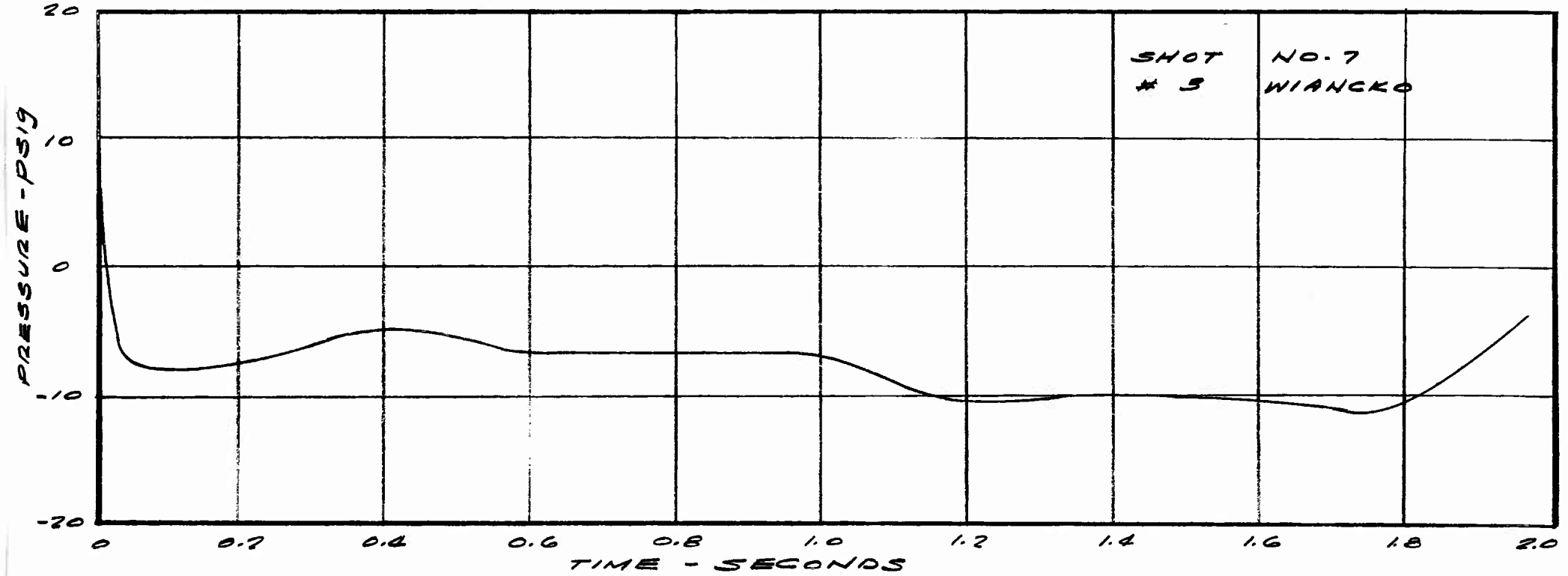

FIGURE A. 26. STATIC PRESSURE, STATION 5, TEST 7

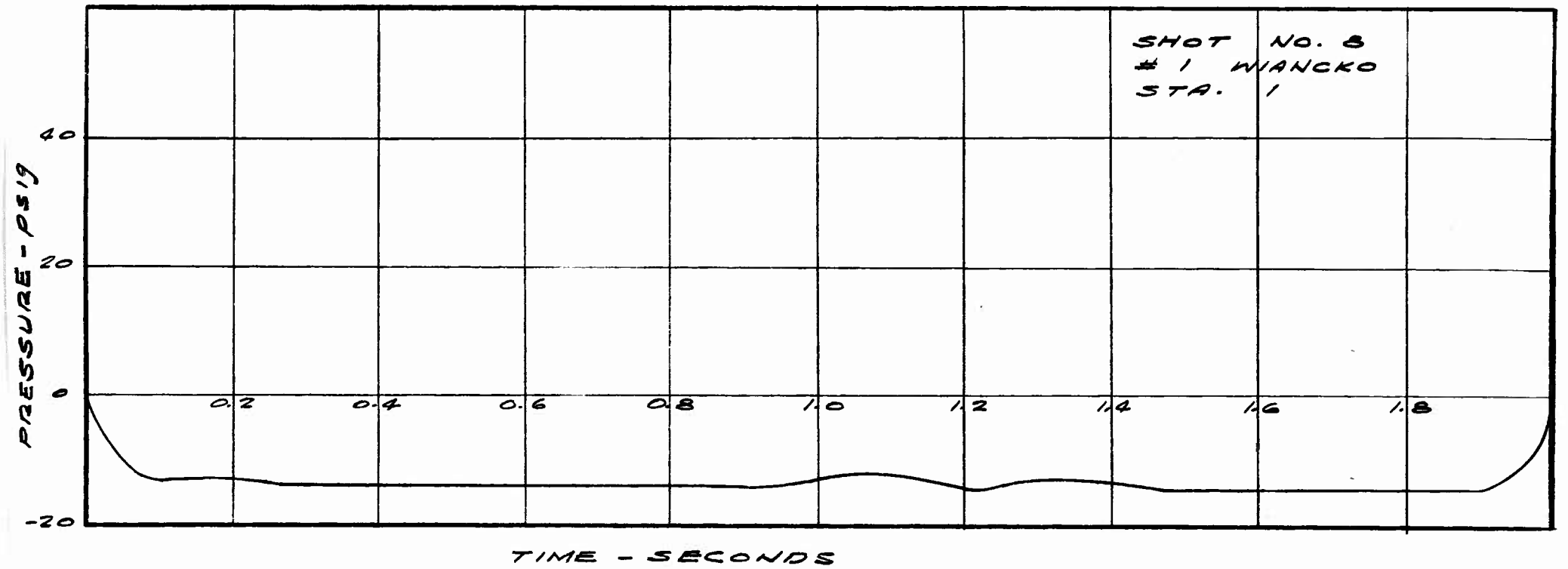

FIGURE A. 27. STATIC PRESSURE, STATION 1, TEST 8

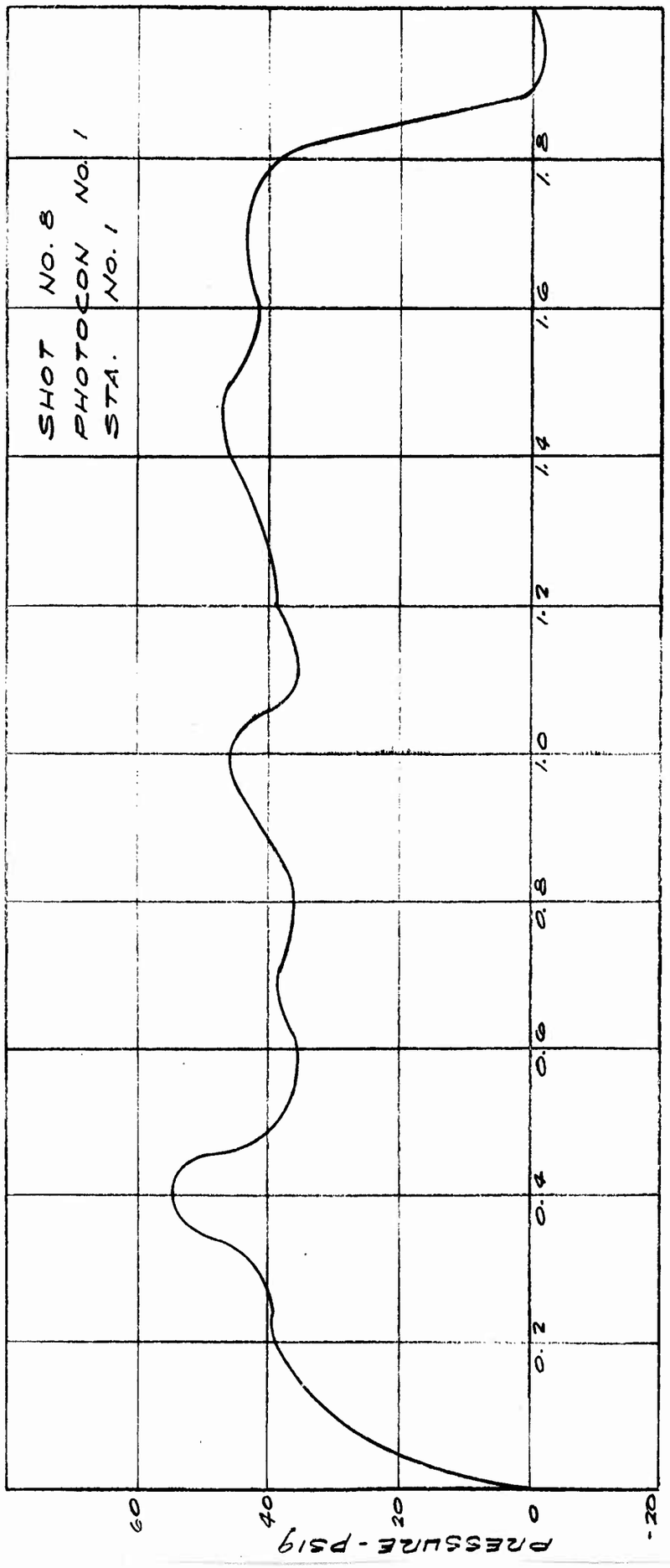

FIGURE A. 28. STAGNATION PRESSURE, STATION 1, TEST 8

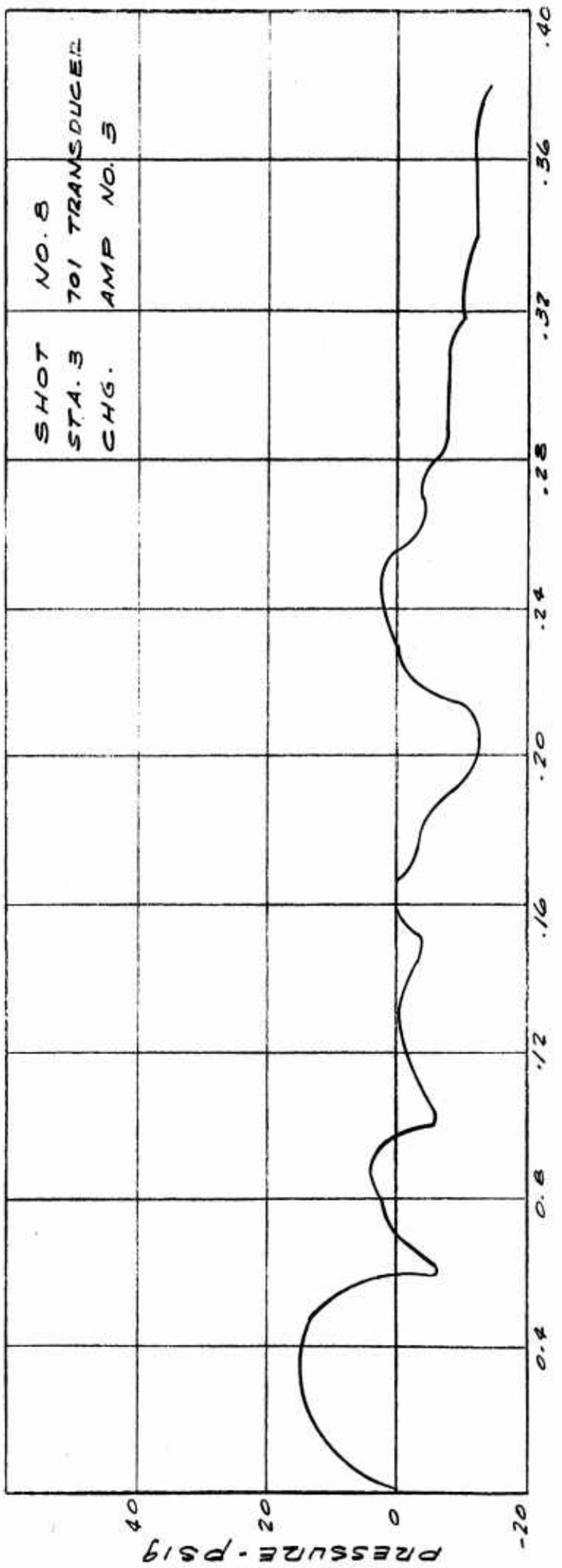

FIGURE A. 29. STAGNATION PRESSURE, STATION 3, TEST 8

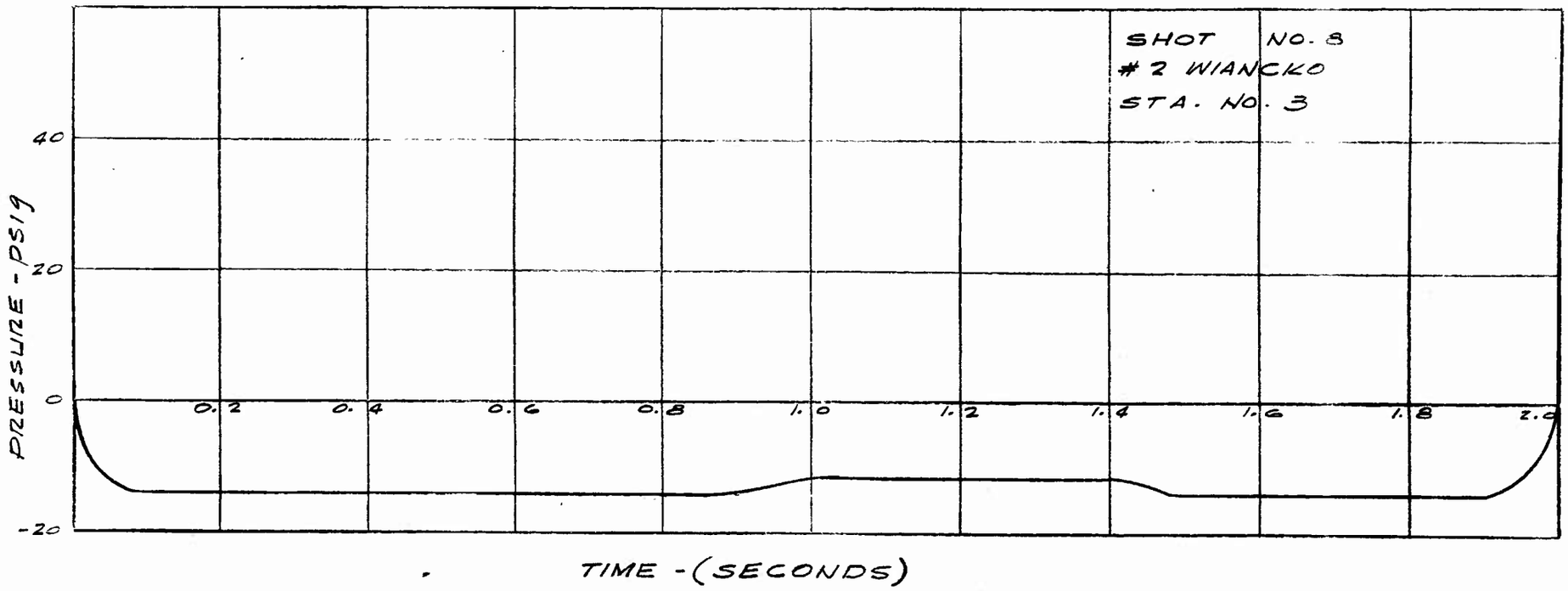

NOTE: 0.1 - 0.8 PRESS. READ LESS THAN -14.5 PSIG

FIGURE A. 30. STATIC PRESSURE, STATION 3, TEST 8

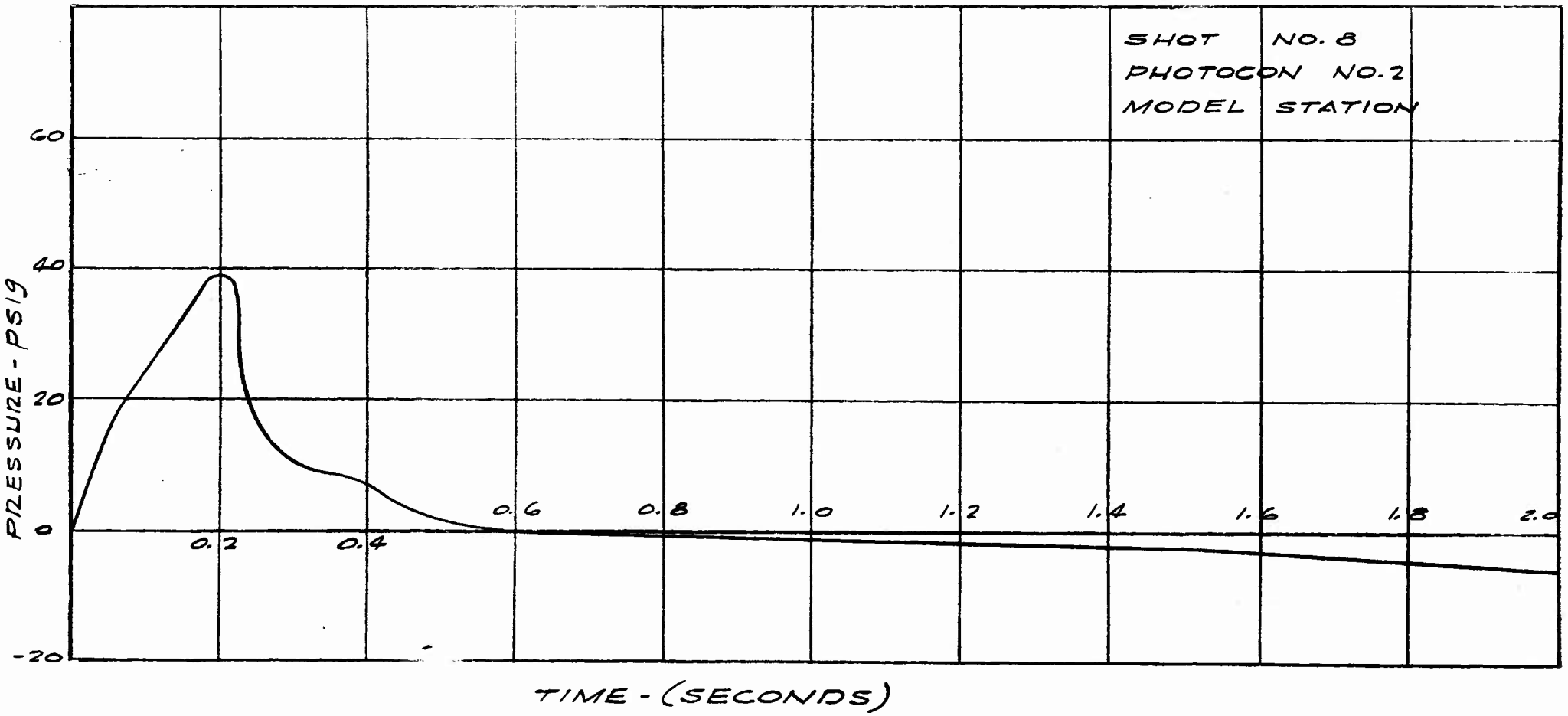

FIGURE A. 31. 0° MODEL PRESSURE, TEST 8

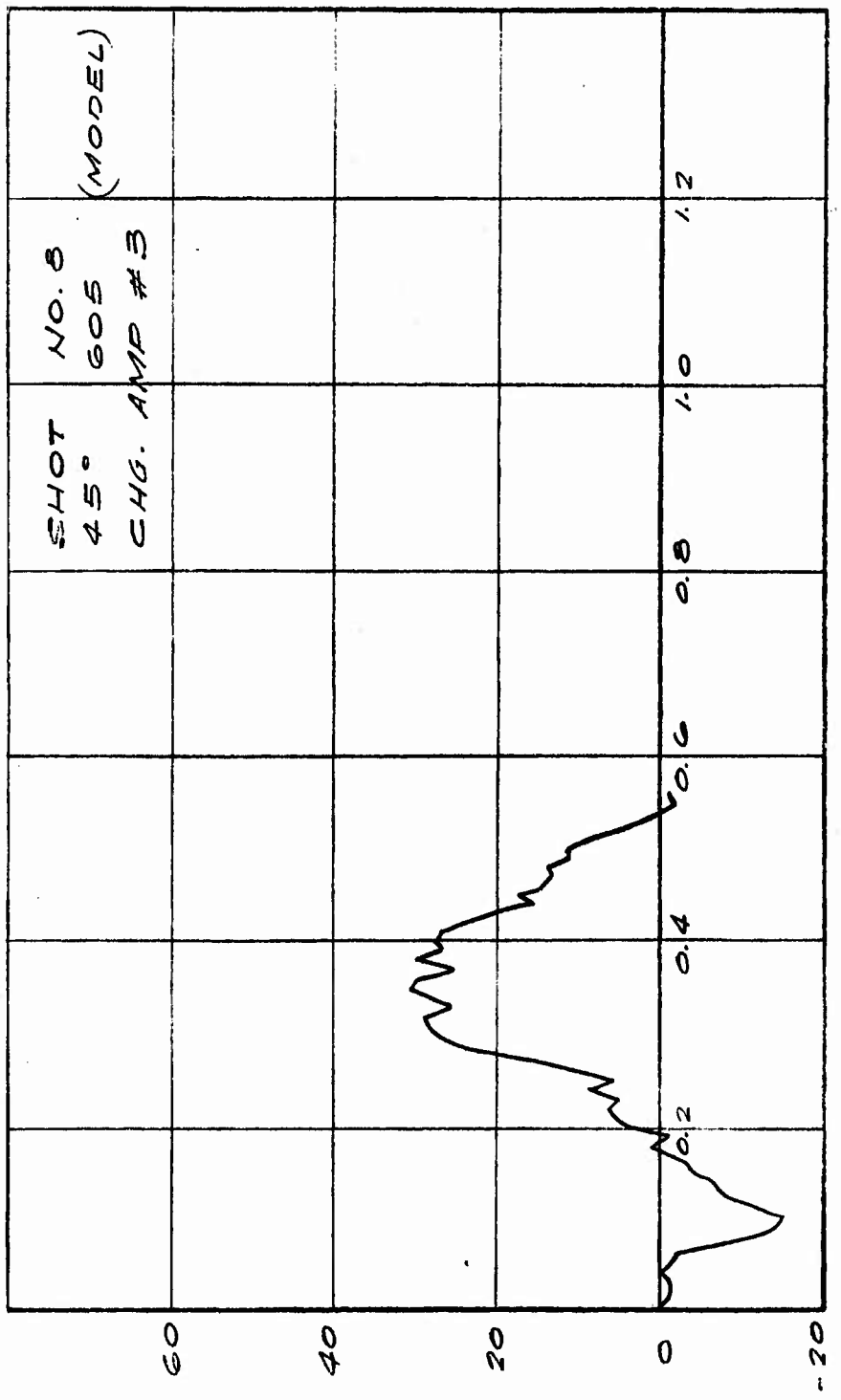

FIGURE A. 32. 45° MODEL PRESSURE, TEST 8

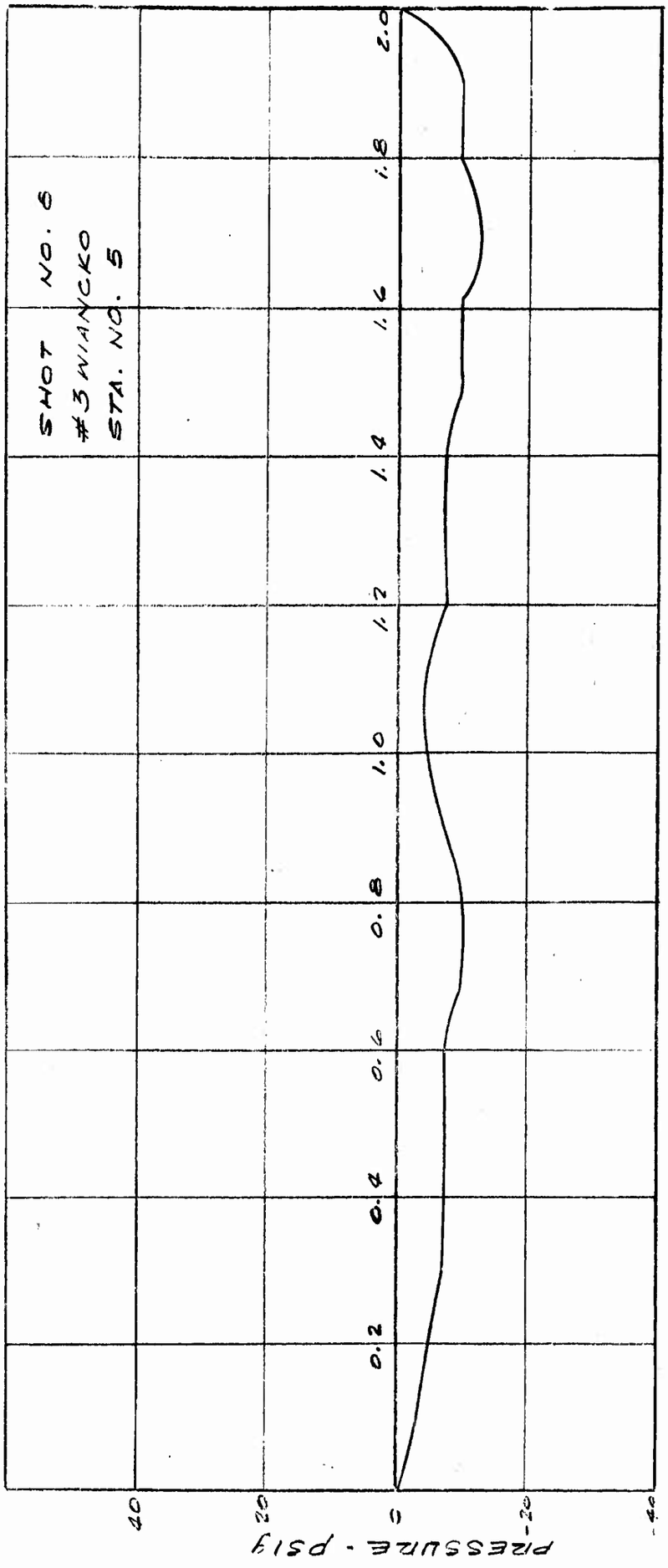

FIGURE A.33. STATIC PRESSURE, STATION 3, TEST 8

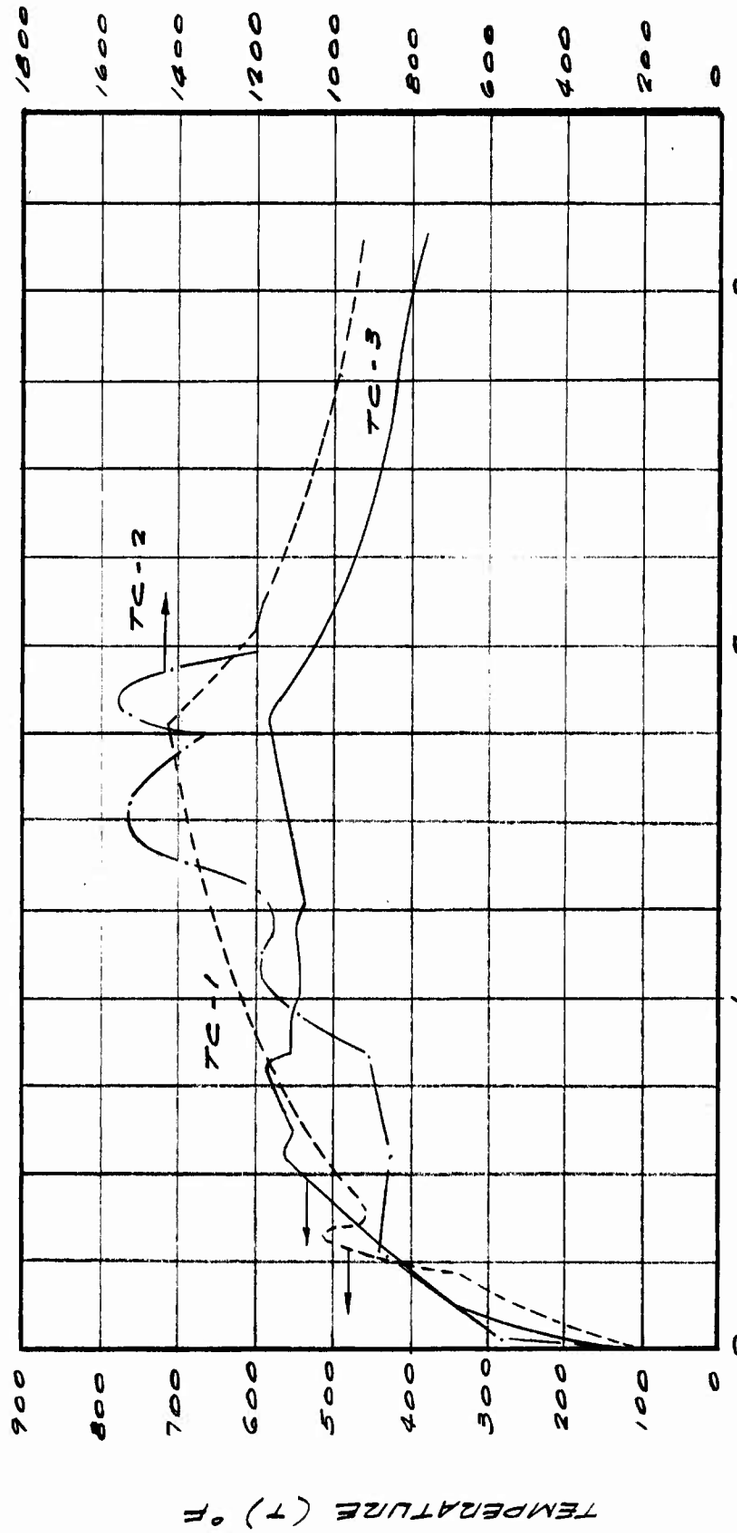

FIGURE A.34. TEMPERATURE RESULTS, TEST 8

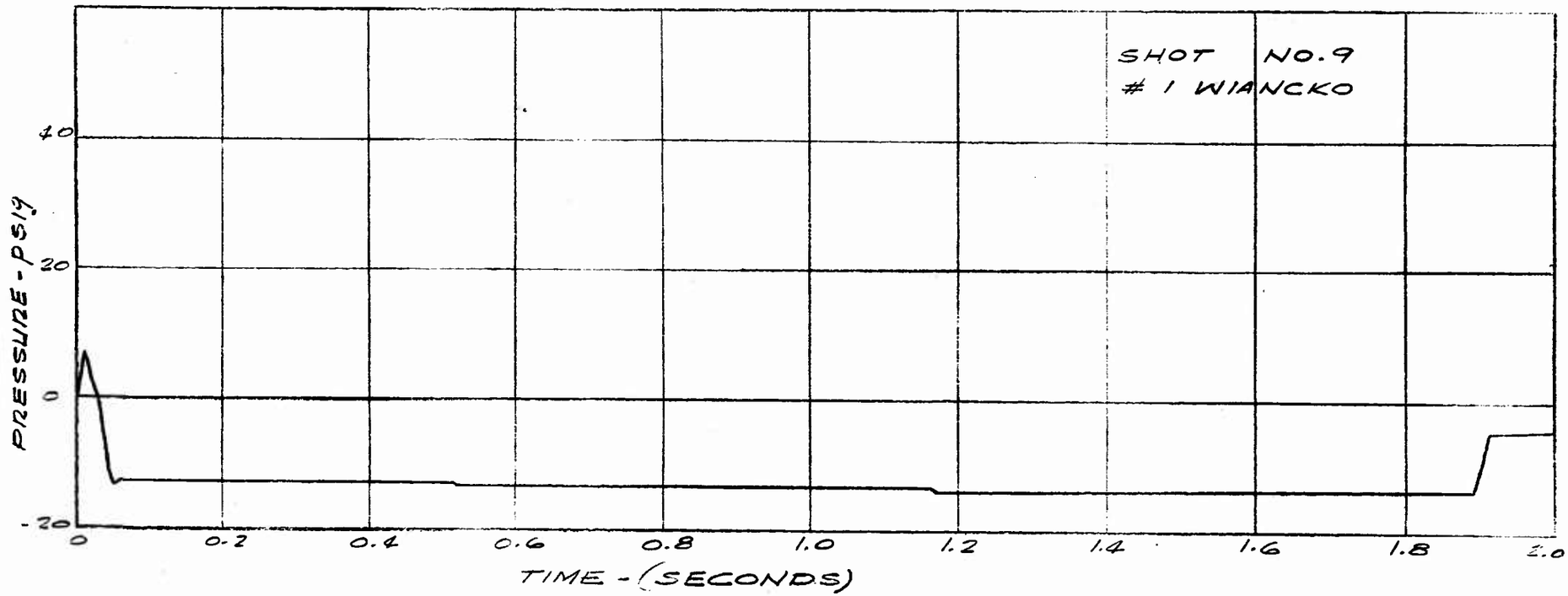

FIGURE A. 35. STATIC PRESSURE, STATION 1, TEST 9

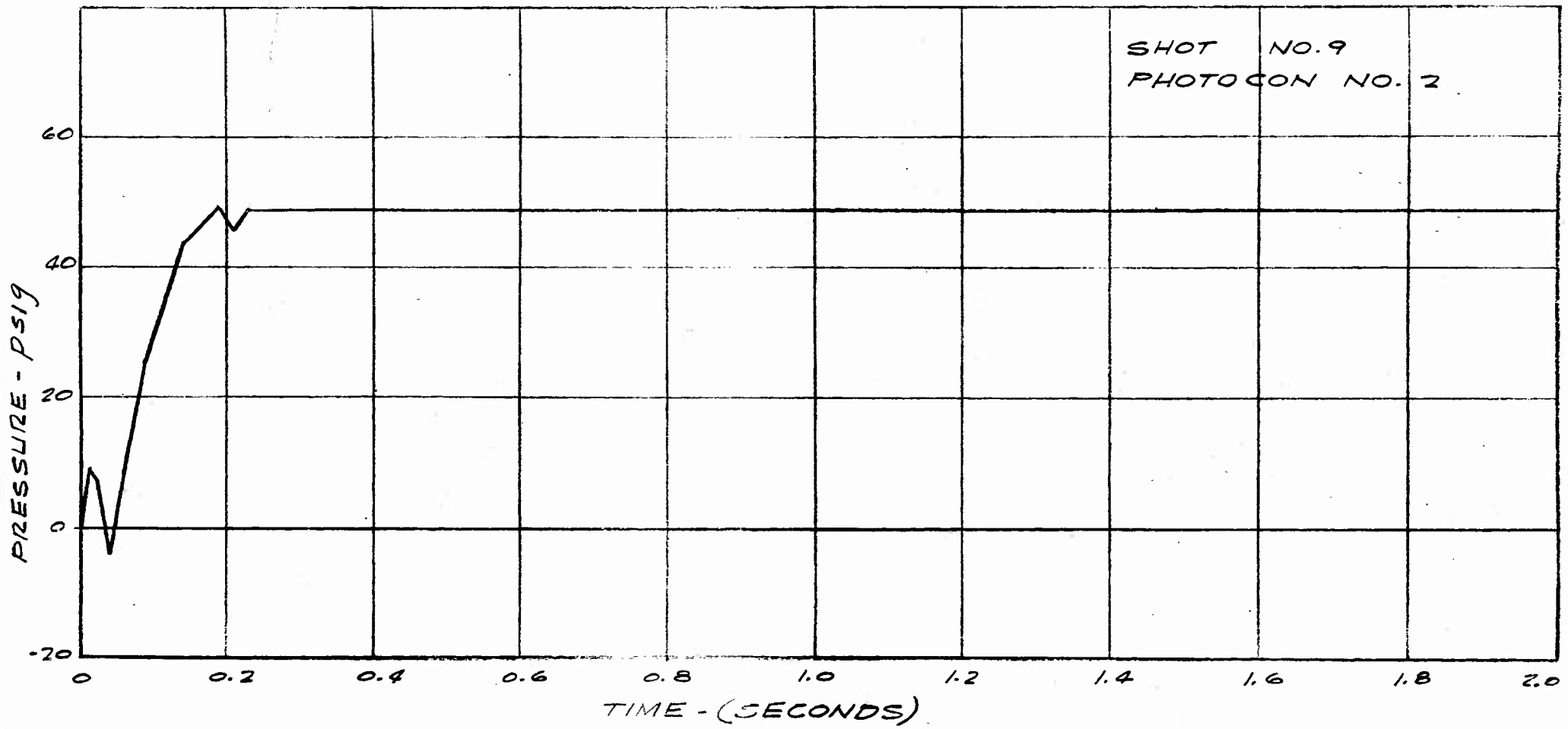

FIGURE A. 36. STAGNATION PRESSURE, STATION 1, TEST 9

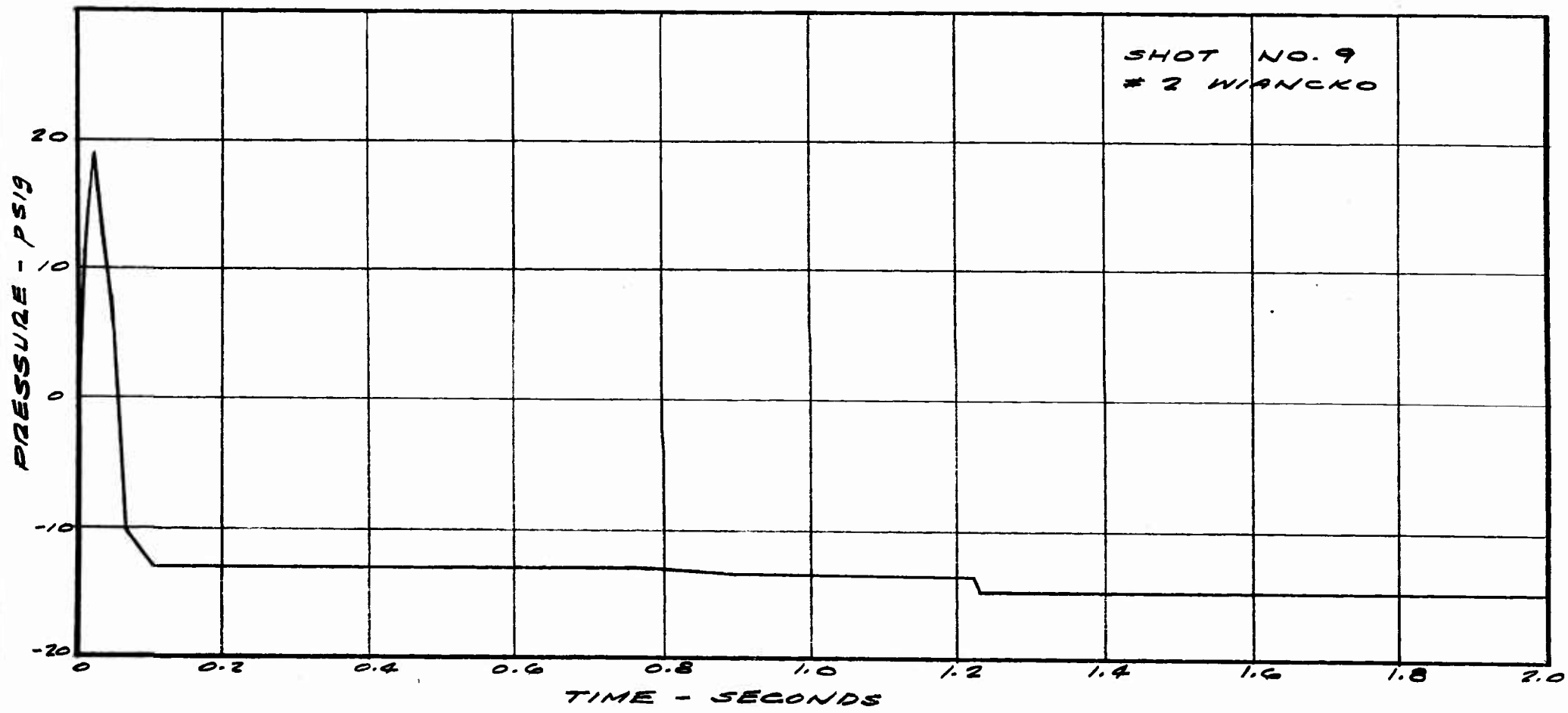

FIGURE A. 37. STATIC PRESSURE, STATION 3, TEST 9

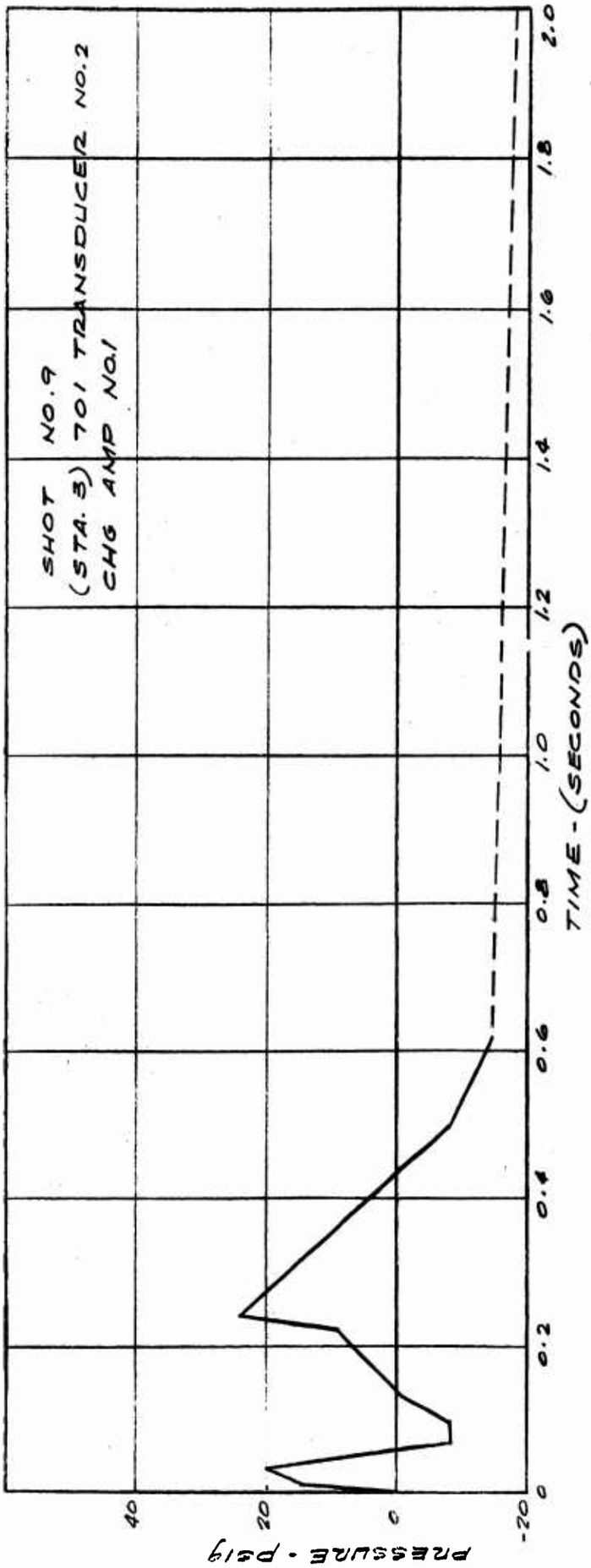

FIGURE A. 38. STAGNATION PRESSURE, STATION 3, TEST 9

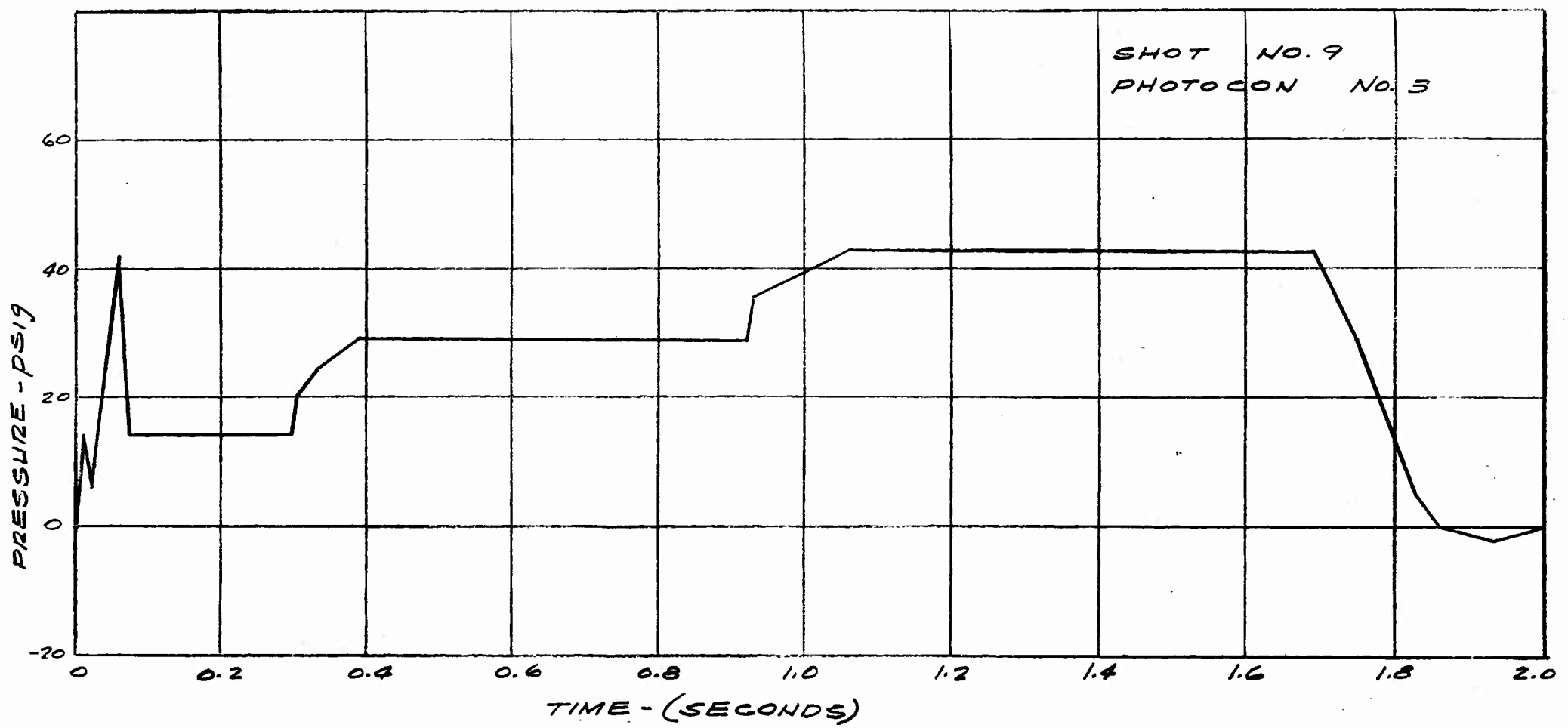

FIGURE A-39. STAGNATION PRESSURE, STATION 3, TEST 9

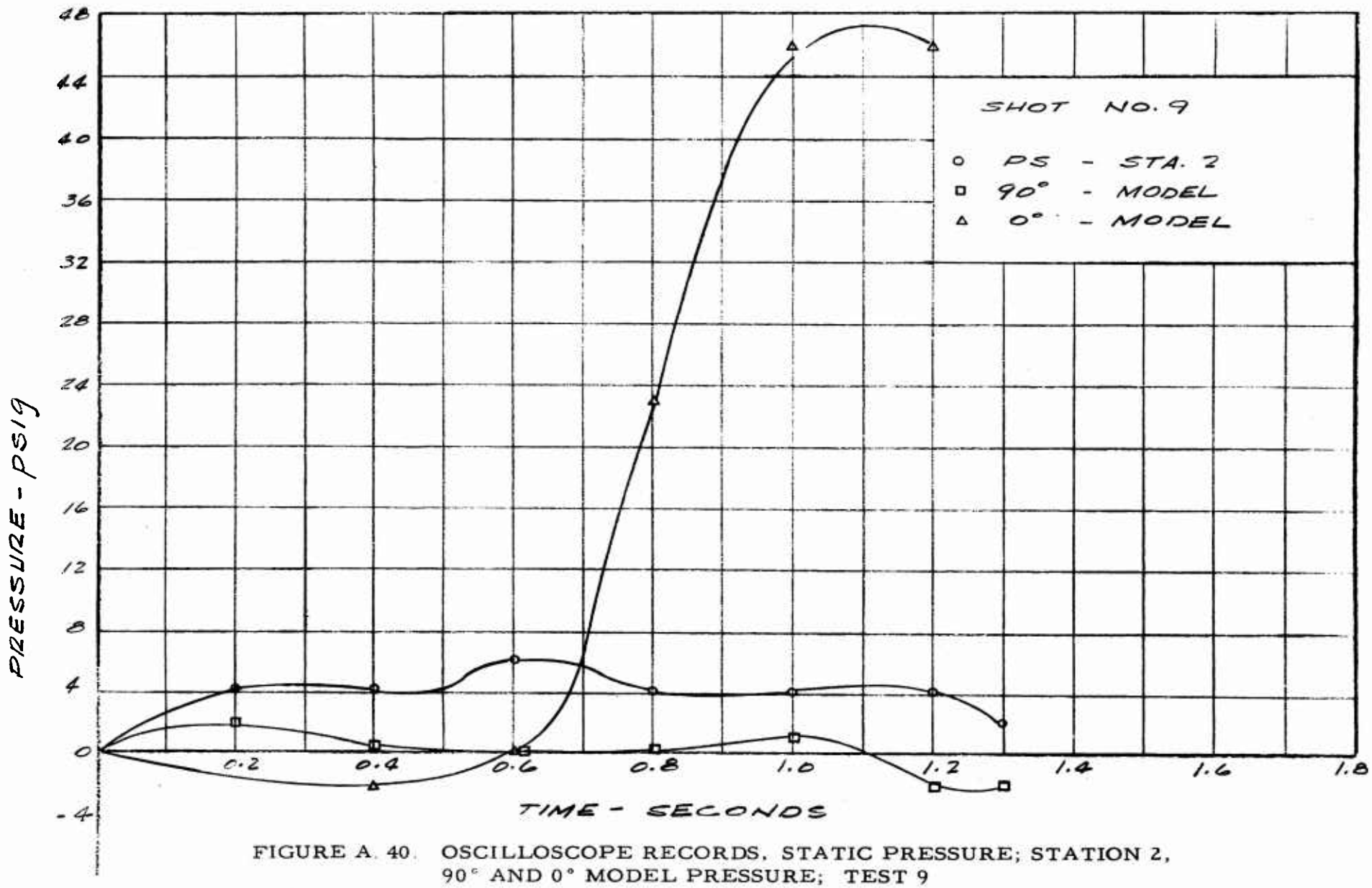

FIGURE A. 40. OSCILLOSCOPE RECORDS, STATIC PRESSURE; STATION 2, 90° AND 0° MODEL PRESSURE; TEST 9

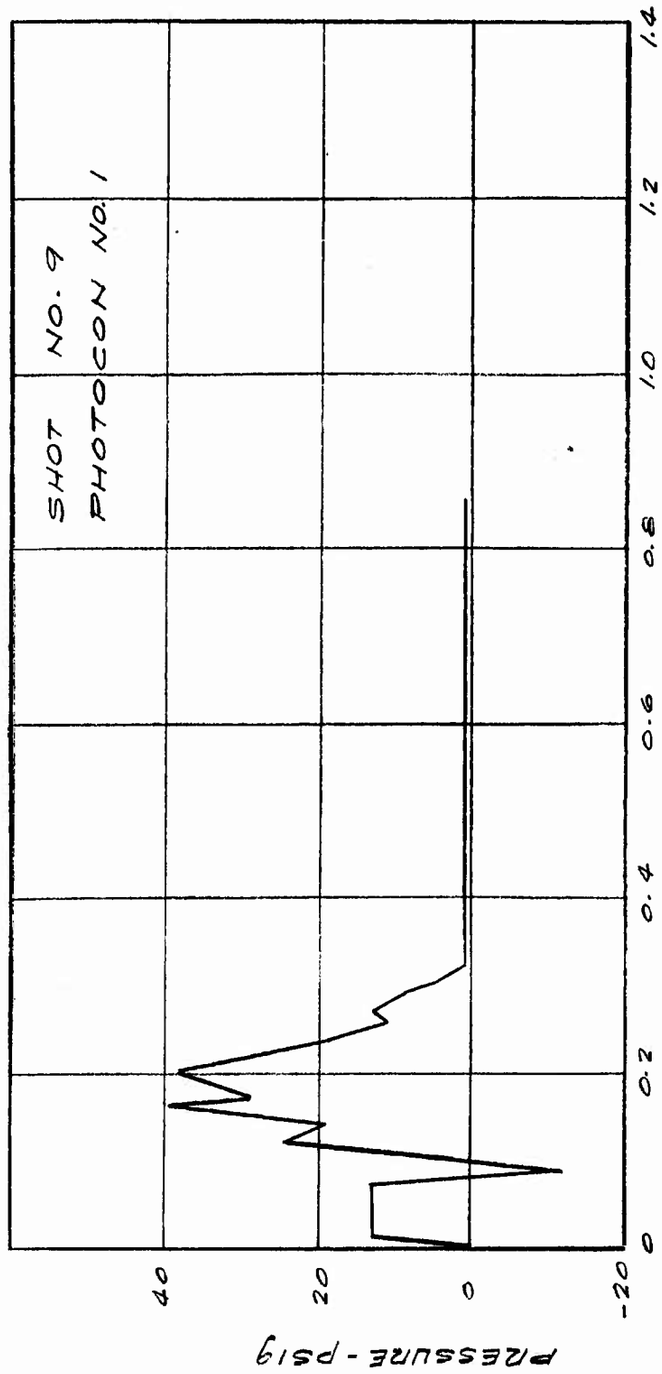

FIGURE A.41. 0° MODEL PRESSURE, TEST 9

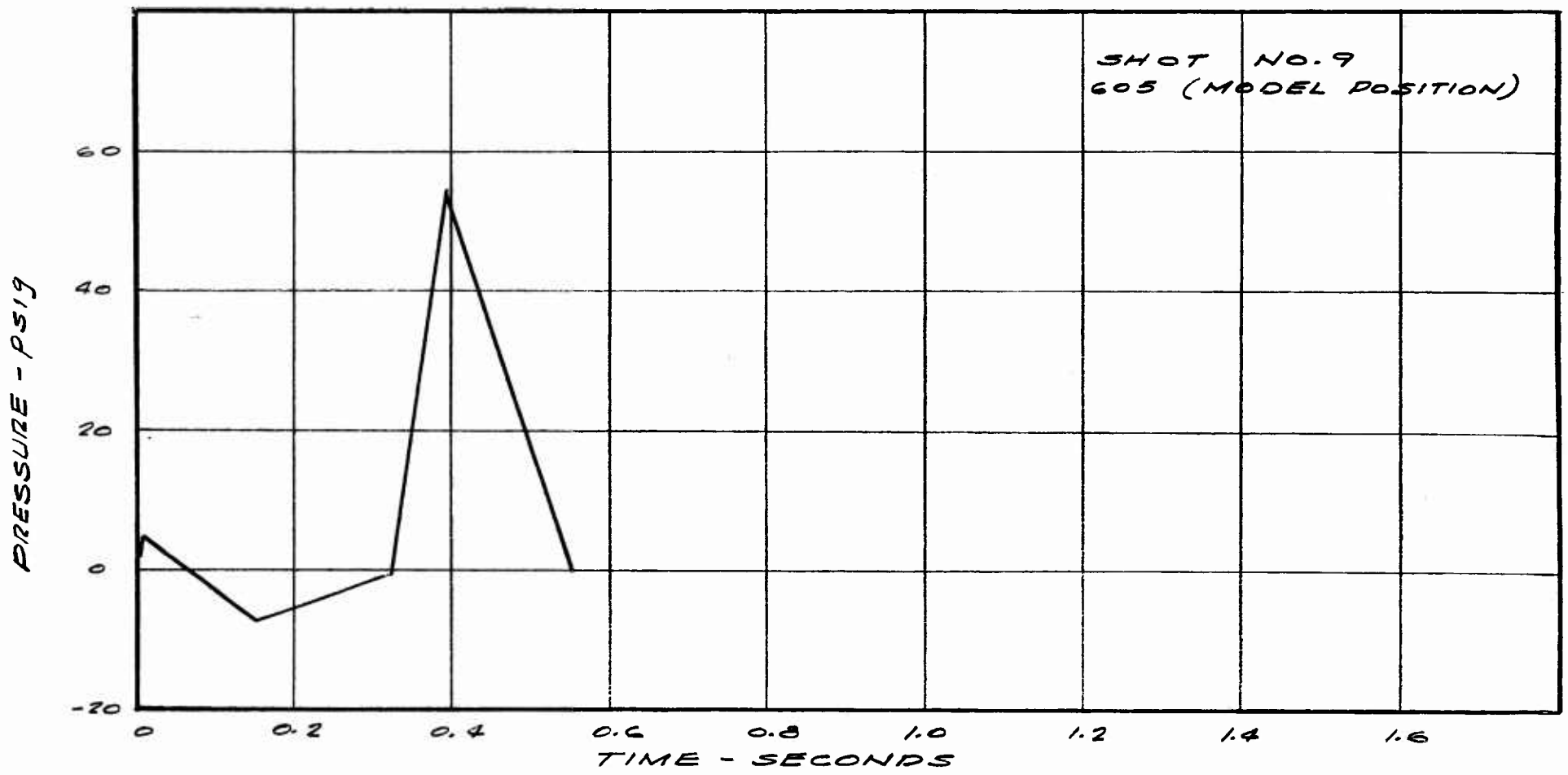

FIGURE A.42. 45° MODEL PRESSURE, TEST 9

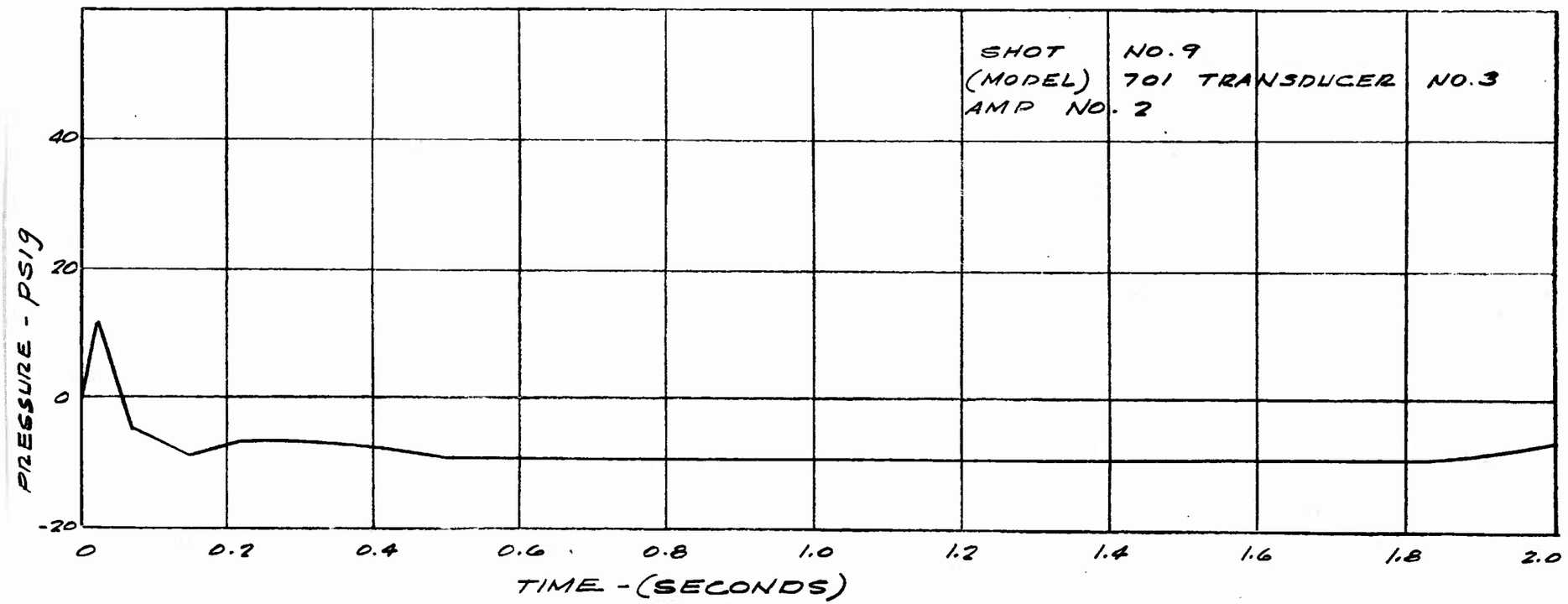

FIGURE A. 43. STATIC PRESSURE, MODEL STATION, TEST 9

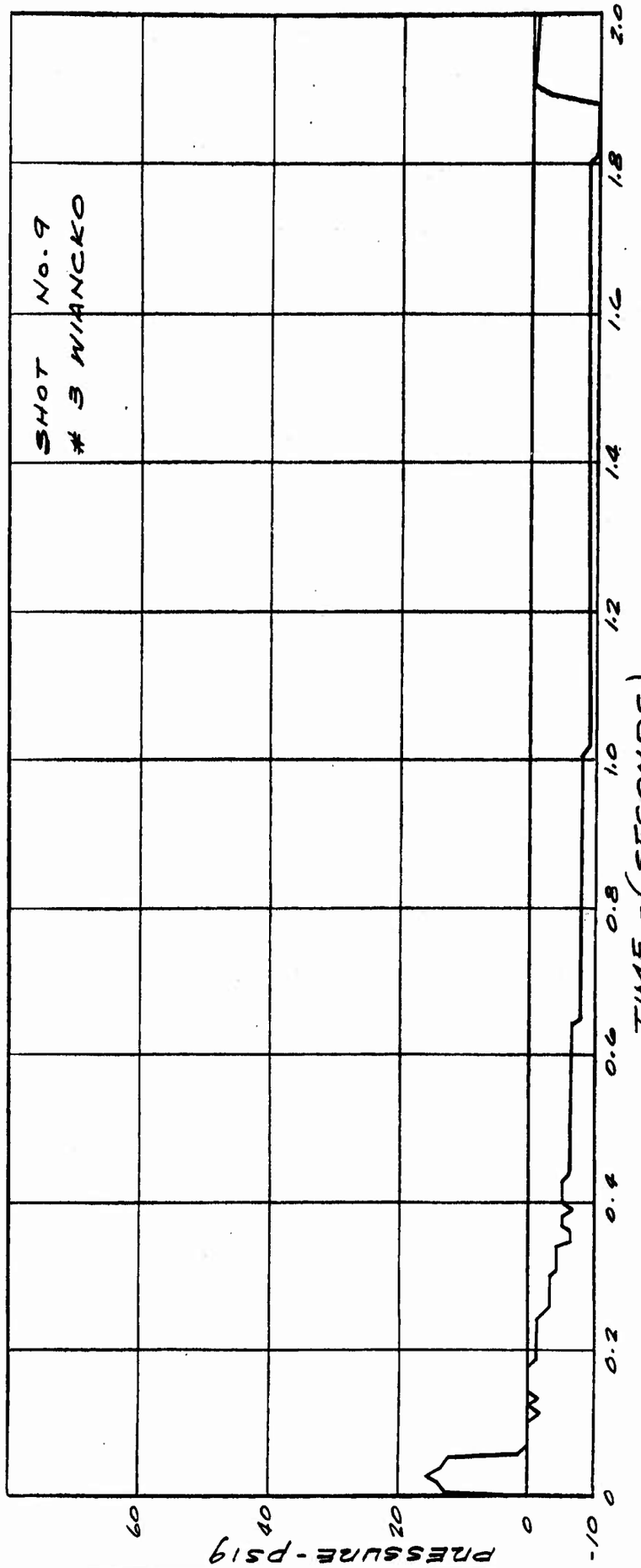

FIGURE A. 44. STATIC PRESSURE, STATION 5, TEST 9

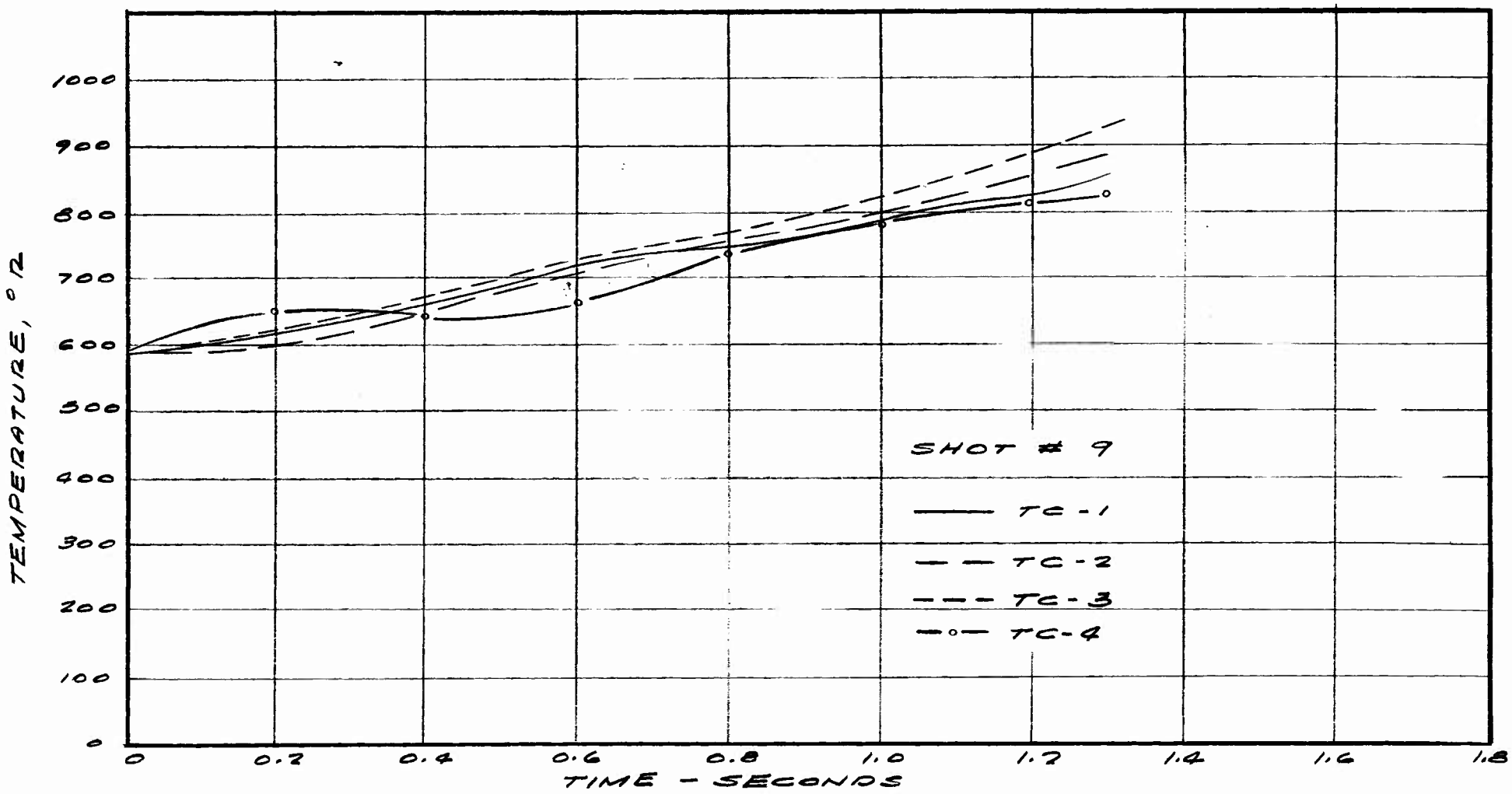

FIGURE A. 45. THERMOCOUPLE MEASUREMENTS, TEST 9 RH/RR-4

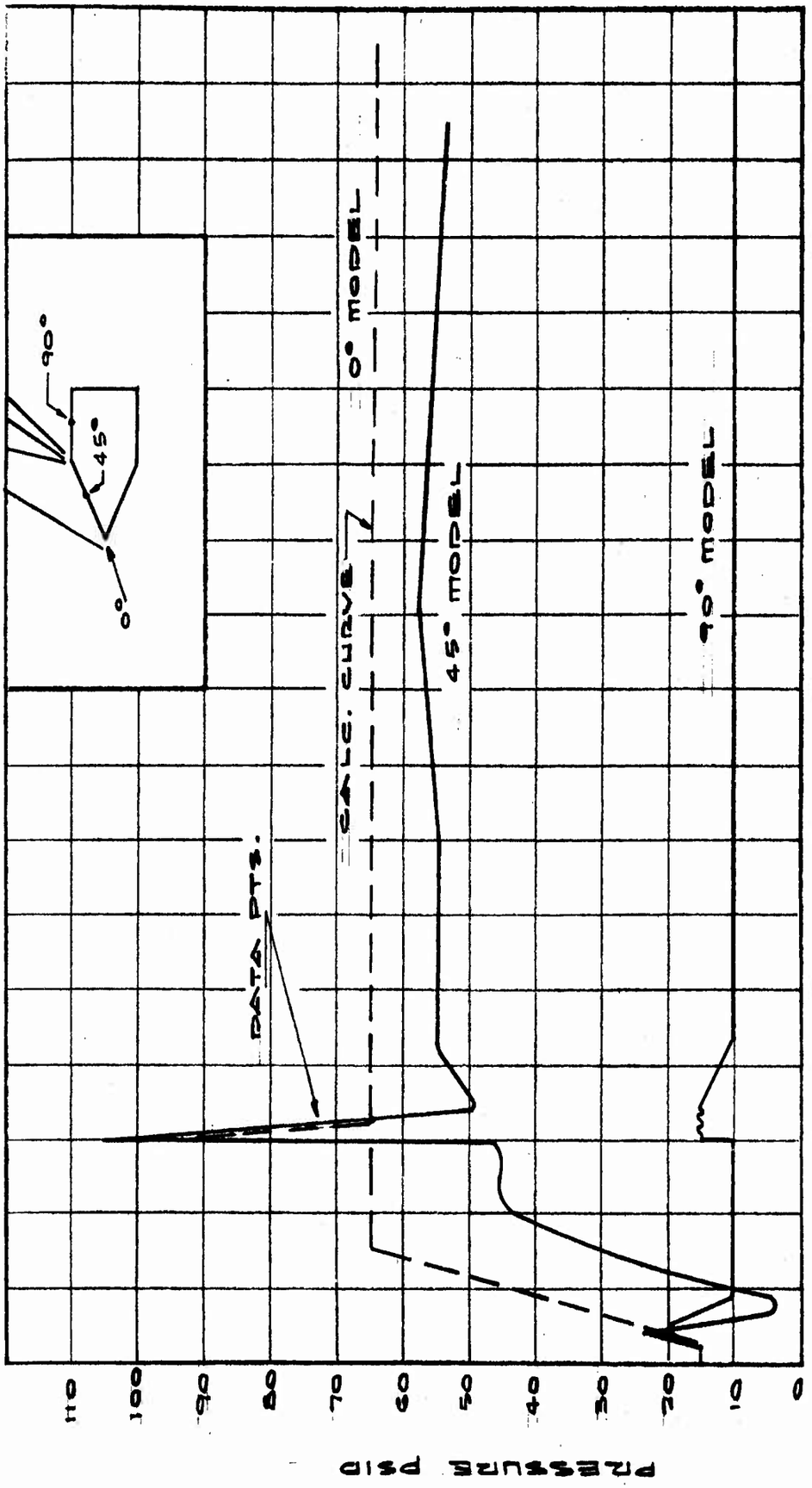

FIG. A46 MODEL PRESSURES, TEST 12

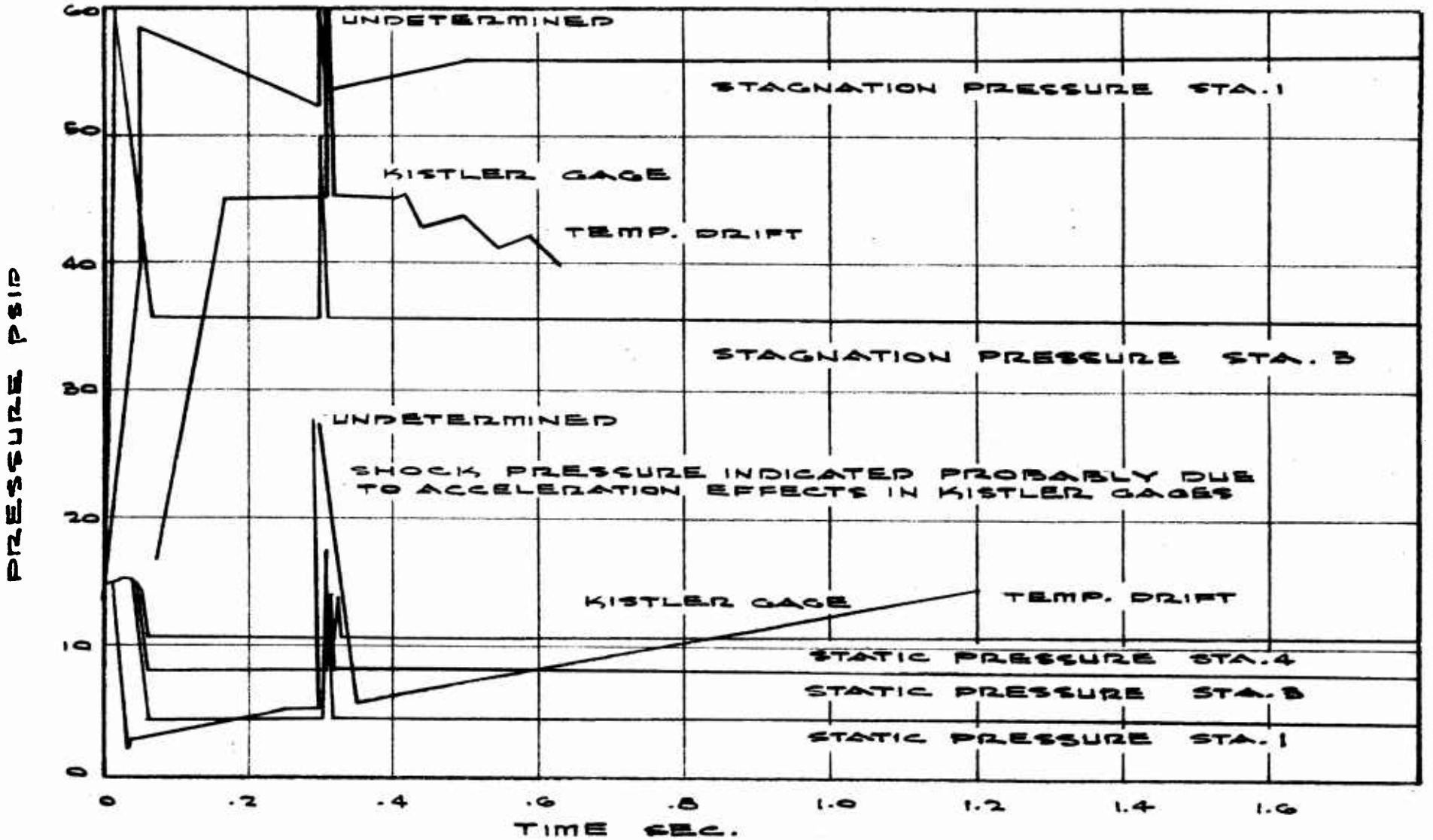

FIG. A47 STATIC AND STAGNATION PRESSURES IN TUNNEL, TEST 12

APPENDIX B

AN ULTRASONIC INSTRUMENTATION SYSTEM FOR MEASURING ROCKET MOTOR EXHAUST VELOCITY AND TEMPERATURE

P. F. Law
T. E. Owen

ABSTRACT

An ultrasonic pulse technique for measuring stream velocity and free stream temperature in a confined rocket motor exhaust is described. The temperatures were calculated from the measured sound velocity under assumptions of uniform flow and zero temperature gradient across the flow. These calculations also include the assumption that nonidealistic dissociations and relaxations do not cause appreciable effects on the sound velocity at the temperatures involved. Temperatures determined with this technique ranged to 2400°F, and flow velocities of Mach three were observed. The theoretical considerations, instrumentation techniques and experimental results are presented in this Appendix. Unfortunately, much data was lost due to lack of prior knowledge concerning inherent flow noise levels.

I. INTRODUCTION

Although the ultrasonic pulse technique of temperature measurement is straightforward in theory, several unique considerations and instrumentation problems appeared due to the adverse environmental conditions of this program. The relatively long transmission distances and the thermal shock and flow noise to which the transducers were exposed created problems not encountered in some related experiments. The use of velocity of sound measurements in temperature determinations has been successfully applied by Suits[17, 14*] at General Electric for determination of arc temperatures. Livengood[10] et al. describe a technique of measurement of internal combustion engine chamber temperature using an ultrasonic technique. Recently, Carnevale[4] and associates at Avco Corporation made use of an ultrasonic pulse technique for temperature determinations in a plasma jet. These experiments were similar to the technique described in this report except that, previously, the velocity of the medium involved was not of concern.

The experimental program in this case concerned the measurement of stream velocity and free stream temperature of a rocket motor exhaust confined in a long, straight tube of circular cross-section. The nominal tube dimensions were 8 inches in diameter by 100 feet long. A single instrumentation station was located near the driven end of the tube where

---

*Numbers refer to BIBLIOGRAPHY AND REFERENCES at end of Appendix.

stream temperatures to 4000°F and velocities to Mach 4 were expected. Instrumentation was developed for the measurement of the time-of-transit of a sharp pressure impulse from a source located in the pipe wall to two separated receivers located across the tube and downstream of the Mach angle. The spherical pressure front emitted by the source expands at the local sound velocity and is swept along at the stream velocity to impinge on the receivers at transit times that are then relatable to these velocities of sound and flow.

II. THEORY

The propagation of sound in a supersonically flowing medium presents several unique considerations. The experimental program discussed here concerns the measurement of time-of-transit of an acoustic impulse across a supersonic flow. The flowing medium is confined to a pipe of circular cross section and of considerable length. If an acoustic impulse is emitted from an omnidirectional source located in the pipe wall (but insulated from the wall), the spherically divergent wave front is swept along the pipe at the flow velocity. A two-dimensional schematic indicating the direct ray effects in the longitudinal pipe section is shown in Figure B. 1. This figure shows the wave front location (primary effect) after a certain time period, t , along with smaller circular arcs indicating past history of the wave front location. A receiving transducer located diametrically opposite the impulse source and downstream of the Mach angle receives the direct ray effect after a time period that is related to the stream velocity and local sound velocity. If the assumption of zero stream velocity gradient and zero local sound velocity gradient across the flow is made (as is intrinsically indicated in the schematic representation of Figure B. 1), the local sound velocity and stream velocity may be readily deduced from the time lapse between impulse emission and direct ray reception for two paths across the flow.

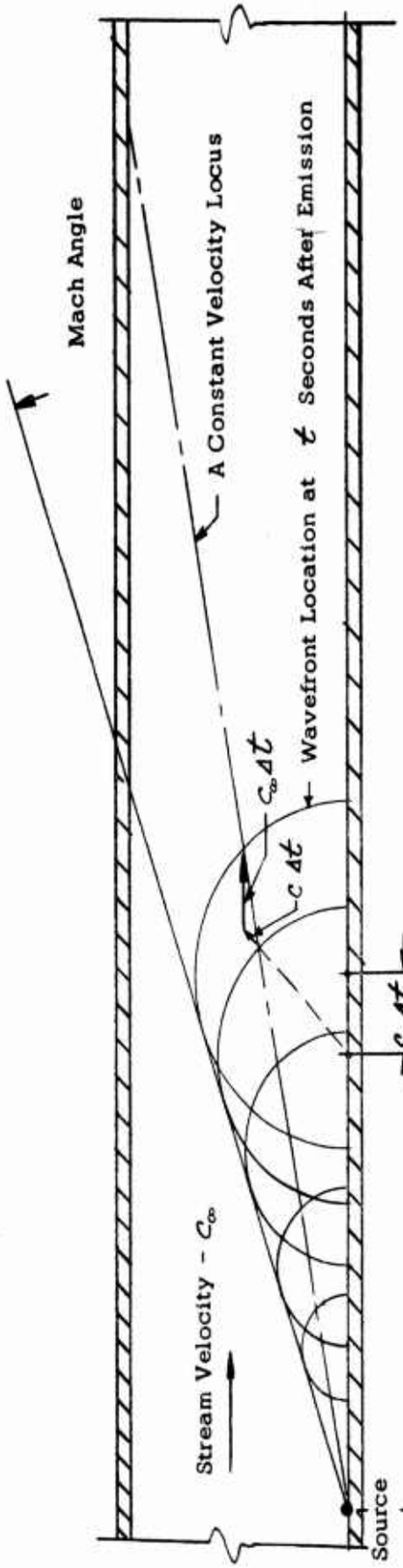

FIGURE B. 1. A PROGRESSIVE WAVEFRONT IN A SUPERSONICALLY FLOWING MEDIUM

A. Determination of Stream Velocity and Local Sound Velocity

The calculations of stream velocity and local sound velocity are based on the assumptions of uniform flow and constant magnitude sound velocity throughout the region of flow under consideration. Under these assumptions, the single transmitter, two receiver configuration of Figure B.2 affords a method of determination of stream velocity, V_∞, and local sound velocity, C, based on apparent propagation velocity along the paths XA and XB. These paths are the shortest time paths from X to A and B, respectively, and the velocities along XA and XB (designated as $\bar{v}_a$ and $\bar{v}_b$) are given by

$$(1) \quad \bar{v}_a = \bar{c}_v + \bar{c}_\infty$$

$$(2) \quad \bar{v}_b = \bar{c}_b + \bar{c}_\infty$$

where the designations $\bar{c}_a$ and $\bar{c}_b$ refer to the vector velocities of the spherical wave front along points lying on the loci XA and XB, respectively. The stream velocity, $\bar{c}_\infty$, is a constant vector throughout the region of flow. The solution of these simultaneous vector equations for the magnitudes $|\bar{c}_a| = |\bar{c}_b| \equiv c$ and $|\bar{c}_\infty| \equiv |c_\infty|$ is made more apparent through the representation of Figure B.3. Here it is seen that the relation

$$(3) \quad (x - c_\infty)^2 + y^2 = c$$

must be satisfied for the two conditions of

$$(4a) \quad (x, y) = (v_a \cos \theta_a, \; v_a \sin \theta_a)$$

$$(4b) \quad (x, y) = (v_b \cos \theta_b, \; v_b \sin \theta_b)$$

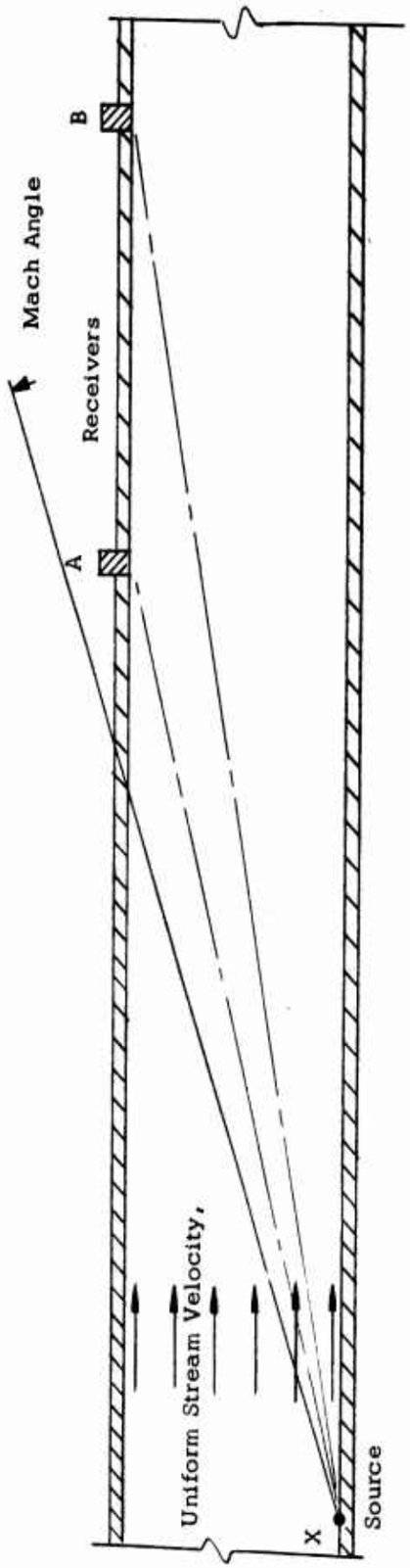

FIGURE B.2. SINGLE TRANSMITTER, TWO RECEIVER METHOD OF INSTRUMENTATION

A substitution of these points leads at once to the conclusion that

$$(5) \qquad c_\infty = \frac{v_b^2 - v_a^2}{2(v_b \cos\theta_b - v_a \cos\theta_a)}$$

from which, in conjunction with the geometry of Figure B.3., it may be inferred that

$$(6) \qquad c = [v_b^2 + c^2 - 2v_b c \cos\theta_b]^{1/2}$$

The parameters θ_a, θ_b, XA, and XB are known from the geometrical layout of the transmitting and receiving transducers. The velocities $v_a = \frac{XA}{t_a}$ and $v_b = \frac{XB}{t_b}$ are then available from the measured data t_a and t_b, the time lapse between transmission and reception of a pressure impulse along the two paths.

The discussions to this point have presented a technique for determination of stream velocity and local sound velocity in a uniform flow based on time of transit of a pressure impulse from a transmitting source to a separated pair of receivers.

B. Determination of Temperature

In an ideal gas mixture which obeys the perfect gas laws, the velocity of sound is related to temperature by the relation

$$(7) \qquad C = \sqrt{\frac{RT\gamma}{M}}$$

where R is the universal gas constant, T is the absolute temperature, γ is the ratio of specific heats and M is the mean molecular weight of the gas mixture. The application of Equation (7) must be made with

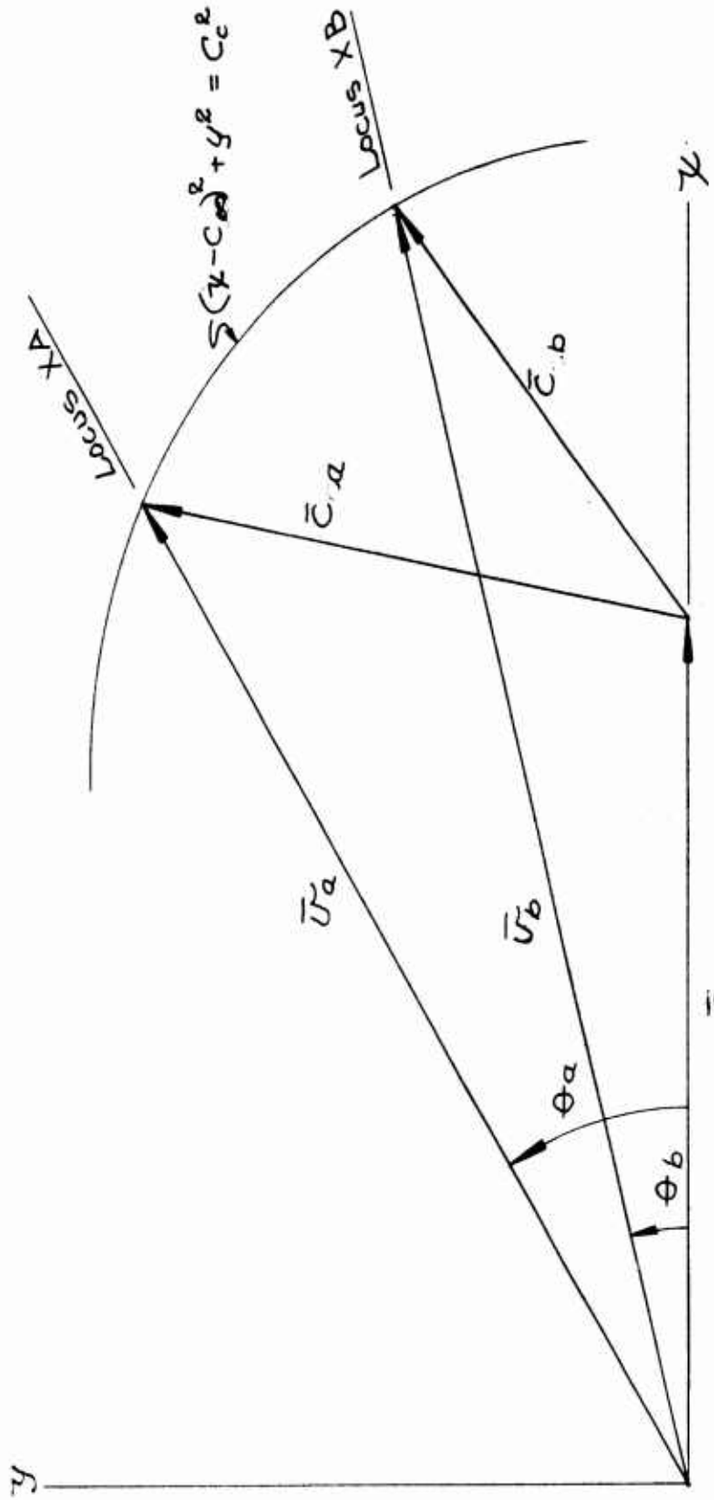

FIGURE B.3. VECTOR REPRESENTATION OF PRESSURE FRONT VELOCITIES ALONG THE CONSTANT VELOCITY LOCI XA & XB

caution as certain dispersive and other nonidealistic phenomena may invalidate the results derived on this simple basis.

To calculate the velocity of sound in a polyatomic gas at high temperatures, it is necessary to know the gas constituents in order to determine the mean molecular weight and the ratio of specific heats. However, at sufficiently high temperatures, the gas molecules tend to dissociate as well as become ionized, changing the basic gas density and the condition of equilibrium. The specific heats also vary with increasing temperature because of energy absorption by atomic and electron vibrations. From work done by Suits[17, 14] on high temperature electric arcs and by Carnevale[4], et al., on plasma jets operating at temperatures up to 8000°K, it was found that less than one per cent dissociation occurred in air at temperatures up to about 4800°F, with the most sensitive molecule being oxygen. Since the flame temperatures of the rocket propellants were not expected to exceed a temperature of 4200°F, dissociation of the rocket motor exhaust gas constituents was neglected as well as ionization effects. Thus, by assumption of constant partial pressures for the various gas constituents, the total specific heat at constant volume for the gas mixture was computed as a function of temperature using standard tables giving the physical properties of the various combustion products.

To facilitate calculations of temperature from the measured local sound velocity, the graphs of Figure B. 4 were prepared for the rocket motors

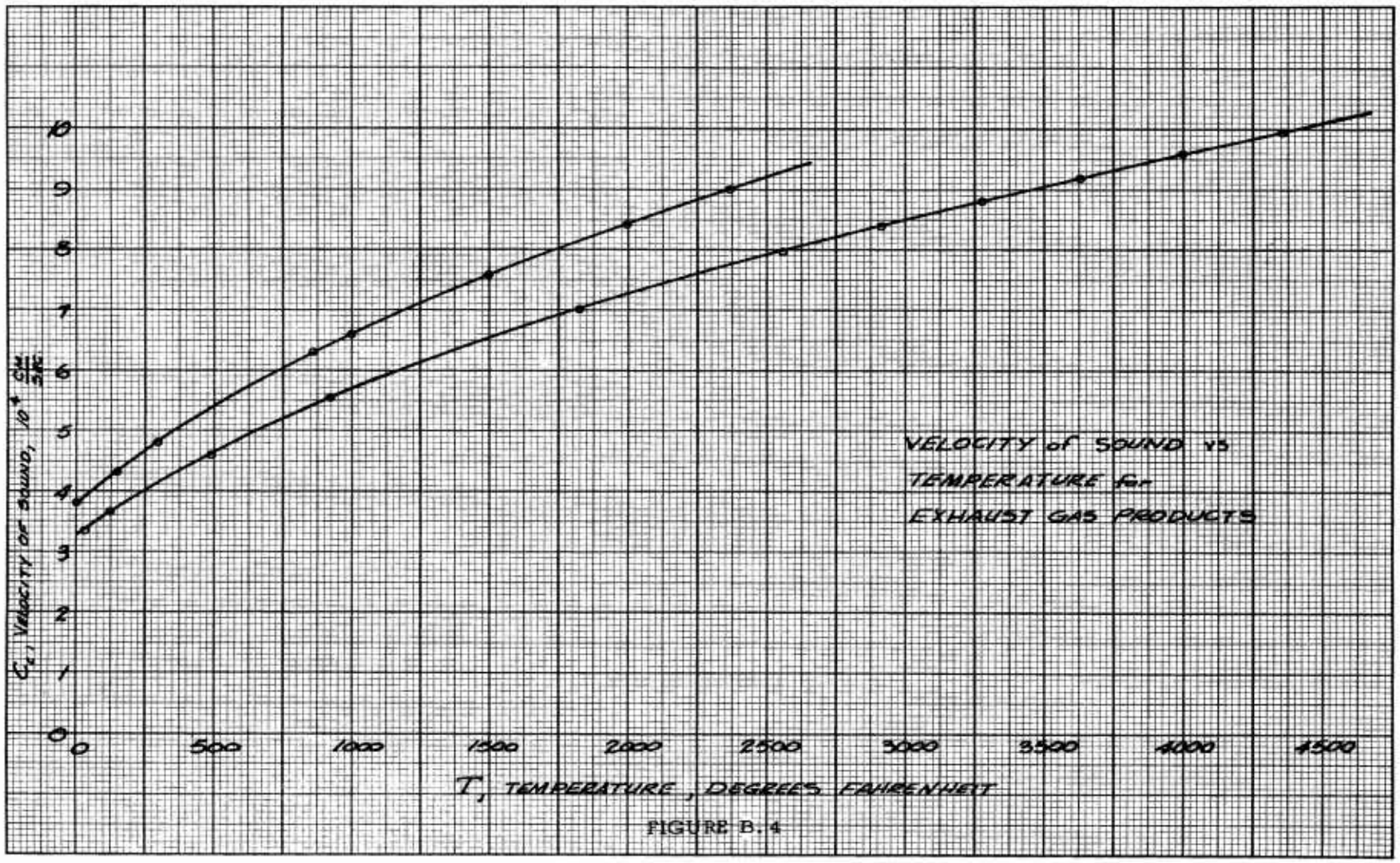
VELOCITY of SOUND vs
TEMPERATURE for
EXHAUST GAS PRODUCTS
C_s, VELOCITY OF SOUND, 10^4 $\frac{cm}{sec}$
0
1
2
3
4
5
6
7
8
9
10
0
500
1000
1500
2000
2500
3000
3500
4000
4500
T_f, TEMPERATURE, DEGREES FAHRENHEIT

FIGURE B.4

involved. These charts show graphically the solution to Equation (7). The parameters γ and M were established from the relationships

$$(8) \quad \gamma = 1 + \frac{R}{c_v}$$

where

$$c_v = \frac{\Sigma p_i c_{vi}}{\Sigma p_i}$$

$$(9) \quad M = \frac{\Sigma p_i M_i}{\Sigma p_i}$$

The definition of symbols

p_i - partial pressure of i^{th} constituent

c_{vi} - specific heat at constant volume for the component i

M_i - molecular weight of i^{th} constituent

apply in these relationships.

It may be further noted that γ is a function of temperature in that c_{vi} is temperature dependent. This variation with temperature was also included in the sound velocity determination. The rocket exhaust constituents for the two different motors as well as their ratios of specific heats as a function of temperature are given in Appendix B.1.

III. INSTRUMENTATION DEVELOPMENT

In order to acquire the necessary data for computation of flow velocity and temperature as discussed in the preceding section, an instrumentation technique for measurement of transit time of an ultrasonic impulse over two different propagation paths was developed. This technique required a single impulsive source and two receiving transducers located opposite and downstream of the source. A simplified block diagram of the various associated equipment is shown in Figure B. 5.

A. High Voltage Source

A high voltage arc discharge was employed as a means of generating an omnidirectional pressure impulse. This high voltage source was capable of discharging an energy storage up to 100 joules at ignition rates of 7. 5 or 15 impulses per second. A ceramic-metal triggered arc gap was used as a high voltage switch in this arcing circuit (see Fig. B. 6).

B. Transducers

A transmitting spark gap was constructed as indicated in Figure B. 7. The insulating body was machined from lava, then vitrified. An adjustable center electrode of brass, tipped with tungsten, was provided as a high voltage electrode, and a tungsten ground electrode was welded to the inner pipe wall.

The receiving transducers were comprised of lead-zirconate titanate piezoelectric crystals coupled to the stream through a monel bar.

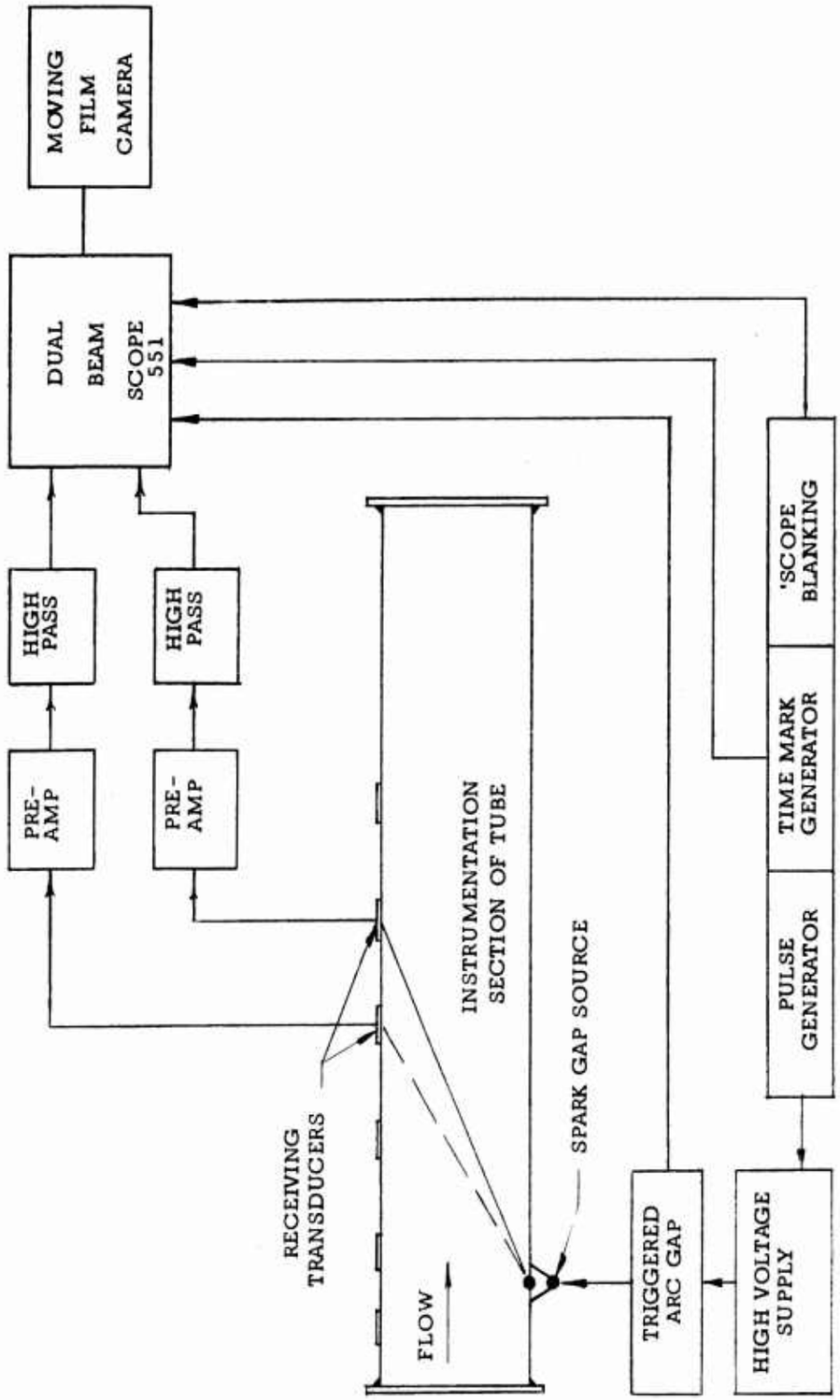

FIGURE B.5. SIMPLIFIED BLOCK DIAGRAM

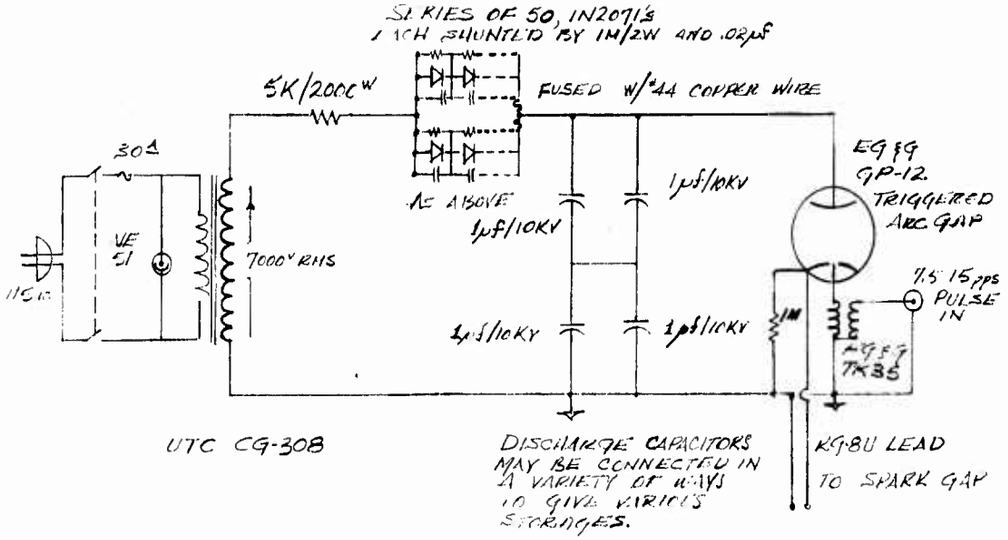

FIGURE B. 6. HIGH VOLTAGE ARCING CIRCUIT

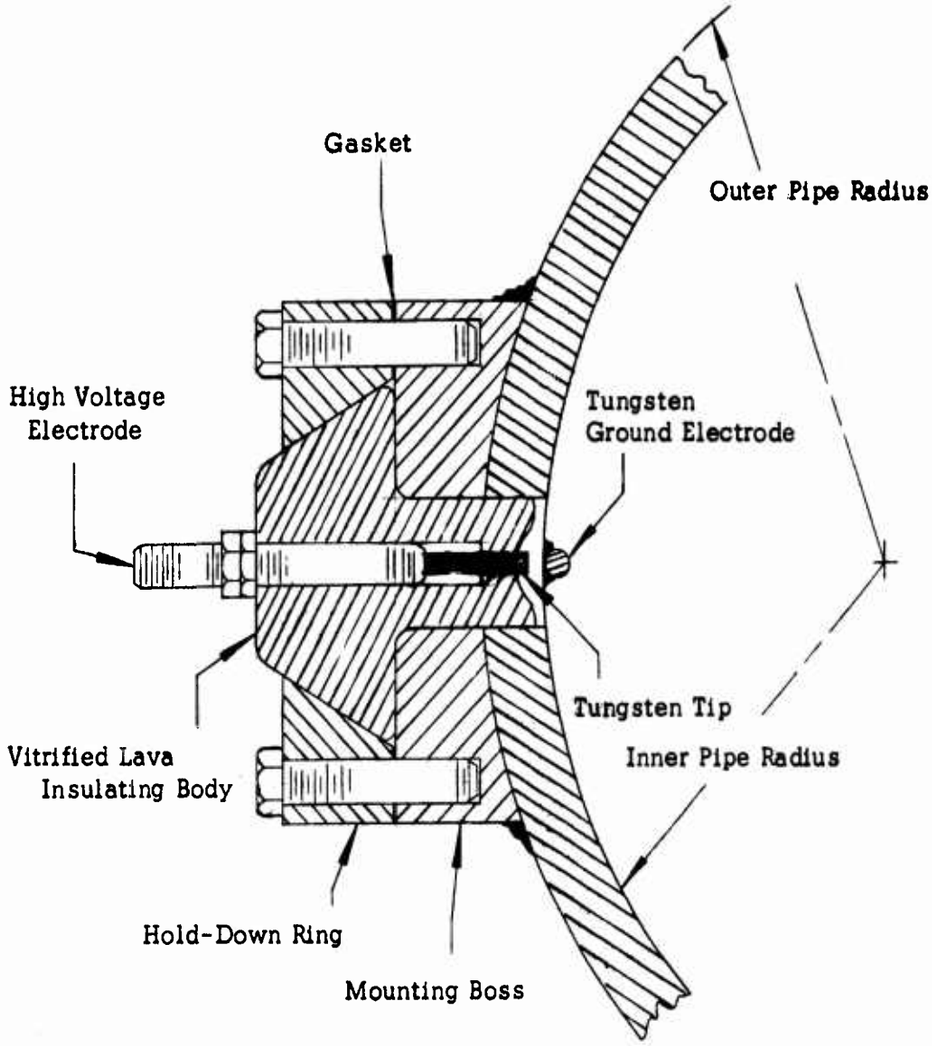

FIGURE B. 7. TRANSMITTING SPARK GAP DETAIL

This system was flange mounted to the pipewall through suitable electrical and acoustical insulating materials as indicated in Figure B. 8.

Initially, antenna beam pattern considerations led to the adoption of a cylindrical bar facing (as indicated in Figure B.8) to produce a 120-degree fan-shaped main beam pattern. This allowed for a wide reception angle in the plane including the transmitting spark gap and an otherwise narrow reception angle. After the first two motor tests, the bars were turned to a 60° convex spherical face to limit protrusion into the flow and consequently improve signal-to-noise ratio especially at those times when the transmitting spark gap was within the more confined beam pattern. Here it is important to note that angle of arrival of a pressure front at the receiver (which is colinear with the source-to-receiver line-of-sight) is not normal to the arriving pressure front, where the medium involved has a velocity component normal to the line of sight. The angle of arrival which is compatible with the ordinary ray theory beam pattern specification is given by the direction of the normal component of the pressure front velocity.

C. Pulse Generation and Time Marker Equipment

A thyratron switch was used to produce a voltage trigger for the triggered arc gap. The 7.5- and 15-pps rates were made available by dividing down from the 60-cps supply. The circuit diagram of the pulse generator is shown in Figure B. 9.

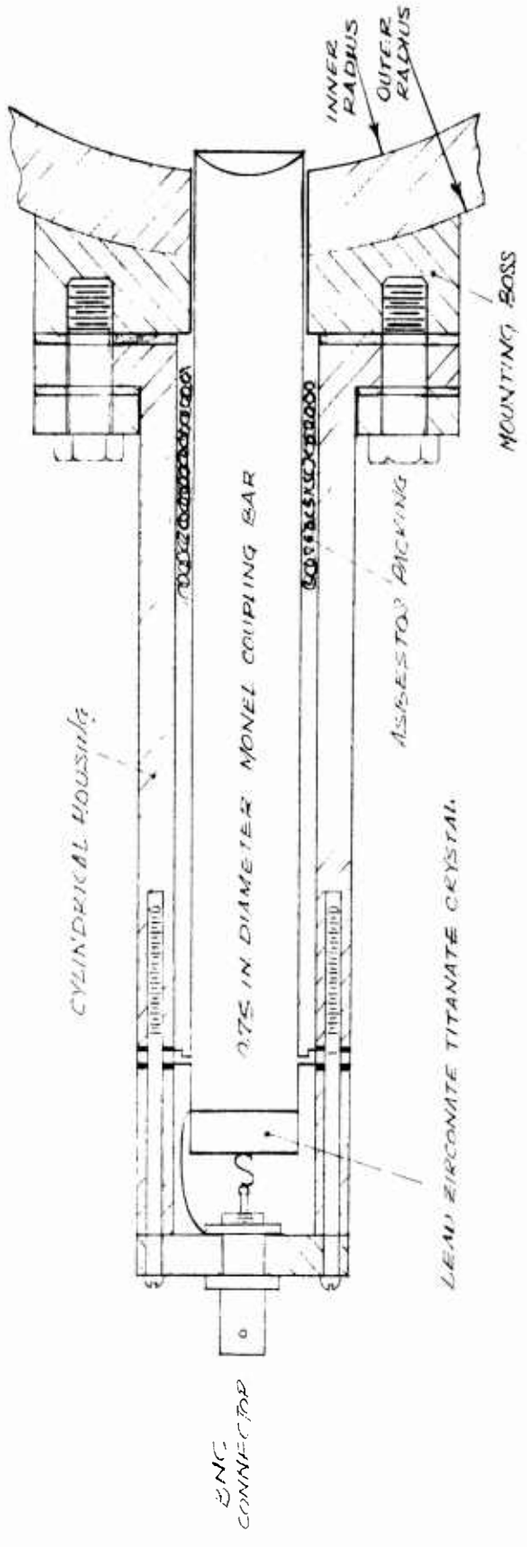

FIGURE B.8. RECEIVING TRANSDUCER DETAIL

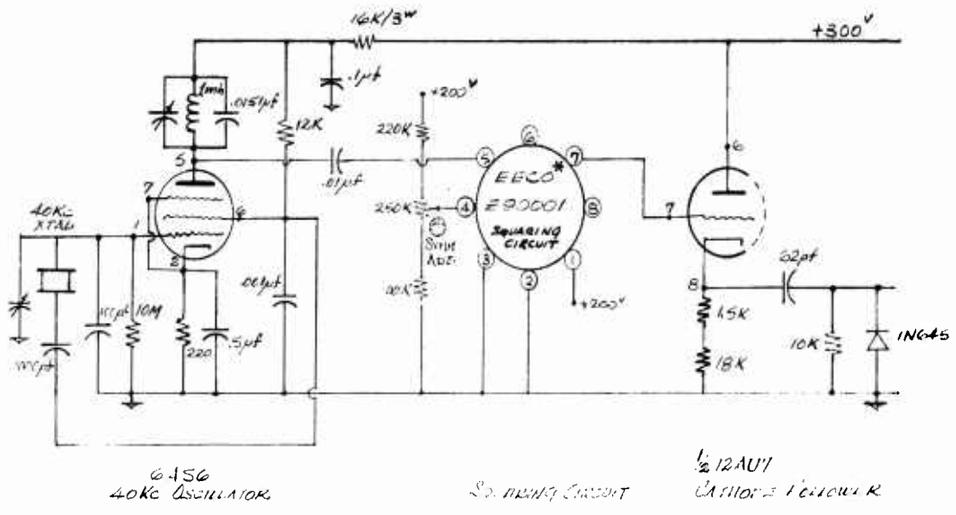

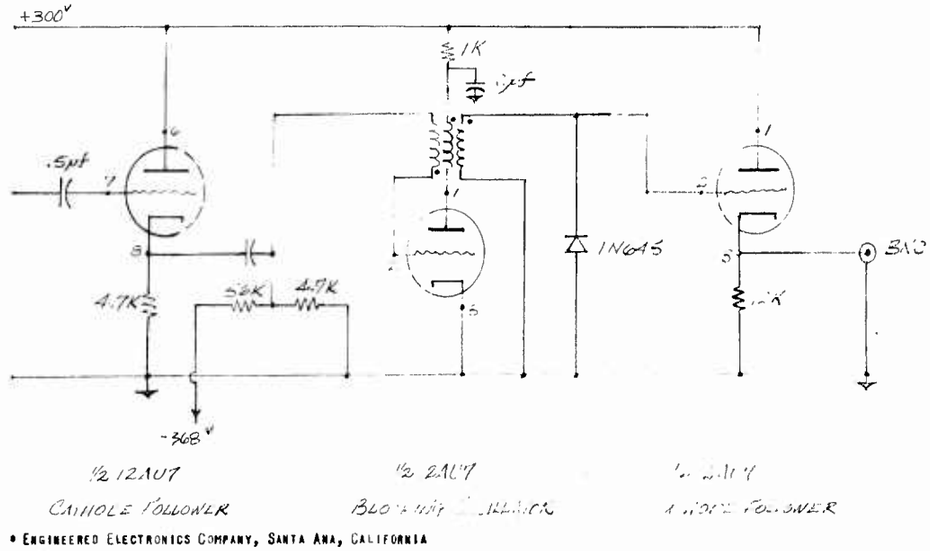

* Engineered Electronics Company, Santa Ana, California

FIGURE B.9. TIME MARK GENERATOR, 40,000 pps.

A time mark generator was also provided in order to display time reference on the oscilloscope display. This circuit included a crystal stablized 40-kc oscillator and a triggered blocking oscillator to produce sharp time mark pulses with a 25-microsecond spacing. This time mark circuit is shown in Figure B.9.

Also included was an oscilloscope blanking square wave-form (z-axis modulation) of controllable duration to circumvent multiple tracing problems in the displayed information signal. This circuit diagram is included in Figure B.10. Figure B.11 shows the overall power supply for the electronic equipment system.

D. Recording

A photographic record of the acoustic pulse arrivals was made by a moving film camera and a dual beam oscilloscope. The paper film speed was sufficient to allow a separated photograph of each oscilloscope display at the 7.5- or 15-cycle rate.

A typical film speed of 1800 inches/minute or 30 inches/second allowed a film exposure interval of four inches at the 7.5 per second data rate. The photographic process reduced the five-inch trace to about one inch. The oscilloscope trace duration of one millisecond per data point was sufficient to cause slight additional foreshortening of the trace as the film moved 0.03 inch during this interval. The short persistence P-5 phosphor of the cathode ray tube caused only slight blurring of the record.

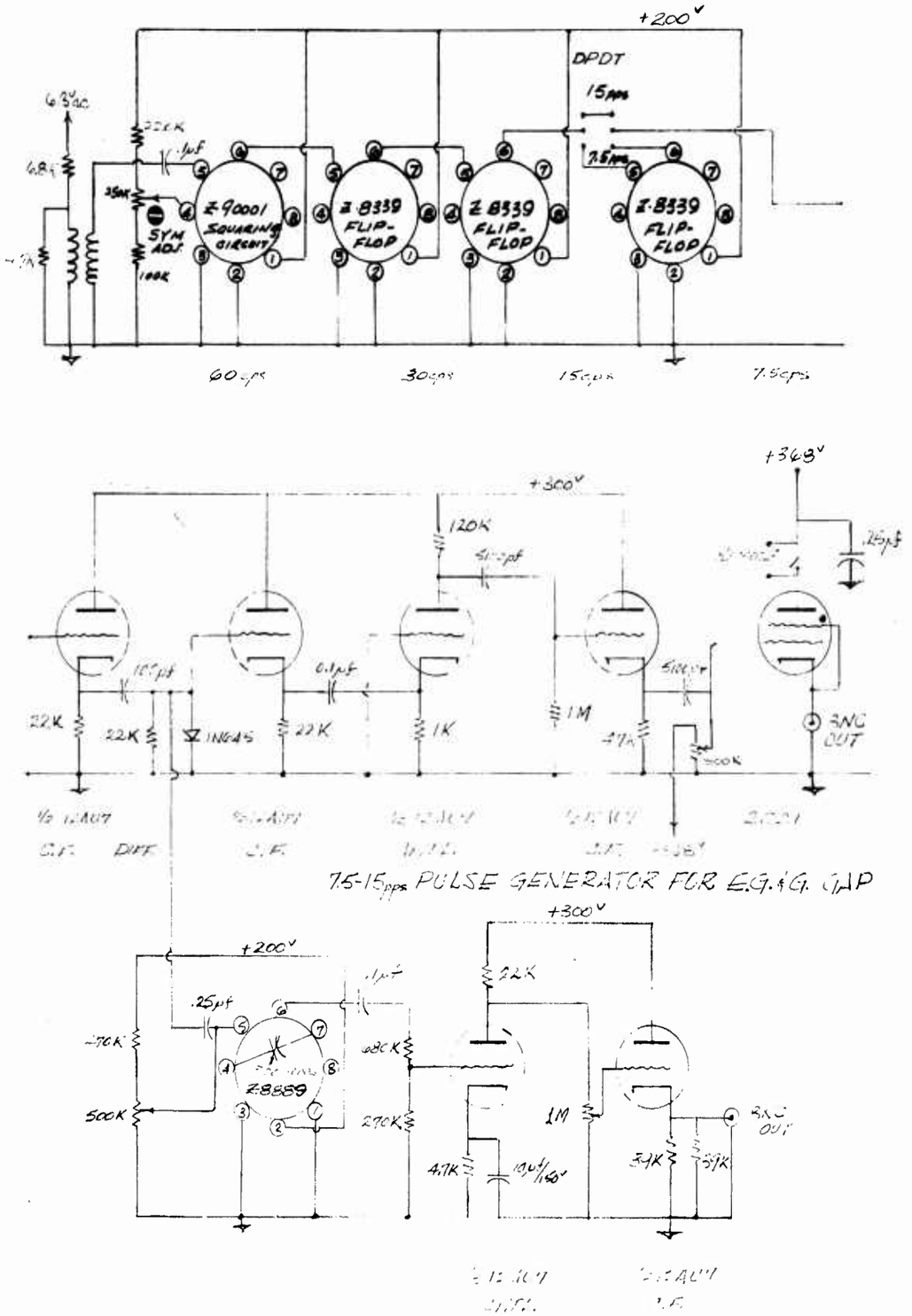

FIGURE B. 10. OSCILLOSCOPE UNBLANKING

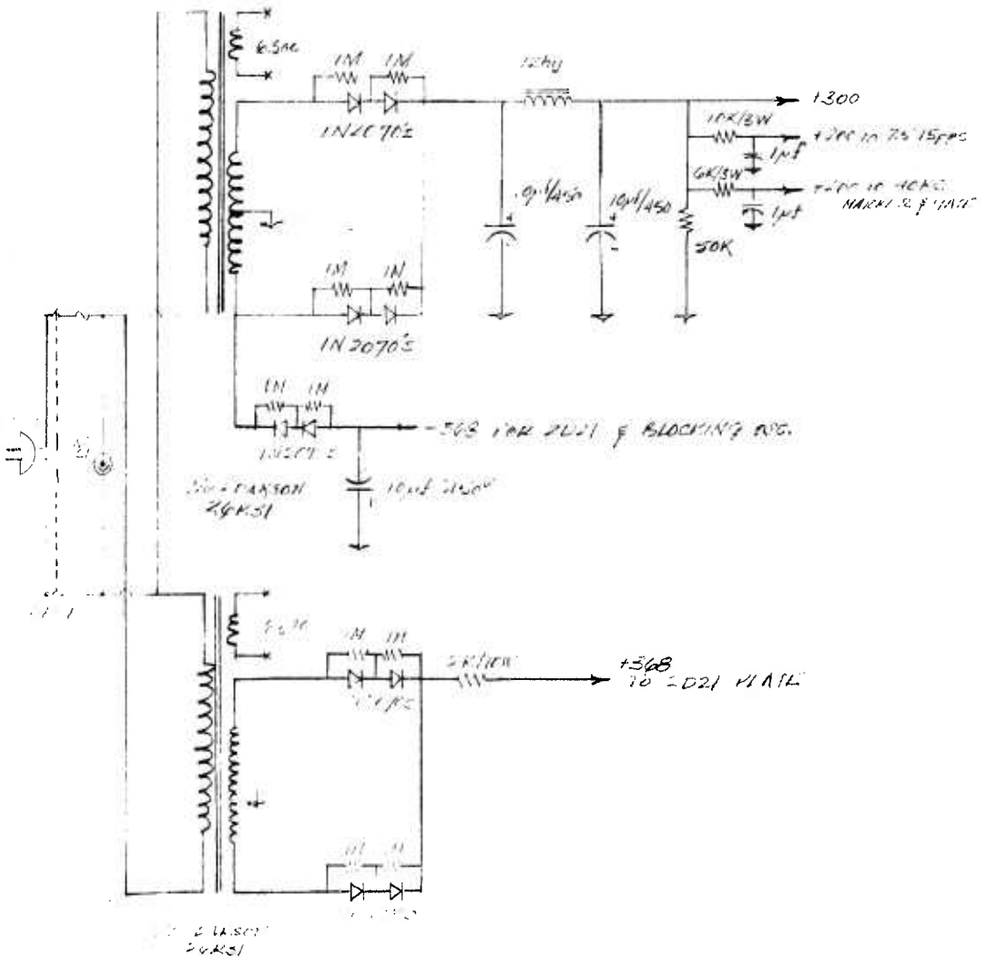

FIGURE B. 11. POWER SUPPLIES

The time resolution was accomplished through the observation of the 25-microsecond spaced time marks, observation of the 1000-microsecond total trace duration and observation of the photographed oscilloscope graticule which was illuminated by the cathode-ray trace. Unfortunately, the 25-microsecond time markers proved generally ineffective in the field operation, and it was found more convenient to rely on the illuminated graticule markers that were spaced at a 100-microsecond interval.

E. Instrumentation Section of Tube

A pipe section six feet in length was tooled with the various mounting bosses for the transmitting gap and receiving transducers. The layout as indicated in Figure B. 12 shows the several choices of receiver locations that are available for the various expected flow velocities.

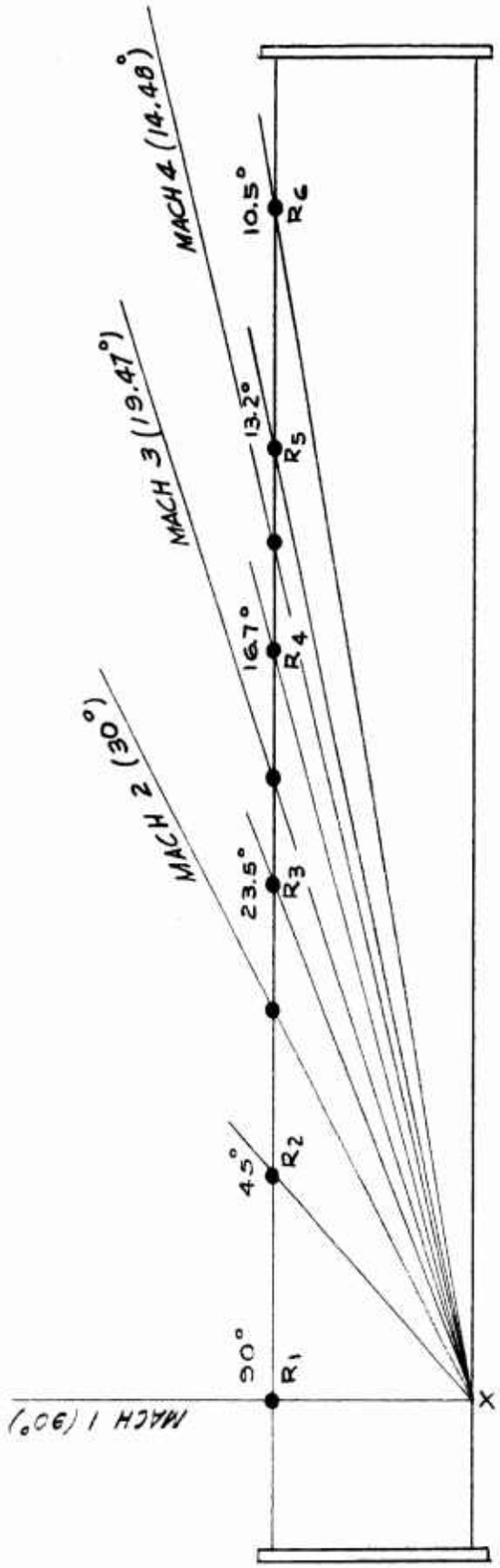

FIGURE B.12. INSTRUMENTATION SECTION OF PIPE

IV. EXPERIMENTAL RESULTS

Four rocket motors were fired during the course of the program including two small (4-pound RDS-135 Rocketdyne) and two large (70-pound TE-82 Thiokol) motors. The gas constituencies of the exhaust products were made available by the various motor manufacturers so that mean molecular weight and specific heat calculations could be made. Also, estimates of flow velocity were possible so that receiving transducer location on the instrumentation of the pipe section could be made compatible with the expected flow velocity. Firing duration on the small motors was of order one second, whereas the large motor duration was about three seconds. A 7.5-impulse-per-second cyclic rate was used at the spark gap pressure transmitter during all tests. The results obtained from two of the experiments were not useable since flow-induced noise as well as breakdown of acoustical and electrical insulation at the pipe wall corrupted the records to the extent that reasonable data interpretations were impossible. The instrumentation pipe section was five feet downstream of the rocket motor exhaust nozzle in these tests. Certain data points of the other two records were reduceable to flow velocity and temperature indications. The test results obtained during the last large motor firing yielded the most significant data points. For this experiment, the ultrasonic instrumentation pipe section was located

about twenty-five feet downstream of the motor exhaust nozzle. Also, a refacing of the receiving transducer bars was made. This combination of adjustments proved effective in suppressing a significant portion of the undesirable effects of flow induced noises in the detected signal. A reproduction of an impulse arrival data point from the moving film record is shown in Figure B.13. The transit time information available from this record indicates a flow velocity and free stream temperature of 30, 380 cm/sec and 782°F, respectively (see Appendix B.2 for this sample calculation).

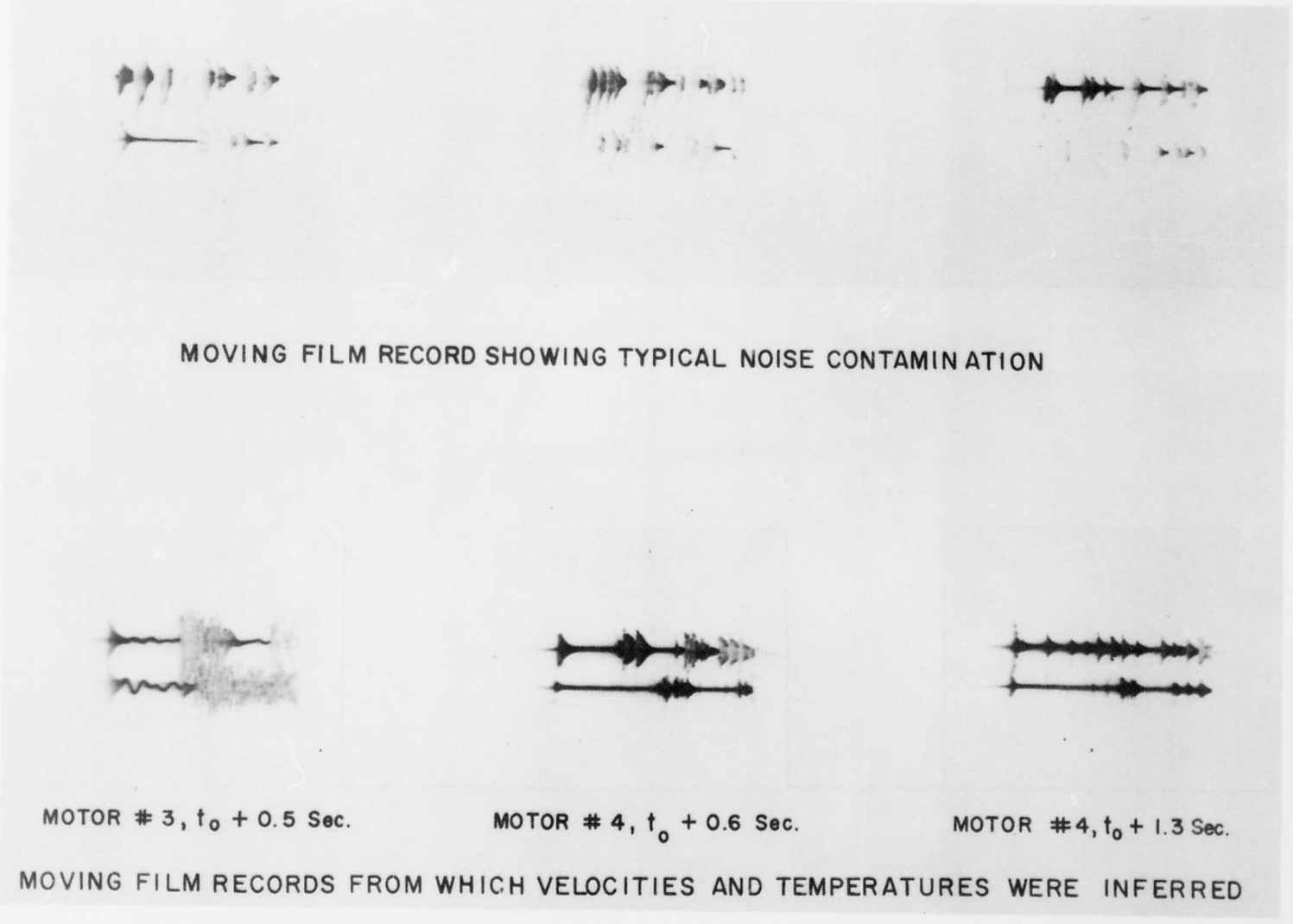
MOVING FILM RECORD SHOWING TYPICAL NOISE CONTAMINATION
MOTOR # 3, t_o + 0.5 Sec.
MOTOR # 4, t_o + 0.6 Sec.
MOTOR #4, t_o + 1.3 Sec.
MOVING FILM RECORDS FROM WHICH VELOCITIES AND TEMPERATURES WERE INFERRED

FIGURE B. 13

TABULATION OF RESULTS

Test	Motor	Time	Mach No.	Temp, °F	Remarks
1	T-S	--	--	--	Velocity data masked by flow noise
2	Cajun	--	--	--	Velocity data masked by flow noise
3	T-S	+0.5	0.493	782	
4	Cajun	+0.6	3.26	1700	
		[illegible]3	2.70	2420	

V. CONCLUSIONS

It is felt that these tests have demonstrated an affirmative indication of the feasibility of an ultrasonic instrumentation scheme for measuring supersonic flow velocity and temperature. The results of the final large motor firing were very gratifying in face of earlier problems, especially those associated with such large motors. It is felt that further refinements of this technique could lead to a useful instrumentation tool in the measurement of high speed flow in adverse environments.

Inherent in this method of instrumentation is its inadequacy to perform in other than uniform flows. The degree of uniformity of flow in these tests is highly questionable, and it appears to be a matter of speculation whether or not the small motors filled the tube at the instrumentation section. Another inherent characteristic of this method is that it averages over a significant volume of flow. Further, the accuracy of this technique is somewhat sensitive to the accuracy to which the gas constituency can be determined. A principle advantage of this instrumentation technique is that the flow perturbation is small in that the transmitters and receivers protrude only slightly into the flow.

The thermal shock and erosion effects of the flow caused considerable damage to the transducers in the earlier tests. Certain of these effects are illustrated in the photographs of Figures B.14 and B.15.

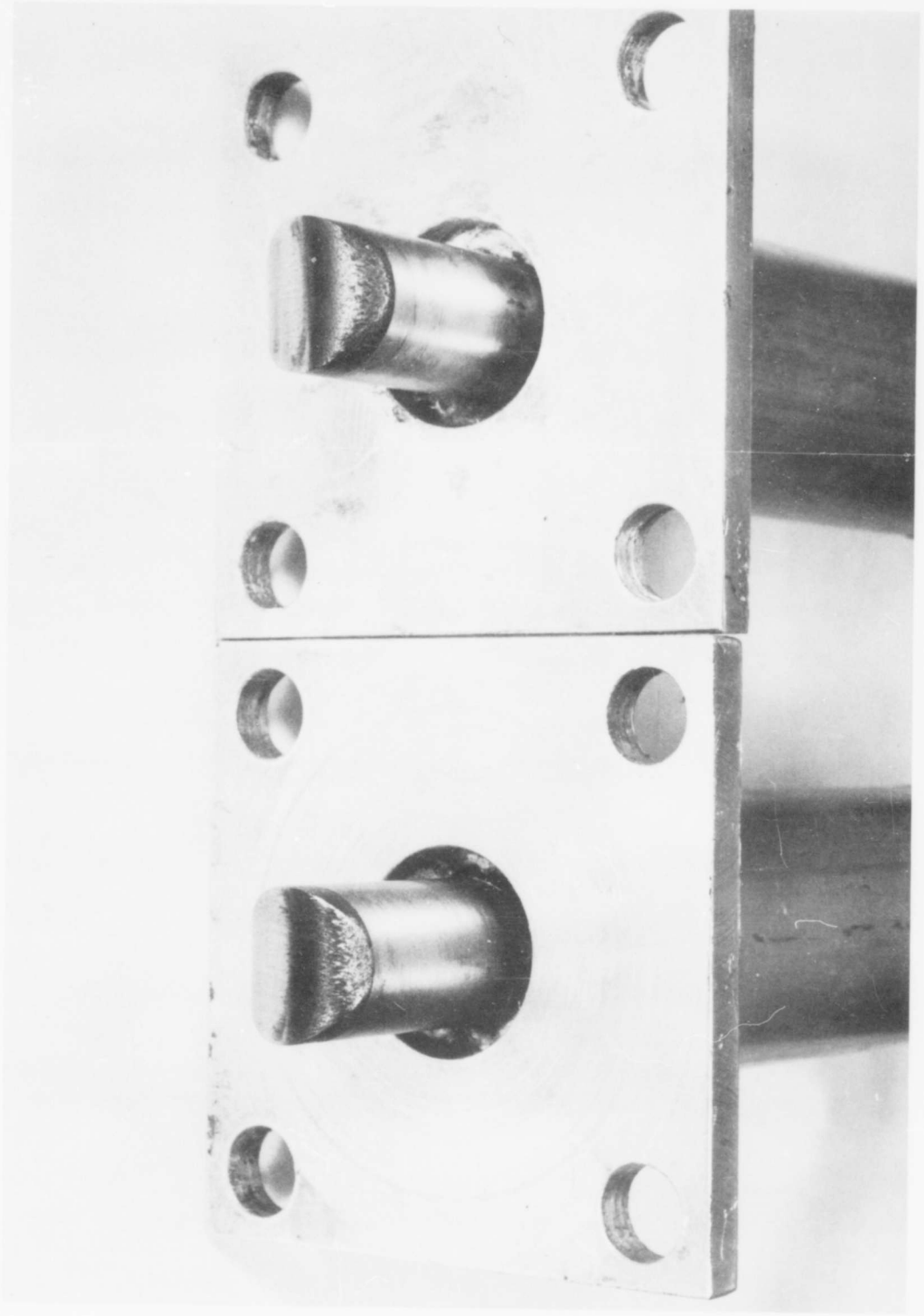

FIGURE B.14. THERMAL SHOCK AND EROSION EFFECTS OF THE FLOW

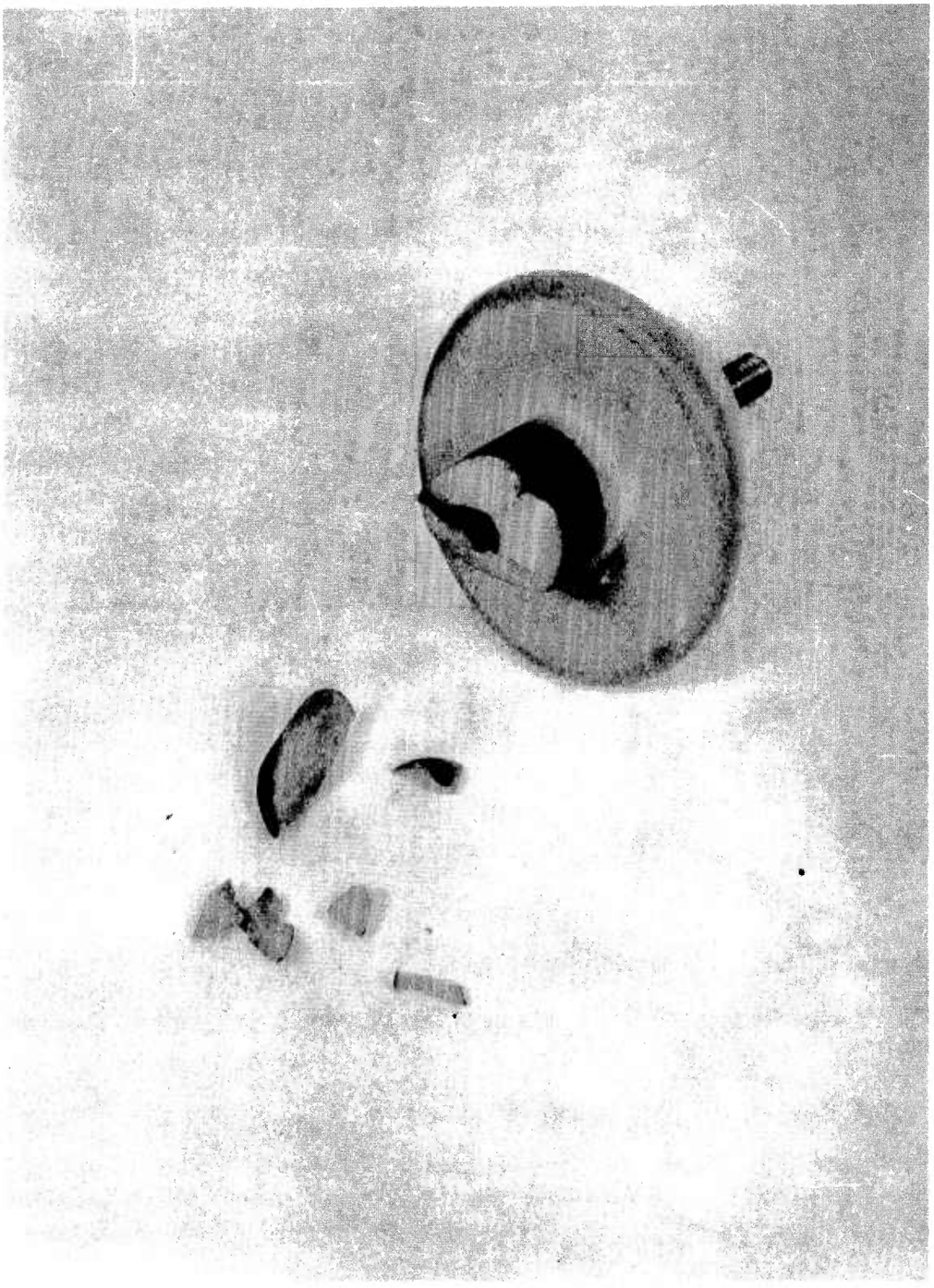

FIGURE B.15. THERMAL SHOCK AND EROSION EFFECTS OF THE FLOW

APPENDIX B.1. GAS MIXTURES INVOLVED

The exhaust gas mixture data on the two rocket motors are displayed here. Also, the relationships of $\gamma = 1 + \frac{R}{c_v}$ with temperature for the two gas mixtures are displayed in the plots of Figure B..16.

RDS-135 ROCKETDYNE EXHAUST GAS COMPOSITION

Constituent	Molecular Percent
H_2O	34.78
CO	14.47
CO_2	7.28
N_2	21.55
H_2	21.18
Solids	

TE-82 THIOKOL EXHAUST GAS PRODUCTS

H_2O	35.1
HCl	16.6
CO_2	15.3
H_2	8.9
CO	8.3
N_2	8.3
H_2S	5.6
S_2	1.5
MgO	.27
COS	.17
SO_2	.16
Remainder	< .05

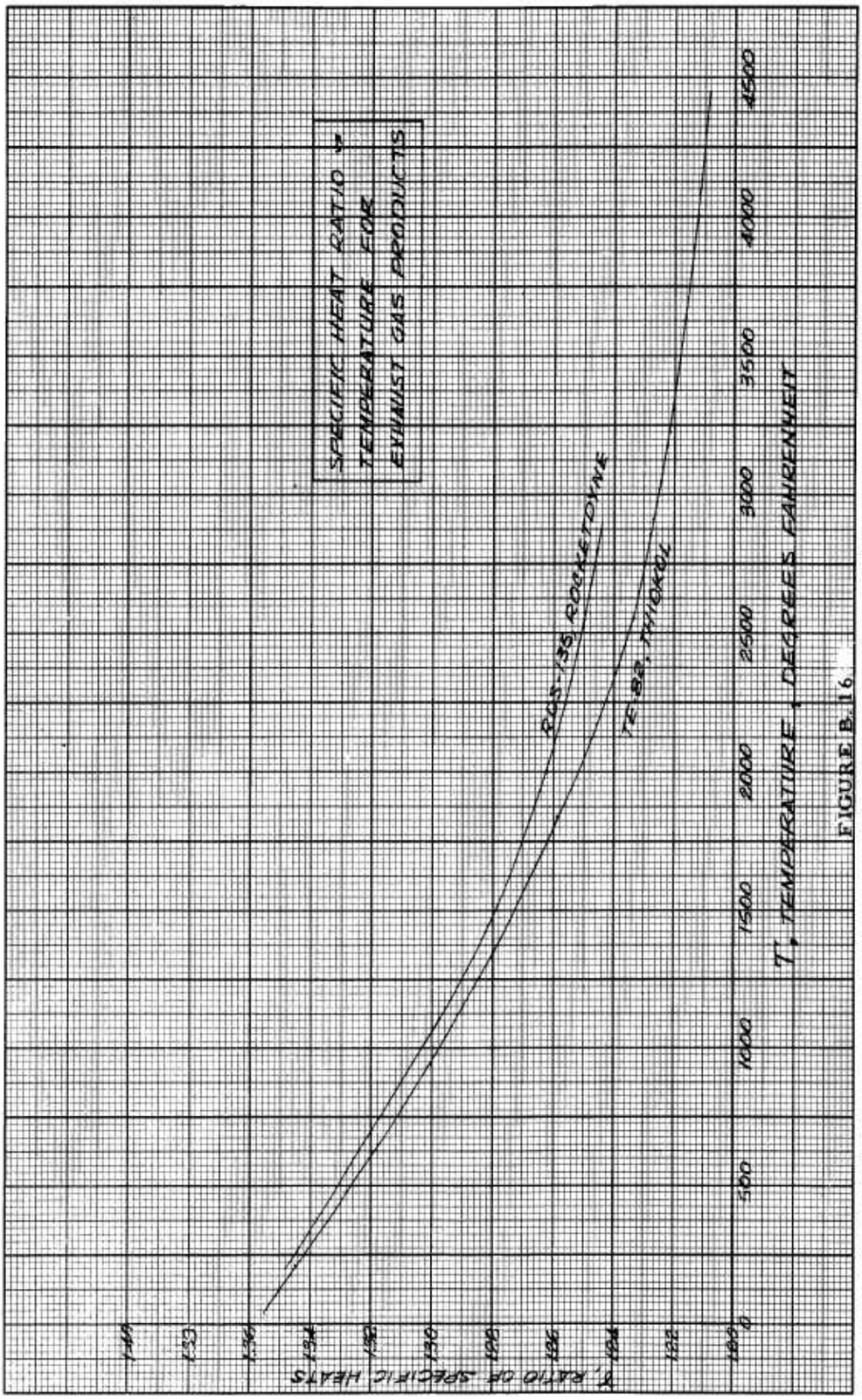
SPECIFIC HEAT RATIO
TEMPERATURE FOR
EXHAUST GAS PRODUCTS
RUS-135 ROCKETDYNE
TE-82, THIOKOL
γ, RATIO OF SPECIFIC HEATS
T, TEMPERATURE, DEGREES FAHRENHEIT
1.38
1.34
1.32
1.30
1.28
1.26
1.24
1.22
1.20
500
1000
1500
2000
2500
3000
3500
4000
4500

FIGURE B.16

APPENDIX B.2. SAMPLE CALCULATIONS

This sample calculation is for the Rocketdyne RDS-135 solid propellant motor. For this test the transmitting spark gap and receiving transducers were geometrically related as indicated in Figure B.17.

MOTOR #3, TO +0.5 SEC

	Direct	Downstream
Trace Length	0.325" ± .0021	0.312" ± .002
Transit Time	$0.325 \div .083 \times 100 = 391.55\mu$ sec	$0.312 \div .083 \times 100 = 376.00\mu$ sec
Arc Gap-Transducer Spacing	7.625"	$7.625\sqrt{2}$"
Velocity	$v_a = 7.625 \div (3.6155 \times 10^{-6})$ $= 21{,}090$ in./sec	$v_b = 7.625\sqrt{2} \div (346.00 \times 10^{-6})$ $= 22{,}040\sqrt{2}$ in./sec

0.083" = > 1cm (Photographic Reduction Factor) and 1cm = > 100μ sec (Trace Time Scale)

Time of Transit in Monel Bar, 30μ sec

$$c_\infty = \frac{v_b^2 - v_a^2}{2(v_b \cos\theta_b - v_a \cos\theta_a)} = 11{,}950 \text{ in./sec} = \underline{30{,}380 \text{ cm/sec}}$$

$$c = [v_a^2 + c_\ell^2 - 2v_a c_\ell \cos\theta_a]^{1/2} = 24{,}300 \text{ in./sec} = \underline{61{,}700 \text{ cm/sec}}$$

Mach Number = 0.493

From Figure B.4, $\underline{T = 782°F}$.

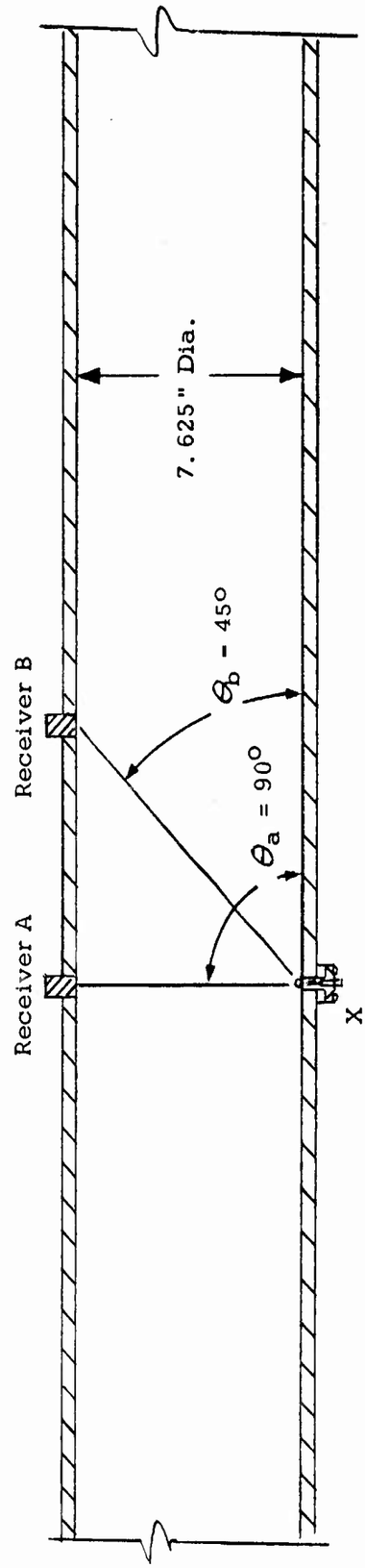

FIGURE B.17. TRANSDUCER LOCATION GEOMETRY FOR SUBSONIC FLOW EXAMPLE

BIBLIOGRAPHY AND REFERENCES FOR APPENDIX B

1. Abello, T. P., "Absorption of Ultrasonic Waves by Various Gases," Physical Review, Vol. 31, June, 1928.

2. American Institute of Physics, Temperature, Its Measurement and Control in Science and Industry, Vol. I, Reinhold, 1941; Vol. II, Reinhold, 1955.

3. Battelle Memorial Institute, Project Rand, "Physical Properties and Thermodynamic Functions of Fuels, Oxidizers, and Products of Combustion," Jan. 1949.

4. Carnevale, E. H., H. L. Poss, and J. M. Yos, "Ultrasonic Temperature Determinations in a Plasma," Tech. Rpt. RAD-TR-61-13, Research and Advanced Development Division, Avco Corporation, Wilmington, Mass., June 1961.

5. Ferri, Antonio, Elements of Aerodynamics of Supersonic Flows, The Macmillan Co., 1949.

6. Hart, R. W., and F. T. McClure, "Combustion Instability: Acoustic Interaction with a Burning Propellant Surface," Journal of Chemical Physics, Vol. 30, No. 6, June, 1959.

7. Herzfeld, K. F., and F. O. Rice, "Dispersion and Absorption of High Frequency Sound Waves," Physical Review, Vol. 31, April, 1928.

8. Hill, J. A. F., J. R. Baron, L. H. Schindel, and J. R. Markham, "Mach Number Measurements in High Speed Wind Tunnels," Naval Supersonic Laboratory, Massachusetts Institute of Technology, Oct. 1956.

9. Johns Hopkins University, Handbook of Supersonic Aerodynamics, Navord Report, 1488, Vol. 3, Nov. 1957.

10. Livengood, J. C., T. P. Rona, and J. J. Baruch, "Ultrasonic Temperature Measurement in Internal Combustion Engine Chamber," Journal of the Acoustical Society of America, Vol. 26, No. 5, 1952.

11. Niordson, F., "Transmission of Shock Waves in Thin-Walled Cylindrical Tubes," Acta Polytechnica, 107 (1952).

12. Parker, J. G., "Rotational and Vibrational Relaxation in Diatomic Gases," The Physics of Fluids, Vol. 2, No. 4, 1959.

13. Perry, J. H., Editor, Chemical Engineers Handbook, McGraw-Hill, 1941.

14. Poritsky, H., and C. G. Suits, "Determination of Arc Temperature from Sound Velocity Measurements, II," Physics, Vol. 6, 1935.

15. Sherratt, G. G., and E. Griffiths, "The Determination of the Specific Heat of Gases at High Tempera res by the Sound Velocity Method," Proceedings of the Royal Society of London, Series A, Vol. CXLVII, Dec. 1934.

16. Stull, D. R., and G. C. Sinke, Thermodynamic Properties of the Elements, Advances in Chemistry Series, 1956.

17. Suits, C. G., "Determination of Arc Temperature from Sound Velocity Measurements, I," Physics, Vol. 6, No. 6, 1935.

18. Vrkljan, V. S., "Uber die Berechnung der Schallgeschwindigkeit in Gasmischungen," Nuovo Cimento, Vol. XVII, No. 6, 1960.

UNCLASSIFIED